2015•2016
FACULTEIT GENEESKUNDE EN LEVENSWETENSCHAPPEN
master in de biomedische wetenschappen

Masterproef

Cellular and molecular effects of iodine deficiency and ionizing radiation on non-cancerous thyroid cells

Promotor :
dr. Patrick VANDORMAEL

Promotor :
Dr.ir. HANANE DERRADJI

Noami Daems

Scriptie ingediend tot het behalen van de graad van master in de biomedische wetenschappen

2015•2016
FACULTEIT GENEESKUNDE EN LEVENSWETENSCHAPPEN
master in de biomedische wetenschappen

Masterproef

Cellular and molecular effects of iodine deficiency and ionizing radiation on non-cancerous thyroid cells

Promotor :
dr. Patrick VANDORMAEL

Promotor :
Dr.ir. HANANE DERRADJI

Noami Daems
Scriptie ingediend tot het behalen van de graad van master in de biomedische wetenschappen

universiteit hasselt | Maastricht University

TABLE OF CONTENTS

LIST OF ABBREVIATIONS

7-AAD	7-aminoactinomycin D
ATC	Anaplastic thyroid cancer
ATM	Ataxia telangiectasia mutated protein
ATR	Ataxia telangiectasia and Rad3-related protein
BAD	Bcl-2-associated death promoter
BCA	Bicinchoninic acid assay
BCL-2	B-cell lymphoma 2
BCL-XL	B-cell lymphoma-extra large
BRCA1	Breast cancer 1
BrdU	5-bromo-2'-deoxyuridine
CHAPS	3-[(3-cholamidopropyl)dimethylammonio]-1-propanesulfonate
CHK	Checkpoint kinase
CM-H_2DCFDA	chloromethyl-2'7'- dichlorodihydrofluorescein diacetate acetyl ester
Cs^{137}	Caesium-137
CT	Computed tomography
CTNNB1	β-catenin
DAPI	4',6-diamidino-2-phenylindole
DDR	DNA damage response
DSB	Double strand breaks
EDTA	Ethylenediaminetetraacetic acid
EGFR	Epidermal growth factor receptor
ERK	Extracellular-signal-regulated kinases
FBS	Fetal bovine serum
FTC	Follicular thyroid cancer
gp-130	Glycoprotein 130
GSK	Glycogen synthase kinase
Gy	Gray
HB-HBSS	HEPES-buffered Hank's balanced salt solution
HCl	Hydrogen chloride
HIF	Hypoxia inducible factor
HRE	Hypoxia response element
H_2O_2	Hydrogen peroxide
I^{131}	Iodine-131
IAP	Inhibitors of apoptosis proteins
ID	Iodine deficiency
IKKα	IκB kinase
IL	Interleukin
IL-6R	Interleukin-6 Receptor
IR	Ionizing radiation
JAK	Janus kinase
JNK	c-Jun N-terminal kinase
kV	kilo voltage
LET	Linear energy transfer
LNT	Linear no threshold

MAPK	Mitogen-activated protein kinase
Mcl-1	Myeloid Cell Leukemia 1
MDC1	Mediator of DNA damage checkpoint protein 1
MDM2	Mouse double minute 2 homolog
MEK	Mitogen-activated protein kinase kinase
$MgCl_2$	Magnesium dichloride
MKK	MAP kinase kinase kinase
MTC	Medullary thyroid cancer
mTOR	Mechanistic target of rapamycin
NaI	Sodium iodide
NBS1	Nibrin
NFκB	nuclear factor kappa-light-chain-enhancer of activated B cells
NO	Nitrogen oxide
NOS3	Nitrogen oxide synthase 3
PPARγ	Peroxisome proliferator-activated receptor γ
PAX8	Paired box gene 8
PBS	Phosphate-buffered saline
PFA	paraformaldehyde
PI3K	Phosphatidylinositide 3-kinases
PIK3CA	phosphatidylinositol-4,5-bisphosphate 3-kinase catalytic subunit alpha
PTC	Papillary thyroid cancer
PTEN	Phosphatase and tensin homolog
QDot	Quantum dots
RIN	RNA integrity number
ROS	Reactive oxygen species
RT	Reverse transcriptase
RYR	Ryanodine receptor
SAPK	Stress-activated protein kinase
SD	Standard deviation
SDS	Sodium-dodecyl-sulfate
SEM	Standard error of the mean
Sr^{90}	Strontium-90
SSB	Single strand breaks
STAT	Signal transducer and activator of transcription
Sv	Sievert
T_3	Triiodothyronine
T_4	Tetraiodothyronine
tBHP	tert-butylhydroperoxide
TBP	Tributyl phosphate
TBS	Tris-buffered saline
TMRM	Tetramethylrhodamine
TNFα	Tumor necrosis factor α
TPO	Thyroid peroxidase
TRAF	TNF receptor associated factors
TRK	Tyrosine protein kinase receptors
TSC	Tuberous Sclerosis Complex 2
TSH	Thyroid-stimulating hormone
VEGF-A	Vascular endothelial growth factor-A

ACKNOWLEDGEMENTS

Coming to the end of writing this thesis, I would like to thank the people who helped me during my practical work in the lab and during the writing process of this thesis. First of all, I would like to express my sincere gratitude towards my SCK•CEN promotor dr. ir. Hanane Deraddji, my institutional promotor dr. Patrick Vandormael and my second examiner dr. ir.Liesbet Peeters for their continuous support and advice throughout the duration of the thesis. In addition, I would like to thank Prof. dr. Sarah Baatout for the opportunity to work in the lab of the SCK•CEN Radiobiology Unit. Furthermore, I had a lot of help from the PhD students Bjorn Baselet and Niels Belmans and from MSc student Emma Coninx in my practical experiments and result analyses. They were always prepared to answer my questions and to support me at all times during my thesis. Without their help, this thesis would not have been possible. My personal gratitude also goes out to all other PhD students in the Radiobiology and Microbiology unit of SCK•CEN for their warm welcome, friendship and support. Finally, I also want to thank my family and friends outside the workspace of SCK•CEN for their love, friendship and support.

SAMENVATTING

Introductie: Uit Post-Chernobyl epidemiologische studies blijkt dat blootstelling aan ioniserende straling (IR) een belangrijk risicofactor is in schildklierkankerontwikkeling. De algemene populatie wordt steeds meer blootgesteld aan IR afkomstig van natuurlijke en kunstmatige bronnen. Vooral lage stralingsdosissen zijn van belang. Bovendien toont de epidemiologie ook aan dat jodiumtekort (ID), waar meer dan 2 miljoen mensen aan lijden, ook een invloed uitoefent op de schildklierkankerontwikkeling. Er is nog steeds onduidelijkheid over het gecombineerd effect van IR en ID op schildkliercellen. We hypothetiseren dat IR en ID stress veroorzaken in schildkliercellen door een verhoogde productie van reactieve zuurstofsoorten (ROS) wat de deling en overleving van de schildkliercellen kan beïnvloeden.

Materiaal & methoden: Rat PCCL3 schildkliercellen werden gekweekt in de aan- of afwezigheid van jodium voor 6u, 24u en 48u en werden bestraald met lage (0 Gy, 0.05 Gy, 0.1 Gy), gemiddelde (0.5 Gy) of hoge (3 Gy) stralingsdosissen. De proteïne expressie van catalase, (p)AKT1, (p)STAT3, NFκB p52 werd bepaald door middel van Western blot. ROS productie en γH2AX/53BP1 foci werden gedetecteerd door respectievelijk CM-H_2DCFDA fluorescerende beeldvorming en immunocytochemie, gevisualiseerd door een fluorescentie microscoop. De cel cyclus werd onderzocht door middel van een BrdU/7-AAD assay en flow cytometrie. Statistische significantie ($p<0.05$) werd geëvalueerd met een two-way ANOVA.

Resultaten: Jodium-deficiënte cellen bestraald met 0.5 Gy en 3 Gy vertoonde een versterkte ROS productie 24u na de behandeling in vergelijking met jodium-sufficiënte cellen. Bovendien was er een algemeen significant effect van de jodiumstatus op de catalase proteïne expressie 6u na de behandeling. Cellen bestraald met 0.5 Gy en 3 Gy vertoonde een significant verhoogd aantal γH2AX foci vergeleken met niet-bestraalde cellen op 30 min na de behandeling, waarna het aantal terug daalt tot 24u na de behandeling. Het aantal 53BP1 foci na een bestraling van 0.1 Gy, 0.5 Gy en 3 Gy was significant hoger vergeleken met niet-bestraalde cellen en bereikte hun piek na 1-4u, waarna het aantal daalde tot 24u na de behandeling. Cellen bestraald met 0.05 Gy en 0.1 Gy vertoonde een continue stijging in het aantal γH2AX foci tot 24u na de behandeling. Het aantal 53BP1 foci veranderde niet tussen 0.05 Gy-bestraalde cellen en niet-bestraalde cellen. Er was ook geen verschil in het aantal foci tussen jodium-sufficiënte en jodium-deficiënte cellen. Op 24u na de behandeling was er een significante verhoging in de hoeveelheid cellen in de G0/G1 fase na bestraling met 3 Gy vergeleken met niet-bestraalde cellen. Bovendien was het aantal jodium-deficiënte cellen blootgesteld aan lage, gemiddelde en hoge stralingsdosissen significant verlaagd in de G0/G1 fase en verhoogd in de G2/M fase en S fase vergeleken met jodium-sufficiënte cellen. Op 48u na de behandeling werden er geen significante verschillen meer gezien in de cel cyclus tussen jodium-deficiënte en jodium-sufficiënte cellen. Tot slot, er werden geen significante verschillen gezien op proteïne niveau 6u na de behandeling voor proliferatie- en overlevingsmediatoren.

Discussie & conclusie: Blootstelling aan 0.5 Gy en 3 Gy veroorzaakt stress in de schildkliercellen tot een bepaald niveau waardoor ze de bijkomende stress van jodiumtekort niet kunnen opvangen, wat leidt tot een versterkte ROS productie in vergelijking met jodium-sufficiënte cellen. Het DNA herstel verloopt bovendien anders na blootstelling aan lage stralingsdosis dan na een hoge stralingsdosis. Dit suggereert dat er een drempelwaarde van DNA schade overschreden moet worden om een efficiënte activatie te verkrijgen van de DDR pathway. PCCL3 cellen zijn relatief radioresistent. Een gecombineerde behandeling van ID en IR maakt de cellen minder gevoelig voor een G1 stop en versterkt de proliferatie 24u na behandeling. Dit kan duiden op een vergankelijke stressreactie met veranderingen in de proliferatie pathways wat nog niet detecteerbaar was 6u na de behandeling. De veranderde catalase proteïne expressie kan ter compensatie dienen voor onvoldoende H_2O_2-detoxificatie dankzij jodiumtekort.

SUMMARY

Introduction: Post-Chernobyl epidemiological studies appointed ionizing radiation (IR) exposure as high-risk factor for thyroid cancer development. Currently, the general population is increasingly exposed to IR deriving from natural and human-made sources. In particular, low-dose IR is of major concern. On the other hand, epidemiological studies demonstrated that iodine deficiency (ID), affecting more than 2 billion individuals worldwide, is also a determinant in thyroid cancer development. However, there are still uncertainties about the combined effects of ID and low-dose IR exposure on thyroid cells. We hypothesize that low-dose IR and ID both stress thyroid cells by an enhanced production of reactive oxygen species (ROS), affecting proliferation and survival.

Material & methods: Rat thyroid PCCL3 cells were cultured in iodine-deficient or iodine-sufficient conditions for 6h, 24h or 48h and were irradiated with low (0 Gy, 0.05 Gy, 0.1 Gy), intermediate (0.5 Gy) or high (3 Gy) X-ray doses. Protein expressions of Catalase, (p)AKT1, (p)STAT3, NFκB p52 were determined by Western blot. ROS production and γH2AX/53BP1 foci were dtected by respectively CM-H_2DCFDA fluorescent imaging and immunocytochemistry visualized using fluorescence microscopy. Finally, cell cycle distribution was examined by a BrdU/7-AAD assay using flow cytometry. Statistical significance ($p<0.05$) was evaluated with two-way ANOVA.

Results: There was an enhanced ROS production at 24h post-treatment in iodine-deficient cells irradiated with 0.5 Gy and 3 Gy compared to iodine-sufficient cells. Furthermore, there was an overall significant effect of the iodine state on the catalase protein expression 6h post-treatment. PCCL3 cells irradiated with 0.5 Gy and 3 Gy exhibited a significantly increased number of γH2AX foci compared to sham-irradiated cells at 30 min post-treatment, after which it decreased up to 24h post-treatment. The number of 53BP1 foci after irradiation with 0.1 Gy, 0.5 Gy and 3 Gy was significantly higher compared to sham-irradiated cells and reached its peak around 1-4h, after which it decreased up to 24h post-treatment. PCCL3 cells irradiated with 0.05 Gy and 0.1 Gy showed a continuously increasing number of γH2AX foci up to 24h post-treatment. The number of 53BP1 foci did not significantly differ between 0.05 Gy-irradiated cells and sham-irradiated cells. There were no major differences in the number of DSBs between iodine-sufficient and iodine-deficient cells. At 24h post-treatment, the percentage of cells in the G0/G1 phase significantly increased after irradiation with 3 Gy compared to sham-irradiated cells. Furthermore, the amount of iodine-deficient cells exposed to low-, intermediate- and high-dose IR was significantly lower in the G0/G1 phase and higher in the G2/M phase and S phase compared to iodine-sufficient cells. At 48h post-treatment, there were no longer significant differences in cell cycle distribution between iodine-deficient and iodine-sufficient cells. No significant differences were observed at protein level 6h post-treatment for proliferation (STAT3, AKT1) and survival (NFkBp52) mediators.

Discussion & conclusions: Irradiation with 0.5 Gy or 3 Gy stresses thyroid cells to a certain extent which makes them unable to cope with the additional stress of ID, leading to an enhanced ROS production compared to iodine-sufficient cells. Furthermore, The DNA repair of thyroid cells after low-dose exposure is different than after high-dose exposure, suggesting the presence of a DNA damage threshold level required for efficient activation of the DDR pathway. Thyroid cells are relatively radioresistant. However, a combined treatment with ID and IR makes thyroid cells less sensitive for a p53-dependent G1 arrest and enhances proliferation 24h post-treatment. This could represent a transient stress response with subtle changes in the proliferation pathways, which was not detected yet at 6h post-treatment and was disappeared at 48h post-treatment. The altered catalase protein expression could be a response to compensate for insufficient detoxification of H_2O_2 by ID.

INTRODUCTION

1. THE THYROID GLAND AND THYROID CANCER

The thyroid gland is one of the largest endocrine glands in the human body and comprises two connected lobes, located anterolaterally to the upper trachea. The functional unit of the thyroid gland is the thyroid follicle, which produces the thyroid pro-hormone, tetraiodothyronine (T_4) and the active thyroid hormone, triiodothyronine (T_3), using the precursors thyroglobulin and iodide. The produced thyroid hormones are then released into the blood stream via rich capillary networks closely surrounding the thyroid follicles. The active, circulating thyroid hormones are essential for normal fetal brain development and regulate many physiological processes in the human body such as the metabolism, cardiovascular function, respiration, mental processing, growth, maturation and reproduction (1).

Thyroid cancer is a common malignancy of the endocrine system and can originate from two different cell types. Most thyroid cancers originate from the follicular thyroid cells and are classified in different subtypes depending on their morphological and clinical characteristics. They encompass the well-differentiated papillary and follicular thyroid carcinomas (PTC and FTC respectively), as well as the undifferentiated, anaplastic thyroid carcinoma (ATC). PTC is the most frequent tumor type of the thyroid gland, accounting for 80% of all cases and can be associated with ionizing radiation (IR) exposure. Common mutations found in thyroid cancers are point mutation of the BRAF and RAS genes as well as RET/PTC and PAX8/PPARγ chromosomal rearrangements (2) **(Supplemental Table 1).** The characteristic chromosomal rearrangements of the receptor tyrosine kinase RET gene are specific for PTC. The most common rearrangement types are RET/PTC1 and RET/PTC3. As a result from these rearrangements, the portion of the RET gene encoding for the intact tyrosine kinase domain is fused to an active promoter of another gene, stimulating the expression and ligand-independent dimerization of the RET/PTC protein. This, in turn, leads to constitutive activation of the MAPK signaling pathway, promoting tumorigenesis of the thyroid cells **(Supplemental Figure 1)**. RET/PTC rearrangements are commonly found in pediatric PTCs and in PTCs of individuals exposed to IR. The accidental radiation exposure after the Chernobyl accident particularly increased the frequency of the RET/PTC3 rearrangement type. FTC represents only 15% of all thyroid cancers and harbor mostly RAS mutations and PAX8-PPARγ rearrangements. PTC and, to a lesser extent, FTC have a good clinical prognosis if adequately treated. In contrast, ATC is a rare (Only 5% of all cases) but aggressive malignancy, associated with a highly lethal clinical course despite therapeutic intervention. Genetic mutations known to occur in ATC involve the RAS, BRAF, TP53 and CTNNB1 genes as well as alterations in the PI3K/AKT signaling pathway **(Supplemental Figure 1)**. Finally, Medullary thyroid cancer (MTC) originates from the para-follicular C cells and accounts for only 3% of all thyroid cancers. MTCs frequently harbor point mutations of the RET gene (2, 3).

Although the contribution of thyroid cancer to global cancer burden is small, thyroid cancer incidence has rapidly increased worldwide in the recent few decades, including in the Flemish region of Belgium **(Figure 1)** (4-6). The increased incidence is limited to the papillary type of

thyroid cancer. It is suggested that advances in medical diagnostic techniques, which increase the detection rate of small thyroid tumors (<1cm), contribute to this worldwide increasing trend. However, whether this can account entirely for this continuous trend, or whether environmental factors also contribute, remains unclear. Since IR is a well-known risk factor for the development of thyroid cancer, concerns remain that the rising incidence might, in part, result from the increased population exposure to medical radiation (2, 7). In addition, imbalanced dietary iodine intake is also associated with the development of thyroid disorders. Since there is little knowledge about the exact etiology of thyroid cancer and many individuals are simultaneously affected by low-dose IR and iodine deficiency (ID), it is relevant to investigate the biological effect of IR and ID on non-cancerous thyroid cells (5, 8, 9).

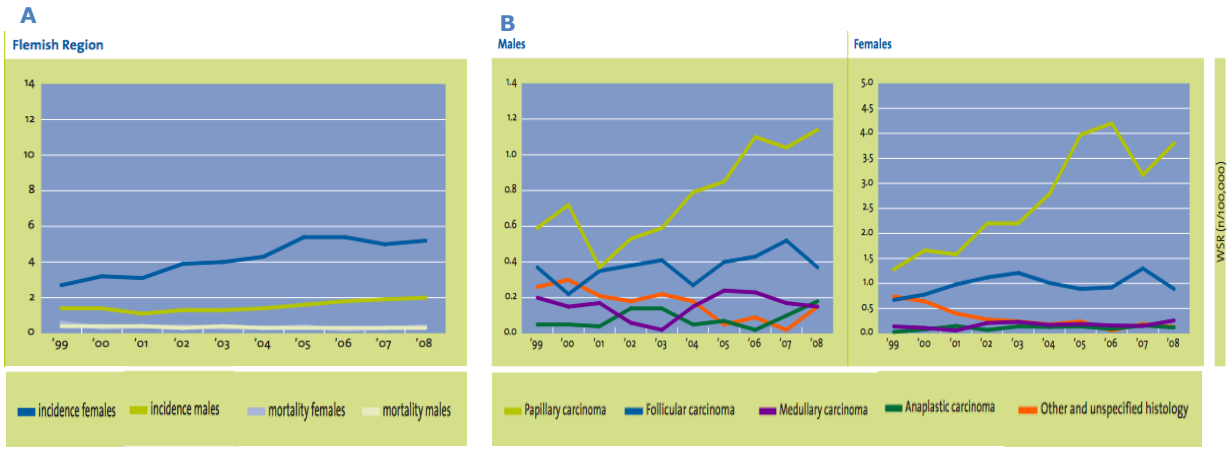

Figure 1: Thyroid cancer incidence and mortality in Belgium (Flemish region). (A) Incidence rate significantly increases in both sexes between 1999-2008 (M: p=0.00; F: p = 0,0). However, mortality decreases (M: p=0.03; F: p=0.07). **(B)** Papillary carcinoma shows a large significant increase (M: p=0.01; F: p=0.00). Other main histological subtypes increase as well, but no significant trend is observed. Due to improved registration practices, a significant decrease is observed in unspecified tumors (M: p=0.05; F: p=0.00). *Adapted from the Belgian Cancer Registry, Cancer Incidence in Belgium, 2008 (6).*

2. IMPORTANT RISK FACTORS FOR THYROID CANCER

2.1 IONIZING RADIATION

2.1.1 Biological effects of ionizing radiation

Currently, the general population is increasingly exposed to IR, originating from natural and manmade sources (10). Ionizing radiation can be classified into two major categories: electromagnetic IR including X-rays and γ-rays and particulate IR including alpha particles, beta particles, neutrons and protons. When passing through a medium, IR can interact with atoms, losing energy along its track. The average energy deposited per unit length is called linear energy transfer (LET) and indicates the efficiency of IR to cause ionizations by ejection of atomic electrons. Alpha particles, beta particles, neutrons and protons are considered as high-LET radiation inducing dense ionizations along their track. Therefore, high-LET radiation is likely to interact directly with essential cellular structures, which makes it highly destructive to biological tissues. Since high-LET radiation rapidly exhausts its energy, it has a low penetrating ability. As a result, high-LET radiation is only of major concern during internal exposure. On the other hand, electromagnetic X-rays and γ-rays are classified as low-LET radiation. The latter primarily acts indirectly through

interaction with the abundant water molecules inside the cell, which results in the generation of a variety of reactive oxygen species (ROS), including hydroxyl radicals, superoxide, singlet oxygen, and hydrogen peroxide (H_2O_2). These produced ROS are able to diffuse over a distance and will in turn interact with critical cellular components such as DNA, proteins and lipids which eventually can result in tissue damage. Low-LET radiation is sparsely ionizing and interacts only randomly along the length of its track. Therefore, low-LET radiation is able to deeply penetrate into biological tissue and is especially of concern during external exposure. The direct and indirect biological effects of IR on the DNA are of major concern since IR can lead to genetic lesions, especially double strand breaks (DSB) (11, 12). These genetic lesions can enhance the mutation rate, which is in turn considered as the underlying basis for radiation-associated carcinogenesis (13, 14). In addition, IR-induced DNA damage and ROS generation are able to induce alterations in intracellular signaling pathways involved in proliferation, survival and apoptosis.

The incidence and severity of IR-induced biological effects depends on several parameters such as the type of radiation, the exposure time, the distance to the radiation source, the type of the exposed biological tissue, the applied radiation dose, the subject's health condition and age, etc. (15). The applied radiation dose can be expressed as 'absorbed dose', measured in grays (Gy) which quantifies the energy deposited per unit mass. The energy deposition of 1 Joule/Kg equals 1 Gy. However, not all types of IR result in the same biological effect after exposure. Therefore, the 'dose equivalent' is mostly used, expressed in Sievert (Sv). The dose equivalent is the product of the absorbed dose and a radiation type-specific weighting factor. The weighting factor for X-rays is 1,0. As a result, 1 Gy is equal to 1 Sv when using X-rays for medical applications. Finally, to assess health risks of IR exposure, the 'effective dose' is used. The effective dose cannot be measured directly since it is a theoretical calculated dose. It is based on which tissues or organs are exposed to the applied radiation by using a tissue specific-weighting factor. These tissue specific-weighting factors can be changed when new research results are available (14, 16).

2.1.2 Thyroid cancer risks following exposure to high and low doses of radiation

Epidemiological studies based on Japanese atomic bomb survivors and the Chernobyl accident in 1986 provide strong evidence of a significantly increased risk of thyroid cancer after exposure to radiation doses above 100 mSv. Thyroid cancer risks are well described by a linear dose-response function and strongly depends on age of exposure (17-19). Indeed, the thyroid gland of children is more radiosensitive than of adults due to their smaller size, rapid growth and the differences in metabolic rate. Furthermore, children have a longer life expectancy than adults which increases the opportunity to develop cancer (20, 21). As a result, thyroid cancer incidence markedly increased in individuals who were exposed to IR as children or adolescents. This has especially been reported in the contaminated areas of Belarus, Ukraine and Russia as early as 4 years after the Chernobyl accident as well as by a data analysis of thyroid cancer incidence from 1958 to 2005 among members of the Life Span Study Cohort of Japanese atomic bomb survivors. Furthermore, also after the more recent Fukushima earthquake in 2011, an excess of thyroid cancer has been detected in children and adolescents who lived in the Fukushima Prefecture within 4 years of the release (22). The data related to thyroid cancer following the Fukushima earthquake need more careful investigations and cannot be ignored. After the Chernobyl accident, most cases

of thyroid cancer occurred in children who were younger than 5 years at the time of the accident, while the risk decreased sharply for adults exposed after age 20 (19, 23, 24). The Chernobyl accident mainly caused internal exposure to radioactive iodine-131 (I^{131}), caesium-137 (Cs^{137}) and strontium-90 (Sr^{90}), by-products of uranium fission, which is used for energy production in the nuclear reactor. The major contribution to radiation dose was exposure to short-lived I^{131}, which was released in large amounts into the environment and primarily accumulated in the thyroid gland after inhalation or ingestion of contaminated food and drinks. Particularly children continued to consume I^{131}-contaminated milk, leading to a median thyroid radiation dose of 0,35 Gy and maximum doses upto 2 Gy. In contrast, survivors of atomic bombing in Hiroshima and Nagasaki were mainly exposed to external radiation. However, the excess relative risks estimated by several case-control and cohort studies indicate that thyroid cancer risks after internal exposure to I^{131} are similar to the well-known risks after external radiation exposure (25-28).

Another extensive body of literature is available about the use of IR for medical diagnostic and therapeutic procedures which continues to expand rapidly as techniques further develop (29). The use of IR for therapeutic purposes involves the delivery of high, fractionated doses to specified tissue volumes of patients while minimizing the irradiation of normal healthy tissue. Conventional fractionation usually consists of daily fractions of 1.8-2 Gy, building up to a total radiation dose of 40 Gy or more dependent on the specific condition to be treated (30, 31). Several studies have linked the use of radiotherapy to treat malignant or benign head and neck conditions, including Hodgkin's disease, with an increased risk to develop secondary malignant thyroid cancer, especially among children (32-36). In contrast to the strong evidence of a linear increase in thyroid cancer risk at radiation doses higher than 100 mSv, radiation-induced cancer risk is less clear at lower doses. This is relevant for medical diagnostic exposures such as X-rays and computed tomography (CT) scans. Medical diagnostic procedures represent the most significant source of artificial exposure to IR **(Figure 2A)** (30). In addition, radiation doses are cumulative. As a result, patients undergoing multiple high-dose diagnostic procedures in a short time period could reach effective radiation doses higher than 100 mSv. Since the number of CT procedures is increasing, there is an upward trend in the contribution of CT scans to the total collective dose from medical examinations **(Figure 2B)** (16, 30, 37, 38). Furthermore, over one third of all CT scans are performed in the head and neck region, exposing the thyroid gland to IR (39). M. Mazonakis, et al. estimated the risk for thyroid cancer induction in pediatric patients undergoing head and neck CT scans. They concluded that exposure of the thyroid gland to the primary CT radiation beam resulted in a thyroid absorbed dose range of 15.2-52.0 mGy, which was related to an increased risk on cancer induction up to 390 thyroid malignancies per one million patients (40).

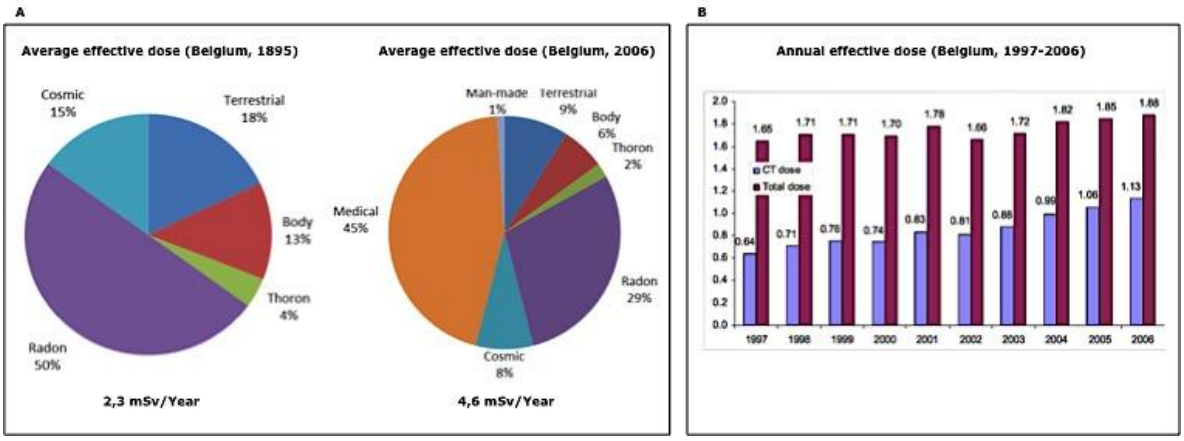

Figure 2: Contribution of medical diagnostic radiation. **(A)** Average annual effective dose (mSv) in Belgium from 1895 and 2006. **(B)** Trends in annual effective dose (in mSv per year) from diagnostic radiological examinations in Belgium (1997-2006). The large and increasing share (77%) from CT is given separately. *Adapted from Vanmarcke et al. IRPA proceedings. 2010;3(1):2216-25* (38).

It is difficult to precisely quantify the risks of low-dose IR exposure. Low-dose risks are likely to be lower compared to high-dose risks. As a result, the signal-to-noise ratio declines and the expected low number of radiation-induced thyroid cancers may be masked by the natural incidence of sporadic thyroid cancers. Therefore, to maintain sufficient statistical power, large epidemiological studies are required (41, 42). Currently, in order to estimate the risks of cancer development at intermediate and low radiation doses, the linear no-threshold (LNT) theory is used **(Supplemental Figure 2)**. This model implies a linear extrapolation of low-dose health risks from high-dose data and thereby indicates that even the lowest radiation doses increase the probability to develop cancer (14). A pooled analysis of 5 cohort studies and 2 case-control studies suggested an increased risk on thyroid cancer at a mean external radiation dose to the thyroid of 50mSv (19). In contrast, several studies believe that low-dose irradiation is stimulatory and beneficial for reproduction, immunity, and average lifespan and decreased cancer death rates (43-47). Indeed, There is still a lot of controversy about the health effects of low-dose IR.

2.2 IODINE DEFICIENCY

Normal thyroid functioning depends on the continuous supply of iodine, the key element for thyroid hormone synthesis. However, iodine is a scarce trace element in the environment and can only be acquired through the diet (48). As a consequence, ID remains a significant public health problem affecting more than 2 billion individuals worldwide (49, 50). Several epidemiological studies demonstrated an association between iodine intake and clinically evident thyroid nodules and benign goitres, occurring more frequently in iodine-deficient populations (51-54). Although nodularity and goitres may precede the development of malignant thyroid cancer, epidemiological data remain controversial about the association between ID and an increased risk to develop thyroid cancer (55-57). Defining this association in certain populations or geographical areas is challenging, since thyroid cancer is relatively rare. As a result, long study periods in large populations are required. In addition, the lag-time between changes in iodine intake and changes in thyroid cancer incidence is unclear and can take several decades (8). However, there are some ecological studies performed in different countries of Europe which describe a significant decrease

in the incidence of ATC and a shift towards more differentiated and less malignant forms of thyroid cancer after correcting ID with iodized salt (58-61). Next to epidemiological and ecological data, several early animal experiments showed an increased development of thyroid tumors, particularly of the follicular and papillary type, in female rats and mice which were fed on a low-iodine diet. Furthermore, the number and size of the thyroid tumors appeared to increase with an increased duration of ID (62-65). Similar results were found in hamsters (66).

A suggested mechanism for the effects of ID is the chronic elevated release of the thyroid-stimulating hormone (TSH) by the pituitary gland as part of the regulating hypothalamus-pituitary-thyroid axis. Short-term actions of TSH include the induction of gene expression and protein synthesis involved in iodine trapping and thyroid hormone production. In addition, TSH promotes the release of thyroid hormones from the thyroid gland. Sustained TSH stimulation due to chronic ID results in hypertrophy and hyperplasia of the follicular thyroid cells combined with an extension of the thyroid vascular network and an increased thyroid blood flow (1). Abdul A. Al-Saadi et al. demonstrated that the development of ID-induced thyroid hyperplasia is associated with chromosomal abnormalities and an increased number of aneuploid rat thyroid cells with an increased duration of ID (67). However, beyond the well-known effects of this delayed phase of increased TSH levels in cases of severe and prolonged ID, thyrocytes are also able to rapidly react to acute mild and moderate decreases in iodine supply without TSH involvement. This early TSH-independent phase is characterised by endothelial cell proliferation and pericyte activation resulting in adaptation of the local microvasculature, an increased blood flow and an enhanced iodine uptake from the blood (68). It has already been demonstrated that an acute intracellular iodine deprivation in thyrocytes induces a rapid and massive production of intracellular ROS, which in turn stabilize hypoxia inducible factor (HIF)-1α. Subsequently, HIF-1 binds to the hypoxia-response element (HRE) site in the promoter region of the vascular endothelial growth factor-A (VEGF-A) gene, stimulating VEGF-A protein synthesis and release (68, 69). Furthermore, J. Craps, et al. (2015) showed that ID activates ryanodine receptors (RYRs) located in the endoplasmic reticulum, leading to intracellular Ca^{2+} release, which in turn phosphorylates and activates nitrogen oxide synthase 3 (NOS3). Subsequently, activated NOS3 produces nitrogen oxide (NO), a reactive nitrogen species with well-known vasodilatory properties, which can induce VEGF synthesis through the activation of the HIF-1/VEGF-A pathway **(Supplemental Figure 3)** (70).

Besides the role of iodine in thyroid functioning, iodine is also involved in other, extra-thyroidal organs, particularly in the stomach and mammary gland. The stomach and the thyroid gland share many morphological and functional similarities, including the capacity to concentrate iodine from the blood by means of the sodium/iodide symporter (NIS). This is probably due to the common embryonic origin of both organs. On the other hand, the mammary gland is highly effective in capturing iodine from the blood during pregnancy and lactation to provide the neonate with sufficient levels of iodine. Then the neonate can produce its own thyroid hormones, which is essential for normal neural development. Several studies reported that iodine deficiency constitutes a risk factor for gastric cancer and breast cancer (71-74). It has been suggested that iodine is a potent antioxidant, which acts as an electron donor, neutralizing free radicals such as H_2O_2 and hydroxyl radicals. Furthermore, iodine inhibits lipid peroxidation and reduces the reactivity of cellular biomolecules with ROS by means of iodination. As a result, iodine protects cells against

damage from oxidative stress. In addition, anti-proliferative, apoptotic and differentiation-promoting effects of iodine have also been observed in several tumor cell lines. These results support that iodine has a protective role against cancer development (75). However, it should be mentioned that an excess of iodine should be avoided as well since iodine excess is also associated with thyroid anomalies such as thyroiditis, hyperthyroidism, hypothyroidism and even thyroid cancer (76).

3. THE COMBINED EFFECT OF IONIZING RADIATION AND IODINE DEFICIENCY ON THE THYROID

Following the Chernobyl accident, it is suggested that ID is a co-factor, which could modify the effects of IR on the thyroid gland. The radioactive isotope I^{131} was the chief component of the accident fallout. Iodine-deficient thyroid glands have a stronger uptake of radioiodine, leading to higher thyroid radiation doses, combined with the continuing effects of ID which may impact the progression of thyroid cancer development (27). Several epidemiological studies focusing on the Chernobyl accident and the link with thyroid cancer indicated that thyroid cancer incidence, especially in children, was higher in territories with severe iodine deficiency than in areas of normal iodine intake (77, 78). These findings suggest that low-iodine diets could potentiate the risk to develop radiation-induced thyroid cancer and that elimination of ID may be important in reducing the effects of radiation exposure on the thyroid (79). Furthermore, Cardis E, et al. even observed a three-fold reduction in thyroid cancer risk among children taking iodine supplements months after exposure to the radioactive fallout from the Chernobyl accident compared to children without iodine supplementation. It is speculated that continuous administration of iodine supplements reduces the size of the thyroid gland, which leads to less cellular proliferation and thus a reduced thyroid cancer risk. Prophylaxis with iodine supplementation could be a favorable approach after exposure to radioactive iodine (78, 79). However, this is more questionable after external thyroid radiation exposure. In a long-term *in vivo* study of Carsten Boltze, et al. it was demonstrated that a low-iodine intake significantly increase the proliferation rate of the thyroid cells and induced thyroid adenomas in rats. However, no malignancies were detected after 110 weeks. When rats were irradiated with an acute exposure of 4 Gy, they observed a significant destruction of the thyroid follicular structure. However, rats under normal iodine supply developed no thyroid malignancies. In contrast, thyroid cancer was detected in rats with ID (80). These results support the idea that ID is an effective tumor promoter, which can enhance thyroid cancer development when a carcinogenic factor like IR is present (8, 80, 81). Therefore, it is interesting to investigate a potential additional effect of the enhanced stress induced by ID and IR on the molecular level of thyroid cells.

4. POSSIBLE MOLECULAR MECHANISMS INDUCED BY IONIZING RADIATION AND IODINE DEFICIENCY IN THE THYROID

4.1. OXIDATIVE STRESS AND THYROID CANCER

As described above, both IR and ID are stress factors for thyroid cells due to the increased generation of reactive oxygen species. Under physiological conditions, ROS are produced in low levels as part of normal cellular biochemical processes such as the defense system against

infectious agents and intracellular signaling. Furthermore, thyroid epithelial cells produce a moderate amount of H_2O_2, which is a co-substrate required for thyroid hormone synthesis. The generated ROS are continuously detoxified during the process of hormone synthesis or by endogenous antioxidant systems including enzymes such as catalase, glutathione peroxidase and peroxiredoxins (82). However, in case of excessive ROS accumulation, ROS levels may exceed the cellular antioxidant defense mechanisms causing oxidative stress, which can result in damage to DNA, proteins and lipids. Oxidative stress and elevated levels of ROS have been considered to be involved in the pathophysiology of many cancers, including thyroid carcinogenesis (83). Several studies already demonstrated an increased generation of ROS and an impairment of the antioxidant system in patients with hyperthyroidism, hypothyroidism and thyroiditis (82, 84-87). Interestingly, Dong Wang, et al. found a stronger association between oxidative stress and thyroid cancer compared to other thyroid disorders. They assessed the total oxidant and antioxidant status and calculated the oxidative stress index of 82 patients who were recently diagnoses with thyroid cancer. The total oxidative status and oxidative stress index were significantly higher, and the total antioxidant status was significantly lower in patients with thyroid cancer compared to healthy controls and patients with benign thyroid diseases (88). These results support the role of oxidative stress in the pathogenesis of thyroid disorders, including thyroid cancer.

4.2 DNA DAMAGE RESPONSE

Ionizing radiation damages DNA through direct ionization but more frequently through indirect actions of water radiolysis. Therefore, it is assumed that the extent of DNA damage is proportional to the received radiation dose. IR-induced DNA damage constitutes a broad range of lesions including single-and double-strand breakages, base modifications, deoxyribose modifications, intra-and inter-DNA cross-linking and promoted DNA-protein cross-linking. These damages overlap substantially with DNA lesions induced by oxidative stress, which can be generated by IR and ID. Therefore, the DNA damage response in thyroid cells could increase when IR and ID are combined, due to the enhanced production of reactive oxygen species. The most deleterious lesion is the DSB (14). Several studies provided data supporting a linear relationship between DSB induction and increasing radiation dose in cultured cells starting from 1 mGy as well as *in vivo* starting from 100 mGy (10, 89, 90). DSBs can be detected by the phosphorylation of the histone variant H2AX (γH2AX). H2AX is a component of the histone octomer in nucleosomes, which compact DNA into chromatin (91). DSBs initiate the phosphorylation of H2AX by ATM and ATR kinases, which are part of the PI3K/AKT pathway. Subsequently, γH2AX is crucial in recruiting and localizing DNA repair proteins and will be dephosphorylated as DNA repair completes. γH2AX foci together with 53BP1 foci are good biomarkers for DSBs (10, 91). To protect the cell against the deleterious effects of DNA damage and to maintain genomic stability, a network of DNA damage response (DDR) pathways are triggered, resulting in several different outcomes **(Supplemental Figure 4)**. DNA damage activates checkpoint pathways, which inhibit the normal progression through the cell cycle. Cell cycle arrest mostly occurs in the G1 or G2 phase so the cell can cope with the induced damage by facilitating repair processes. Besides H2AX, activated ATM phosphorylates several other key proteins of the global DDR such as the tumor suppressor proteins p53 and BRCA1, the negative regulator of P53 MDM2, the checkpoint kinases CHK1 and CHK2, the

regulator of damage-induced cell cycle arrest checkpoints MDC1, and the DNA repair protein NBS1 which is recruited to DSBs in complex with MRE11/RAD50 by direct binding to γH2AX. These events promote cell cycle arrest, chromatin remodeling and up-regulation of DNA repair (14, 92, 93). When the extent of DNA damage is too large, damaged cells will be eliminated by induction of apoptosis, in which p53 plays an important role in the regulation of this process. Conversely, failure of the cell cycle checkpoints or inefficient DNA repair in cells may lead to accumulation of genetic damage and genomic instability. In particular DSBs can lead to genetic mutation which play an important role in the process of carcinogenesis in humans. In addition, IR-induced DNA lesions typically occur in clusters, increasing the complexity. This may compromise DNA repair and contribute to cancer risk (14, 94).

4.3 ALTERED SIGNALING PATHWAYS

There is still a limited understanding about the effects and molecular mechanisms of IR-and ROS-induced alterations in signaling pathways. For instance, the duration of activation of kinases - transient or persistent - may lead to a different decisive outcome in regard to proliferation, cell cycle arrest or cell death (95). Deregulation of these key pathways controlling cellular proliferation and survival together with a suppressed apoptosis constitute the minimal underlying platform for neoplastic evolution and are part of the hallmarks of cancer cells (96). DNA damage, IR and oxidative stress are reported to alter these cellular responses and signaling transduction pathways such as the MAPK/ERK, PI3K/AKT, NFκB and the JAK/STAT pathways (97). These signaling pathways may be more strongly modified in thyroid cells when they are affected by a combination of IR and ID due to enhanced oxidative stress.

4.3.1 PI3K/AKT pathway

The PI3K/AKT signaling pathway is a cytoprotective response with anti-apoptotic effects, downstream of the EGFR family receptors **(Supplemental Figure 5)**. It is reported that cellular exposure to low-dose IR (0,1 Gy) may promote PI3K/AKT signaling by rapid activation of transcription factors and tyrosine kinases (98). In addition, reactive oxygen species induced by IR and ID can function as intracellular messenger molecules. In particular H_2O_2 is able to induce AKT phosphorylation at the Ser473 and Thr308 residues by inhibiting the activity of PTEN. This dually phosphorylated, active AKT protein is then able to directly phosphorylate and inactivate the pro-apoptotic BAD protein, which controls the release of cytochrome c from mitochondria. In addition, AKT also controls apoptosis through indirect inhibition of pro-apoptotic gene expression and increasing expression of anti-apoptotic genes by phosphorylation of various transcription factors. Interestingly, AKT also indirectly regulates p53. Indeed, AKT specifically phosphorylates the MDM2 protein, an important negative regulator of p53, promoting its translocation to the nucleus and targeting p53 for degradation. As a result, AKT impairs the cellular stress response and thereby increases cellular survival. In addition, the PI3K/AKT pathway cross-talks with the NFκB pathway by phosphorylating and activating IκB kinase α (IKKα), which in turn pshorphorylates IκB, targeting it for degradation. This leads to the nuclear translocation and activation of NFκB, inducing expression of NFκB-dependent pro-survival genes, such as the anti-apoptotic proteins BCL-XL, BCL-2 and Mcl-1 as well as caspase inhibitor proteins. Furthermore, cross-talk between PI3K/AKT

pathway and the MAPK/ERK pathway is reported in which AKT co-operates with ERKs to shift the apoptotic threshold in cells to higher inputs by both inactivating BAD. In addition, AKT inhibits the cytotoxic-activation of the non-classical JNK pathway. Besides the anti-apoptotic effects, activated AKT is also able to modulate the function of various substrates, which play a role in the regulation of cell cycle progression, such as GSK-3, mTOR, TSC2 and the cyclin-dependent kinase inhibitors p21 and P27. The PI3K/AKT pathway is frequently disrupted in human cancers and is a major contributor to tumor radio-resistance (99, 100). Therefore, it is of interest to investigate the combined effect of IR and ID on the PI3K/AKT pathway in non-cancerous rat thyroid cells.

4.3.2 NFκB pathway

NFκB is able to activate a wide variety of genes, which are involved in the regulation of stress responses, inflammation and apoptosis **(Supplemental Figure 6)**. The NFκB family comprises five members: RelA (p65), RelB, c-REL, p50/p105 (NFκB1) and p52/p100 (NFκB2). Activated NFκB typically occurs as a dimeric protein, which possesses both a DNA binding domain and a transactivation domain. Different combinations of homo-and heterodimers can be formed to modulate the intrinsic properties of NFκB and its regulation. However, p50/p65 is the most abundant heterodimer (101). Under non-stimulated conditions, the activity of the NFκB complex is suppressed by binding to members of the NFκB inhibitors (the IκB family), which sterically hinder the NFκB nuclear translocation sequence, and thereby causing NFκB cytoplasmic retention (101, 102). IκB phosphorylation is the key event in NFκB activation and is catalyzed by the IKK complex. IR is able to induce NFκB activation by directly damaging the DNA, causing DSBs and SSBs. The damaged DNA activates nuclear ATM, which in turn regulates IKK activity. On the other hand, ROS generated by IR as well as ID in thyroid cells not only induce DNA damage but also activate NFκB via the TRAFs pathway. Furthermore, IR and ROS induce the release of cytokines such as TNFα and IL-1, which also stimulates the activation of NFκB. Phosphorylation of the IκB proteins by activated IKK leads to rapid IκB degradation, allowing the NFκB complex to translocate to the nucleus where it regulates the transcription of various genes (101). Expression of the NFκB effector genes, which include both anti-apoptotic and cell cycle elements, is required for an enhanced cellular survival to allow stressed cells to repair their damaged DNA. NFκB regulates the cell cycle by promoting expression of cyclin D1 and B1, which is required for cell cycle progression through the G1/S phase and G2/M phase transition respectively. In combination with the expression of anti-apoptotic genes such as Bcl-2, Bcl-XL and inhibitors of apoptosis proteins (IAPs), sustained activation of NFκB could permit cells with accumulated DNA damage to proliferate and to escape apoptosis, increasing the risk on malignant transformation (101, 103). Elevated levels of NFκB activation has been linked to increased radio-resistance of tumor cells. Furthermore, activation of NFκB has been demonstrated following high and low doses of IR (104, 105). Therefore, modulations of the NFκB pathway will be investigated in thyroid cells treated with different doses of IR combined with ID.

4.3.3 JAK/STAT pathway

The JAK/STAT pathway mediates signaling transduction via cytokine and growth factor receptors. Upon receptor stimulation, activated JAK phosphorylates and thereby activates the latent, cytoplasmic members of the STAT proteins **(Supplemental Figure 7)**. STAT3 is a critical

factor in the JAK/STAT pathway and has been acknowledged as a prominent oncogenic protein. The major mechanism of STAT3 activation is mediated by the IL-6/IL-6R/gp-130 signaling which leads to the activation of JAKs. In turn, JAKs induce phosphorylation of STAT3, which then forms homo- or hetero dimers. In this activated form, STAT3 translocates to the nucleus where it regulates the expression of various target genes involved in cellular survival, proliferation, differentiation, invasion and angiogenesis (106-108). On the other hand, unphosphorylated STAT3 is also able to regulate gene expression in complex with NFκB, in which STAT3 enables nuclear translocation, while NFκB provides DNA binding and transactivation domains (108). It has been demonstrated that STAT3 and its phosphorylated form, pSTAT3, was present in low levels in benign thyroid disorders, while it was ubiquitous in PTC and in lymph nodes of patients with lymphatic thyroid cancer metastases. These findings suggest that a constitutive activated JAK/STAT3 pathway is involved in the development, progression, and metastasis of thyroid cancer (109). IR and ROS can lead to the activation of STAT3. Furthermore blockage of STAT3 signaling using JAK inhibitors was able to abrogate radiation-induced malignant progression of glioma cells (110). Preliminary data demonstrated that the protein expression level of pSTAT3/STAT3 was significantly increased in rat FRTL5 thyroid cells exposed to a radiation dose of 3 Gy combined with ID as compared to iodine-sufficient, rat FRTL5 thyroid cells solely exposed to a radiation dose of 3 Gy. Therefore, it is of interest to monitor the changes in STAT3 and pSTAT3 protein expression levels in rat PCCL3 thyroid cells treated with ID and low-dose IR and compare them to the available preliminary data in rat FRTL5 cells.

5. RESEARCH PLAN

The main goal of this research was to monitor the basic cellular and molecular responses of thyrocytes to ID and low-dose IR. Since both ID and IR are important stress factors for the thyroid gland, we hypothesized that ID and low-dose IR would both stress thyrocytes due to an enhanced production of reactive oxygen species, which would eventually affect cellular proliferation, survival and resistance to apoptosis. In order to investigate this, non-cancerous rat PCCL3 cells were cultured under the presence or absence of a physiological level of sodium iodide (10^{-8}M NaI). The latter created iodine-deficient thyrocytes. In each condition, thyrocytes were subdivided in different groups depending on the X-ray radiation dose they received, i.e. the sham-irradiated cells which were used as controls, the low-dose irradiated cells (0,05 Gy and 0,1 Gy), the intermediate-dose irradiated cells (0,5 Gy) and the high-dose irradiated cells (3 Gy) **(Supplemental Figure 8)**. We investigated changes in gene expression and the modulations on protein levels using quantitative RT-PCR and Western blot respectively. We focused especially on genes and proteins involved in signaling pathways important for cellular survival, proliferation, DNA repair and antioxidant defense. The extent of DNA damage, more specifically DSBs, was visualized with γH2AX fluorescent staining. On the other hand, apoptosis of thyroid cells and their cell cycle profile was measured by means of a TUNEL assay and a 7-AAD/BrdU assay respectively flow cytometry. Finally, the cellular redox state was assessed under the fluorescence microscope using the cell-permeable, non-fluorescent CM-H_2DCFDA probe.

1. CELL CULTURE AND IRRADIATION

Rat PCCL3 thyroid cells were a gift from Professor F. Miot (Université Libre de Bruxelles, institute de Recherche Interdisciplinaire en Biologie Humaine et Moléculaire, Brussels, Belgium). PCCL3 cells were cultured in Coon's modified Ham's F12 medium (Life Technologies, Merelbeke, Belgium) supplemented with 5% fetal bovine serum (FBS) (Gibco, Ghent, Belgium), 2.4 mM glutamine (Sigma-Aldrich, Diegem, Belgium), 1mU/mL TSH (Sigma-Aldrich, Diegem, Belgium), 100 U/mL penicillin-streptomycin (Invitrogen, Ninove, Belgium), 2.5 µg/mL Fungizone (Invitrogen, Ninove, Belgium), 1 µg/mL insulin (Sigma-Aldrich, Diegem, Belgium) and 5 µg/mL transferrin (Sigma-Aldrich, Diegem, Belgium) in a humidified atmosphere of 37°C and 5% CO_2 **(Supplemental Figure 9)**. At least seven days before the start of the experiments, the cells were grown in fresh media containing a physiological concentration of 10^{-8}M NaI. On the day of the experiment, the culture media were removed, cells were washed with 1x PBS (Gibco, Ghent, Belgium) and fresh media were added, containing or lacking NaI to create iodine-sufficient or iodine-deficient thyroid cells respectively. Following media replacement, the cells were irradiated with low (0.05 Gy and 0.1 Gy), intermediate (0.5 Gy) or high (3 Gy) radiation doses at a dose rate of 8.5 Gy/hour using the Xstrahl 320 kV generator. Non-exposed control cells were sham-irradiated. The cells were then returned to the humidified incubator until the start of the experiments.

2. RNA ISOLATION AND REVERSE TRANSCRIPTION

Three days before induction of ID and irradiation, cells were seeded in five 6-well plates at a density of 2 x 10^5 cells/well for cell lysis 6 and 24 hours after induction of ID, and 1.5 x 10^5 cells/well for cell lysis 24 hours after ID and irradiation. Each 6-well plate corresponded to a single radiation dose and comprised three biological replicates of iodine-sufficient thyroid cells and three biological replicates of iodine-deficient thyroid cells. The cells were washed twice with 1x PBS and lysed in 350 µl of RNeasy Lysis Buffer Plus from the Qiagen RNeasy Plus Mini Kit (Qiagen, Antwerp, Belgium). Then, total RNA was purified according to the manufacturer's instructions and resuspended in 30 µl of nuclease-free water. RNA quantification and RNA quality control was assessed using the DropSense 16 spectrometer (Trinean, Ghentbrugge, Belgium) and the RNA integrity number (RIN) number (Agilent's lab-on-chip Bioanalyzer 2100, Agilent Technologies, Diegem, Belgium) respectively. Subsequently, one microgram of total extracted RNA was reversed transcribed to first-strand cDNA by using the GoScript Reverse Transcription System (Promega, Leiden, The Netherlands) according to the manufacturer's instructions. Briefly, 1 µg of total RNA was mixed with 0.5 µg of random primers and 0.5 µg of oligo$(dT)_{15}$ primers, thermally denatured at 70°C for 5 minutes, and chilled on ice for 5 minutes. Subsequently, GoScript 5X reaction buffer, 1.5 mM $MgCl_2$, the PCR nucleotide mix (0.5 mM of each dNTP), the recombinant RNasin ribonuclease inhibitor and the GoScript reverse transcriptase were added. This final mixture was

incubated at 25°C for 5 minutes to allow primer annealing, at 42°C for 60 minutes to allow first-strand cDNA synthesis and finally at 70°C for 15 minutes to inactivate reverse transcriptase. The obtained cDNA samples were then stored at -20°C until their use in quantitative PCR.

3. WESTERN BLOT ANALYSIS

Three days before induction of ID and irradiation, cells were plated in 75-cm^2 tissue culture flasks at a density of 2 x 10^6 cells/flask. We included three biological replicates per condition. Six hours after ID and irradiation, cells were collected by trypsinization (0.05% Trypsin-EDTA) and the cell pellet was frozen at -80°C until protein extractions. Proteins were isolated from the PCCL3 cells using Bio-Rad's ReadyPrep II including 8M urea, 4% CHAPS, 40 mM Tris and 0.2% Bio-Lyte 3/10 ampholyte (Bio-Rad, Temse, Belgium) supplemented with ½ cOmplete™ Mini Protease Inhibitor Cocktail Tablet (Roche Diagnostics, Brussels, Belgium) and 1% tributyl phosphate (TBP) (Sigma-Aldrich, Diegem, Belgium). Thryoid cells were suspended in 100 µl of the extraction buffer and homogenized by means of 1.4 mm ceramic beads (Labconsult, Brussels, Belgium) and the TissueLyser II (Qiagen, Antwerp, Belgium). Subsequently, the protein samples were quantified, using the bicinchoninic acid (BCA) protein assay kit (Sigma-Aldrich, Diegem, Belgium) according to the manufacturer's instructions with standard protein solutions of 0.125 mg/mL, 0.25 mg/mL, 0.5 mg/mL, 0.75 mg/mL, 1 mg/mL, 1.5 mg/mL and 2 mg/mL (Bio-Rad, Temse, Belgium). Absorbance of the Cu-BCA chelate formed in the presence of protein was measured at 562 nm and normalized at 750nm by means of the Nanodrop spectrophotometer (Thermo Scientific, Ghent, Belgium). Twenty µg of the sample proteins were mixed with 4X Laemmli buffer (25% of the total volume) (Bio-Rad, Temse, Belgium), Beta-Mercapto-ethanol (Sigma-Aldrich, Diegem, Belgium) (2.5% of the total volume) and MilliQ to get a final volume of 20 µl. Samples were heated at 95°C for 5 minutes and were separated by a horizontal 15-well 10% (Amersham ECL™ Gel, GE healthcare Life Sciences, Diegem, Belgium) or a vertical 26-well 4-15% (TGX Stain-free Precast Protein Gel, Bio-Rad, Temse, Belgium) sodium-dodecyl-sulfate (SDS) polyacrylamide gel at 160V for 60 minutes or at 300V for 25 minutes respectively. Then, proteins were transferred onto a nitrocellulose membrane using the iBlot dry gel transfer system (Invitrogen, Ninove, Belgium) for the horizontal 15-well western blot and the Trans-Blot Turbo Transfer System (Bio-Rad, Temse, Belgium) for the vertical 26-well western blot. Membranes were blocked for 1 hour at room temperature in blocking buffer (WesternDot™ blocking buffer, component A of the WesternDot™ 625 Western Blot Kit or SuperBlock™ Blocking buffer, Invitrogen, Ninove, Belgium). Then, membranes were incubated with the primary antibody diluted in blocking buffer at 4°C overnight **(Table 1)** and washed three times for 5 minutes in 1X washing buffer (0.05M Tris-HCl, 0.15M NaCl, 0.05% Tween 20, pH 7.4; Component B of the WesternDot™ 625 Western Blot Kit, Invitrogen, Ninove, Belgium). Subsequently, a biotinylated secondary antibody (Component C of the WesternDot™ 625 Western Blot Kit, Invitrogen, Ninove, Belgium), 1/4000 times diluted in 1X washing buffer **(Table 1)**, was added and incubated for 1 hour at room temperature, followed by three times 5 minutes of washing. The antibody complexes were visualized using QDot® 625 streptavidin conjugates (Component D of the WesternDot™ 625 Western Blot Kit, Invitrogen, Ninove, Belgium), 1/4000 times diluted in blocking buffer and incubated for 1 hour at room temperature. After three times 5

minutes of washing, protein bands were detected by exposing the membranes to UV-light by means of the Fusion FX Imager (Vilber Lourmat, Eberhardzell, Germany). Protein bands were quantified by densitometry using the Bio1D analysis software (Vilber Lourmat, Eberhardzell, Germany). In order to verify equal loading, the protein levels were normalized against the level of the housekeeping proteins ß-actin or viniculin, which were always probed on the same membrane of the proteins of interest.

Table 1: Characteristics of the used primary antibodies for Western blot.

Primary antibody	**Host species**	**Supplier**	**Clonality**	**Dilution**
Akt1 (B-1) (sc-5298)	Mouse	Santa Cruz	Monoclonal	1/500
B-actin (C4) (sc-47778)	Mouse	Santa Cruz	Monoclonal	1/2000
Catalase (H-300) sc-50508	Rabbit	Santa Cruz	Polyclonal	1/500
eNOS/NOS Type III (610296)	Mouse	BD Biosciences	Monoclonal	1/800
HIF-1α (MAB1536)	Mouse	R&D Systems	Monoclonal	1/800
NFκB p52 (K-27) (sc-298)	Rabbit	Santa Cruz	Polyclonal	1/1000
p-Akt1 (Thr308) (sc-135650)	Rabbit	Santa Cruz	Polyclonal	1/500
p-eNOS (S1177) (9571S)	Rabbit	Cell Signaling	Polyclonal	1/800
p-STAT3 (B-7) (sc-8059)	Mouse	Santa Cruz	Monoclonal	1/800, 1/1000
p-STAT3 (Y705) (9145P)	Rabbit	Cell Signaling	Monoclonal	1/800
STAT3 (C-20) (sc-482)	Rabbit	Santa Cruz	Polyclonal	1/800
Viniculin (7F9) (sc- 73614)	Mouse	Santa Cruz	Monoclonal	1/2000
Secondary antibody	**Host species**	**Supplier**	**Clonality**	**Dilution**
Biotin XX anti-rabbit	Goat	Invitrogen	Polyclonal	1/4000
Biotin XX anti-mouse	Goat	Invitrogen	Polyclonal	1/4000

4. ROS ASSAY

One day before induction of ID and irradiation, cells were seeded in transparent bottom 96-well plates with dark rims at a density of 1 x 10^3 cells/well. Each 96-well plate corresponded to a single dose and comprised 12 biological replicates of iodine-sufficient thyroid cells and 12 replicates of iodine-deficient thyroid cells. 24 hours after ID and irradiation, culture media were removed and cells were washed twice in 37°C-preheated HEPES-buffered Hank's balanced salt solution (HB-HBSS; Thermo Scientific, Ghent, Belgium, 1X HBSS + Ca^{2+} + Mg^{2+} + 20 mM HEPES, pH: 7.2). Then, to detect general intracellular ROS levels, the cells were incubated for 25 minutes at room temperature and protected from light with a staining solution containing a final concentration of 2 µM CM-H_2DCFDA (Thermo Scientific, Ghent, Belgium) dissolved in DMSO after a 1/500 dilution in HB-HBSS buffer. After washing the cells twice in HB-HBSS, the cells were imaged using the inverted fluorescence Nikon Eclipse Ti microscope. The CM-H_2DCFDA signal was detected under the Green Fluorescent Protein (GFP) channel. Exposure time and gain were optimized and kept constant among all experimental groups during the imaging procedures. The fluorescent signal was quantified and analyzed using a macro developed by Drs. Winnok de Vos and Tom Sieprath from UGhent.

5. YH2AX/53BP1 IMMUNOFLUORESCENCE STAINING

One day before induction of ID and irradiation, cells were plated in 8-well lab-teks (Thermo scientific, Ghent, Belgium) at a density of 5 x 10^4 cells/well. Each labtek corresponded to a single dose and comprised three biological replicates of iodine-sufficient thyroid cells and three biological replicates of iodine-deficient thyroid cells. 30 minutes, 1 hour, 4 hours and 24 hours after ID and irradiation, culture media were removed and cells were washed in 1X PBS before fixation in 2% paraformaldeyhde (PFA) (Life Technologies, Merelbeke, Belgium) for 15 minutes at room temperature. Then, cells were washed twice and permeabilized by incubation in 1X PBS containing 0.25% Triton-X for 3 minutes at room temperature. After two washing periods of 15 minutes, cells were blocked in pre-immunized goat serum (Invitrogen, Ninove, Belgium), diluted 1/5 times in TNB blocking buffer (0.5% w/v blocking reagent in 1X TBS-0.05%Tween, Perkin Elmer, Zaventem, Belgium), for 1 hour at room temperature. This was followed by incubation with primary mouse monoclonal anti-γH2AX antibody (Millipore, Overijse, Belgium) and rabbit polyclonal anti-53BP1 antibody (Novus Biologicals, Abingdon, UK), respectively 1/300 times and 1/1000 times diluted in TNB blocking buffer, for 1 hour at 37°C. After two washing periods of 15 minutes, cells were incubated with Alexa fluor 488-labeled secondary goat anti-mouse antibody and Alexa fluor 568-labeled secondary goat anti-rabbit antibody (Life Technologies, Merelbeke, Belgium), respectively 1/300 times and 1/1000 times diluted in TNB blocking buffer containing 4',6-diamidino-2-phenylindole (DAPI) (Sigma-Aldrich, Diegem, Belgium), for 1 hour at 37°C and protected from light. Following two washing periods of 15 minutes, glass coverslips were mounted using ProLong Diamond Antifade mountant with DAPI (Invitrogen, Ninove, Belgium) which was dried overnight at 4°C. Up to 150 to 250 cells/well were visualized and captured using the inverted fluorescence Nikon Eclipse Ti microscope. The laser exposure time and gain were optimized and kept constant among all experimental groups. γH2AX foci were analyzed using a macro developed by Drs. Winnok de Vos from UGhent.

6. CELL CYCLE ANALYSIS

Two days before induction of ID and irradiation, cells were seeded in 25-cm^2 culture flasks at a density of 5 x 10^5 cells/flask. We included three biological replicates per condition. Five, 23 hours and 47 hours after ID and irradiation, 10 µM of BrdU (Thermo Scientific, Gent, Belgium) was added to the culture media for 1 hour. Then, cells were harvested by trypsinization (0.05% trypsin-EDTA) and fixed in ice-cold ethanol with a final concentration of 70%. After centrifuging the cells at 500g for 5 minutes, acidic antigen recovery was achieved by treating the cells with 2M HCl for 30 minutes at room temperature, followed by washing twice with 1X PFT buffer (1X PBS supplemented with 5% FBS and 0.25% Triton X-100). Subsequently, cells were blocked with 1X PFT buffer for 1 hour at room temperature and were incubated with the primary rat monoclonal anti-BrdU antibody (AbD Serotec, Bio-Rad, Temse, Belgium), 1/300 times diluted in 1X PFT buffer, overnight at 4°C, protected from light. After washing twice with 1X PFT buffer, cells were incubated with Alexa fluor 488-labeled secondary goat anti-rat antibody (Life Technologies, Merelbeke, Belgium), 1/200 times diluted in 1X PFT buffer, for two hours at room temperature, followed by washing twice with 1X PFT

buffer. Then, cells were resuspended in 10 µg/mL 7-amino-actinomycin D (7-AAD) (Sigma-Aldrich, Diegem, Belgium) in 1X PFT buffer for 15 minutes at room temperature and were applied on a 5 mL Falcon Polystyrene tube with a cell-strainer snap cap (Corning Science, Wiesbaden, Germany) for centrifugation at 500G for 2 minutes. The samples were stored on ice, protected from light, and were analyzed using the Becton Dickinson Accuri C6 flow cytometer (BD Biosciences, Erembodegem, Belgium). First, singlet cells were identified according to their forward scatter and their fluorescence area to height ratio. Then, gates were set to identify the cells in the G1 phase, the G2/M phase and the S phase which were expressed as percentage of the total cell number acquired.

7. TUNEL ASSAY

One day before induction of ID and irradiation, cells were seeded in 25-cm^2 culture flasks at a density of 4 x 10^5 cells/flask. We included three biological replicates per condition. 48 hours after ID and irradiation, cells were harvested by trypsinization (0.05% trypsin-EDTA) and fixed in ice-cold ethanol with a final concentration of 70%. After centrifuging the cells at 500g for 5 minutes and removal of ethanol, cells were washed in 1X PFT buffer (1x PBS supplemented with 5% FBS and 0.25% Triton X-100). Then, positive control samples were treated with DNase 1 (Qiagen, Antwerp, Belgium) in DNase 1 buffer solution (50 nM Tris-HCl pH 7.5, 1 mg/ml BSA) for 10 minutes at room temperature to induce DNA strand breaks. Negative control samples were incubated in DNase 1 buffer solution lacking DNase 1. After incubation, control cells were washed in 1X PFT buffer. Subsequently, all sample pellets were resuspended in 50 µl of 20% TdT 5X reaction buffer (125 mM Tris-HCl, 1 M Sodium Cacodylate, 1.25 mg/ml BSA, pH 6.6, Roche Diagnostics, Brussels, Belgium), 4% BrdUTP stock solution (2 mM Br-dUTP in 50 mM Tris-HCl, pH 7.5, Sigma-Aldrich, Diegem, Belgium), 1% TdT in TdT storage solution (4% TdT in 60 mM K-phophate, 150 nM KCl, 1 mM 2-Mercaptoethanol, 0.5% Triton X-100, 50% glycerol, Roche Diagnostics, Brussels, Belgium), 4% 25 mM cobalt chloride stock solution (Roche Diagnostics, Brussels, Belgium), and 71% distilled H_2O for 60 minutes at 37°C. After washing with 1X PFT, the cell pellets were incubated with the primary rat monoclonal anti-BrdU antibody (AbD Serotec, Bio-Rad, Temse, Belgium) and the primary rabbit monoclonal anti-cleaved caspase 3 (Asp175) antibody (Cell Signaling, Leiden, The Netherlands), both 1/300 times diluted in 1X PFT buffer, overnight at 4°C, protected from light. After washing twice with 1X PFT buffer, cells were incubated with Alexa fluor 488-labeled secondary goat anti-rat antibody (Life Technologies, Merelbeke, Belgium) and Alexa fluor 568-labeled secondary goat anti-rabbit antibody (Life Technologies, Merelbeke, Belgium), both 1/200 times diluted in 1X PFT buffer, for two hours at room temperature. Subsequently, cells were washed twice with 1X PFT buffer and were applied on a 5 mL Falcon Polystyrene tube with a cell-strainer snap cap (Corning Science, Wiesbaden, Germany) for centrifugation at 500G for 2 minutes. The samples were stored on ice, protected from light, and were analyzed using the Becton Dickinson Accuri C6 flow cytometer (BD Biosciences, Erembodegem, Belgium).

8. STATISTICAL ANALYSIS

GraphPad Prism 5.01 was used to perform statistical analysis of the results. All experiments included at least three biological replicates. Therefore, results are presented as mean ± Standard deviation (SD). To test for significant differences between iodine-sufficient and iodine-deficient conditions and among different radiation doses, a two-way Anova was performed, followed by a Bonferonni or a Tukey-Kramer post hoc test. The results are considered statistically significant when $p < 0.05$.

1. ROS PRODUCTION.

Our hypothesis states that ID and IR would both stress thyroid cells due to enhanced generation of reactive oxygen species. To assess the production of reactive oxygen species upon irradiation and ID, non-cancerous rat PCCL3 cells were cultured in an iodine-sufficient or iodine-deficient condition for 24 hours and exposed to low, intermediate or high radiation doses. Subsequently, the cell-permeable, non-fluorescent CM-H_2DCFDA probe was used to indicate general oxidative stress. Reactive oxygen species oxidize the probe yielding a fluorescent adduct captured inside the cells. The fluorescent signal was then quantified and normalized against the total cell number.

There was a significant, radiation dose-dependent increase in the production of reactive oxygen species compared to lower irradiation doses and to non-irradiated control cells, both in iodine-sufficient as in iodine-deficient conditions **(Table 2)**. Furthermore, the production of reactive oxygen species was significantly upregulated in iodine-deficient PCCL3 cells that were irradiated with 0.5 Gy and 3 Gy, compared to the corresponding irradiated, iodine-sufficient PCCL3 cells (0.5 Gy: $P<0.001$; 3 Gy: $P=0.012$) **(Figure 3)**.

These results suggest that starting from an intermediate radiation dose of 0.5 Gy and higher upto 3 Gy, thyroid cells are stressed to this extent, so that the additional stress of ID leads to an enhanced production of reactive oxygen species, compared to iodine-sufficient thyroid cells.

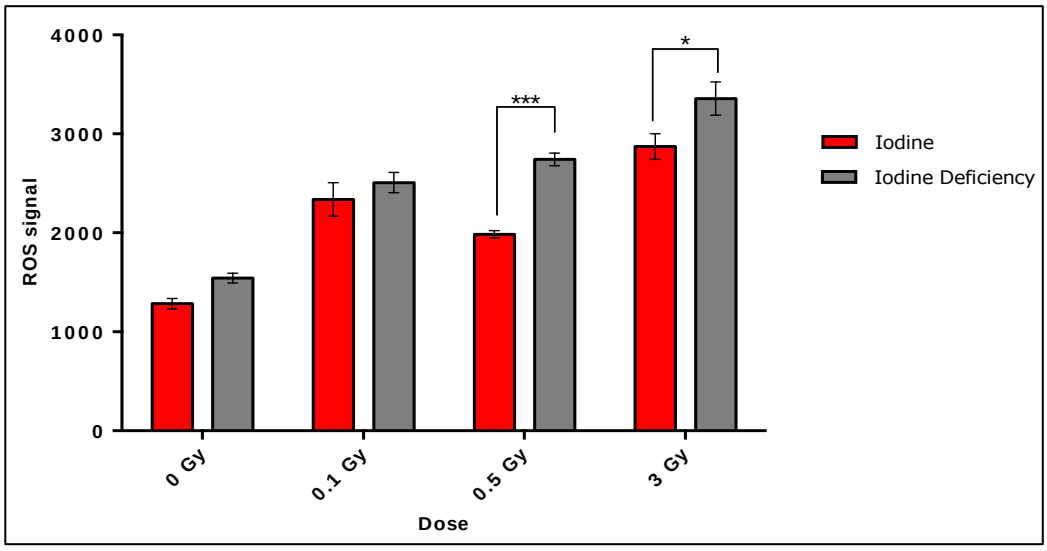

Figure 3: ROS production significantly increased with increasing radiation doses and is enhanced under iodine-deficient conditions at 0.5 Gy and 3 Gy. ROS production was analyzed using the cell-permeable, non-fluorescent CM-H_2DCFDA probe in PCCL3 cells that were iodine deprived for 24 hours and irradiated at low, intermediate and high radiation doses. Results are expressed as mean fluorescent signal intensity ± standard error of the mean and are normalized against the number of cells. ns, not significant, *, $p<0.05$; **, $p<0.002$, ***, $p<0.001$.

Table 2: Table of significance of the ROS assay 24 hours after iodine deficiency and ionizing radiation, comparing changes between the different radiation doses in iodine-sufficient and iodine-deficient PCCL3 cells.

Iodine			Iodine deficiency		
Comparisons test	Significance	P-value	Comparisons test	Significance	P-value
0 Gy vs 0.1 Gy	***	<0.001	0 Gy vs 0.1 Gy	***	<0.001
0 Gy vs 0.5 Gy	***	<0.001	0 Gy vs 0.5 Gy	***	<0.001
0 Gy vs 3 Gy	***	<0.001	0 Gy vs 3 Gy	***	<0.001
0.1 Gy vs 0.5 Gy	ns	0.09	0.1 Gy vs 0.5 Gy	ns	0.42
0.1 Gy vs 3 Gy	**	0.005	0.1 Gy vs 3 Gy	***	<0.001
0.5 Gy vs 3 Gy	***	<0.001	0.5 Gy vs 3 Gy	***	<0.001

2. ANTIOXIDANT DEFENSE

Preliminary data showed that rat thyroid FRTL5 cells exhibited a resistant profile to DNA damage and apoptosis after exposure to high doses of IR and iodine deprivation. A possible explanation is the presence of effective mechanisms to regulate antioxidant responses in thyroid cells, limiting cellular damage and apoptosis induced by ROS, such as H_2O_2, a required co-substrate together with iodide in the synthesis of thyroid hormones. Therefore, together with our previously described ROS assay, an increased protein expression of antioxidant enzymes, such as catalase, an enzyme that detoxifies H_2O_2, could be expected when exposing thyroid cells to IR and ID, both factors leading to ROS production. To examine the change in catalase protein expression upon irradiation and iodine deprivation, non-cancerous rat thyroid PCCL3 cells were cultured in an iodine-sufficient or iodine-deficient state for 6 hours and exposed to low, intermediate or high radiation doses. Protein expression of catalase was analyzed using Western blot.

Bands were detected at approximately 60 kDa and 120 kDa for catalase protein expression **(Supplemental Figure 10C)**. The predicted band size of a catalase monomer is 60 kDa. A two-way Anova statistical analysis indicates that there was an overall significant effect of the PCCL3 iodine state on the results we observe (P=0.0242). However, post-hoc testing could not define a specific significant difference between groups. We can see a trend of an increased catalase protein expression in iodine-deficient thyroid cells compared to iodine-sufficient thyroid cells. In contrast, irradiation, even with high IR doses, did not significantly change catalase protein expression in the exposed thyroid cells. As a result, there was no enhanced effect observed when combining IR and ID **(Figure 4)**. Under iodine-deficient conditions, the production of H_2O_2 cannot be sufficiently detoxified by the thyroid peroxidase (TPO)-catalyzed oxidation of iodide to iodine during the process of thyroid hormone synthesis. These data indicate that deprivation of iodine activates antioxidant protein expression of catalase, which could represent an acute compensatory response to the decreased presence of iodide as a H_2O_2 antioxidant-scavenging agent.

There are relatively high standard deviations observed at n=3 for each condition. This could mask potential significant effects of IR and a potential enhanced effect of IR and ID on catalase protein expression. Reconsidering optimization of the Western blot protocol and including more

biological replicates could reduce the SD values of the observed results and could increase the reproducibility of the experiment.

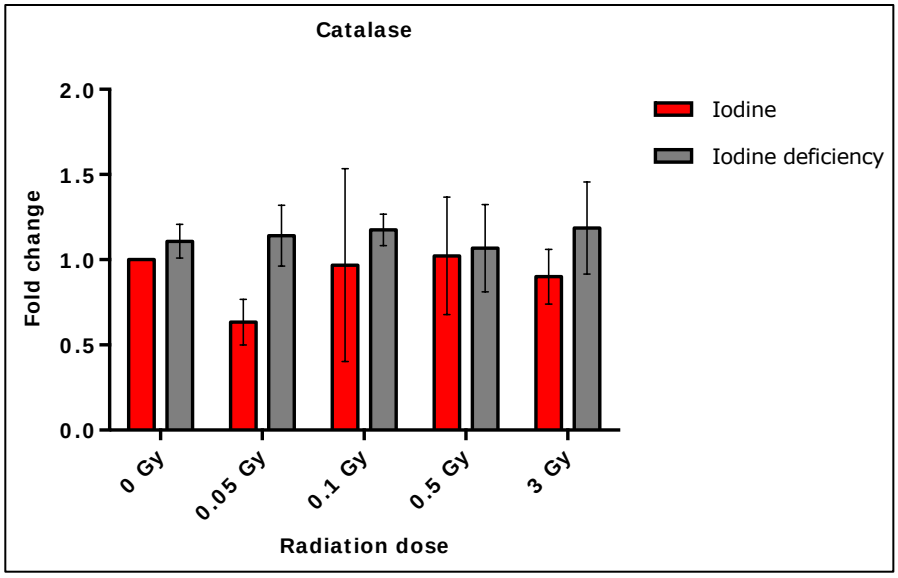

Figure 4: ID had an overall significant effect increasing catalase protein expression (p=0.0242). In contrast, there were no significant differences observed in catalase protein expression among the different radiation doses and after combined exposure to IR and ID. Catalase protein expressing was analyzed by Western blotting in PCCL3 cells that were iodine deprived for 6 hours and irradiated with low, intermediate or high radiation doses. Densitometric values were normalized against ß-actin. Results are expressed as the mean fold change relative to non-irradiation, iodine-sufficient thyroid cells ± standard deviation (SD) of 3 biological replicates (n=3) from 1 representative experiment.

3. APOPTOSIS

In order to investigate the effect of a combined treatment with ID and low-, intermediate- and high-dose irradiation on the induction of apoptosis in thyroid cells, we wanted to measure the proportion of living, early and late apoptotic rat PCCL3 cells, 48 hours post-treatment. We performed a TUNEL assay using BrdUTP and cleaved caspase-3 fluorescent immunocytochemistry, followed by flow cytometry analysis. However, during this assay, we encountered complications in pellet formation after centrifugation of the samples, causing cell loss in many treated samples. Furthermore, we were not able to visualize clearly separated cellular populations of living and apoptotic cells, questioning the quality of the staining protocol **(Supplemental Figure 11)**.

4. DNA DAMAGE: DOUBLE STRAND BREAKS

DNA damage is intrinsic to cells and is aggravated by genotoxic events such as exposure to ionizing radiation and oxidative stress. Cells are able to sense and react on damaged DNA through activation of the DDR pathway, causing cell cycle arrest, allowing cells to repair the damaged DNA. Repair proteins rapidly assemble around the damaged sites. γH2AX and 53BP1 are often used as markers representing sites of DSBs, which can be detected as foci. Preliminary data showed that rat thyroid FRTL5 cells exhibited resistance to DNA damage following high-dose irradiation and iodine deprivation. Therefore, in order to evaluate the extent of DNA damage and the subsequent

DNA repair kinetics, a fluorescent immunocytochemistry double staining was performed, targeting γH2AX and 53BP1 foci in rat thyroid PCCL3 cells that were iodine deprived for 30 min, 1 hour, 4 hours or 24 hours and were irradiated with low, intermediate or high irradiation doses **(Supplemental Figure 12)**. The mean number of γH2AX and 53BP1 foci per nucleus was calculated for at least 250 cells per biological replicate in each condition **(Figure 5 and Figure 6)**.

H2AX phosphorylation appears immediately after irradiation, typically reaching its maximal number of γH2AX foci around 10-30 minutes post-irradiation, after which it continuously decreases up to 24 hours. This specific trend is observed in both iodine-sufficient and iodine-deficient cells exposed to sham-irradiation, 0.5 Gy and 3 Gy. In contrast, PCCL3 cells that were exposed to low irradiation doses (0.05 Gy and 0.1 Gy) showed a continuous increase in the number of γH2AX foci over time. When comparing iodine-sufficient, sham-irradiated control cells to the corresponding irradiated cells, we observed a significantly increased number of γH2AX foci after exposure to intermediate and high irradiation doses (0.5 Gy and 3 Gy) at all measured time points. This also counts for iodine-deficient conditions, except for the 3 Gy-irradiated, iodine-deficient cells at 24 hours after the co-treatment, in which the cells showed a strong DNA repair and thus no longer significantly differentiated in the amount of γH2AX foci from the control cells at this specific time point. Unexpectedly, PCCL3 cells that were exposed to low-dose irradiation (0.05 Gy and 0.1 Gy) showed significantly less γH2AX foci compared to the control cells at the early time point of 30 minutes after the co-treatment up to approximately 4 hours. This also counts for both iodine-sufficient and iodine-deficient conditions. However, at 24 hours post-irradiation and ID, the low-dose irradiated cells accumulated significantly more γH2AX foci than the corresponding control cells due to their continuously increasing trend over time **(Figure 5A and B, Table 3A)**. When comparing between iodine-sufficient and iodine-deficient thyroid cells per radiation dose, they clearly follow the same trend over time with only significantly more γH2AX foci under iodine-deficient conditions in sham-irradiated control cells at 24 hours post-treatment **(Figure 5C;** P=0.005**),** in 0.1 Gy-irradiated cells at 4 hours and 24 hours **(Figure 5E;** P<0.001 and P=0.04 respectively**)** and in 3 Gy-irradiated cells at 30 minutes **(Figure 5G;** P=0.022**)**. There were significantly more γH2AX foci under iodine-sufficient conditions in 0.5 Gy-irradiated **(Figure 5F;** P=0.011**)** and 3 Gy-irradiated cells **(Figure 5G;** P<0.001 **)** respectively at 1 hour and 4 hour post-treatment.

Kinetically, the appearance of 53BP1 foci and their hyper-phosphorylation occur later than the appearance of γH2AX foci, since 53BP1 first need to be recruited to the sites of DNA damage in contrast to H2AX, which is already present at the DSBs. In our results, there is no significant difference in the number of 53BP1 foci between sham-irradiated control cells and cells exposed to 0.05 Gy. This counts for both iodine-sufficient and iodine-deficient conditions, except for a small significant higher number of 53BP1 foci in 0.05 Gy-irradiated iodine-deficient cells compared to the corresponding control cells at 30 minutes post-ID and -irradiation (P=0.01). The control cells and 0.05 Gy-irradiated cells both exhibit their maximal number of 53BP1 foci after 30 minutes post-ID and –irradiation after which it continuously decreases over time. This is in contrast to the cells exposed to higher irradiation doses from 0.1 Gy up to 3 Gy, reaching their peak of 53BP1 foci

between 1 hour and 4 hours after ID and irradiation. More specifically, iodine-sufficient cells exposed to 0.1 Gy started to significantly differ from the sham-irradiated control cells in their number of 53BP1 foci at 1 hour post-irradiation, reaching their peak at this time point. Then, their number of 53BP1 foci continuously decreased up to 24 hours post-irradiation and thus no longer significantly differentiated from the control cells. Their counterparts, the iodine-deficient, 0.1 Gy-irradiated cells also started to significantly differ from the sham-irradiated control cells in their number of 53BP1 foci after 1 hour post-ID and -irradiation, but reached their peak at 4 hours instead of 1 hour. In case of the 0.5Gy-irradiated cells, the number of 53BP1 foci was already significantly higher compared to the 53BP1 foci in the sham-irradiated control cells at 30 minutes post-treatment in both iodine-deficient and iodine-sufficient conditions. Both cell groups reached their peak in 53BP1 foci at 1 hour post-treatment, after which the number of 53BP1 foci decreases over time up to 24 hours, but still remains significantly higher compared to the control cells at 4 hours post-treatment. 24 hours post-treatment, the number of 53BP1 foci in the 0.5 Gy-irradiated iodine-sufficient cells no longer significantly differentiated from the number of 53BP1 foci in the control cells, in contrast to the iodine-deficient cells which still exhibited a small significant increase in 53BP1 foci compared to the control cells (P=0.035). Finally, in case of the 3 Gy-irradiated cells, the number of 53BP1 foci started to significantly differ from the sham-irradiated control cells at 1 hour post-treatment, but reaches their peak at 4 hours post-treatment in both iodine-sufficient and iodine-deficient conditions. After 4 hours, the number of 53BP1 foci strongly decreased up to 24 hours post-treatment in both conditions, but was still significantly higher compared to the number of 53BP1 foci in the control cells **(Figure 6A and B, and Table 3B)**. When comparing the differences between iodine-sufficient and iodine-deficient cells per radiation dose, they follow the same trend over time **(Figure 6C, D, G)** with only significantly more 53BP1 foci in iodine-deficient, 0.1 Gy-irradiated cells at 4 hours post-treatment **(Figure 6E**; P<0.001**)** and in iodine-sufficient 0.5 Gy-irradiated cells at 1 hour post-treatment **(Figure 6F**; P=0.003).

Taken together, these results suggest that exposure of thyroid cells to low irradiation doses of only 0.05 Gy and 0.1 Gy result in a slower induction of γH2AX foci compared to exposure to intermediate and high irradiation doses (0.5 Gy and 3 Gy) which reach their maximum number of γH2AX foci at 30 minutes or even earlier post-irradiation, suggesting a reduced efficiency of the DDR system after low-dose radiation exposure. This could also indicate that phosphorylation of H2AX is not robust enough to trigger DDR activation and initiate subsequent DNA repair, which could explain the continuous increase in γH2AX foci over time after low-dose radiation exposure in contrast to the strong disappearance of foci at 24 hours after intermediate- and high-dose radiation exposure. The reason for the high baseline presence of γH2AX foci and the DNA repair at 24 hours in sham-irradiated cells is not clear. Furthermore, low-dose irradiation with 0.05 Gy does not trigger the late 53BP1 recruitment to DSBs and its hyper-phosphorylation compared to sham-irradiated control cells, even though γH2AX foci are increasingly induced over time. This effect can be observed starting from a low-dose irradiation with 0.1 Gy upto 3 Gy. Finally, there are no major differences observed between iodine-sufficient and iodine-deficient conditions in the extent of DNA damage and their subsequent DNA repair kinetics.

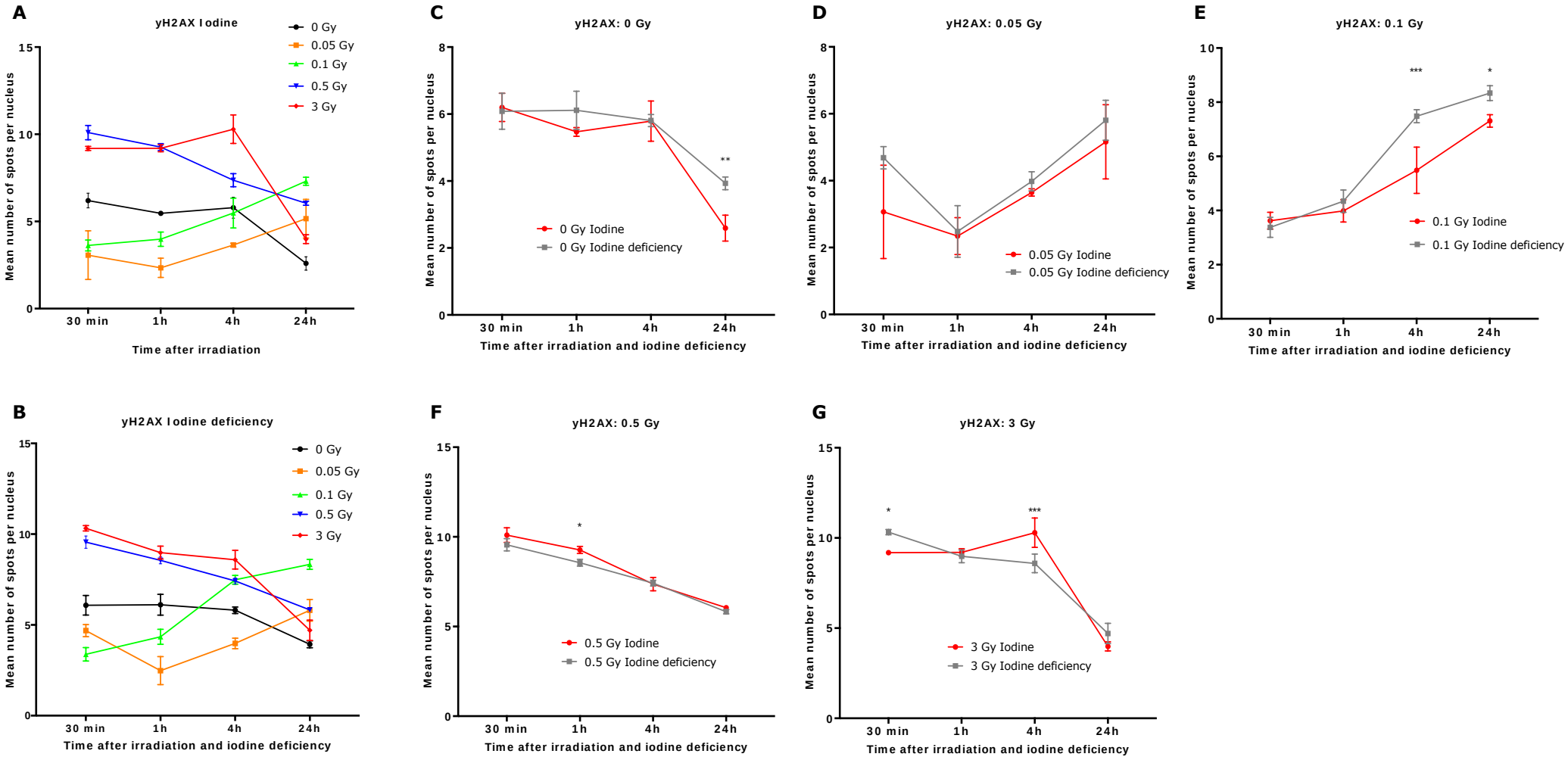

Figure 5: Intermediate and high irradiation doses induce double strand breaks leading to γH2AX foci in iodine-sufficient and iodine-deficient PCCL3 cells with a maximal number at 30 min post-irradiation and ID, and decreasing over time with a minimal number at 24 hours post-irradiation and ID. This is in contrast to exposure to low irradiation doses of 0.05 Gy and 0.1 Gy, increasing in γH2AX foci over time. γH2AX foci were detected using immunocytochemistry staining of PCCL3 cells that were iodine deprived for 30 min, 1hour, 4 hours and 24 hours and irradiated with low, intermediate and high radiation doses. Results are expressed as mean number of foci per nucleus at each time point in iodine-sufficient conditions **(A)** and iodine-deficient conditions **(B)** ± standard deviation (SD) of three biological replicates (n=3) from 1 representative experiment. Furthermore, the differences between iodine-sufficient and iodine-deficient conditions per radiation dose is visualized for 0 Gy **(C)**, 0.05 Gy **(D)**, 0.1 Gy **(E)**, 0.5 Gy **(F)** and 3 Gy **(G)**. Per biological replicate of each condition, at least 250 nuclei were investigated.

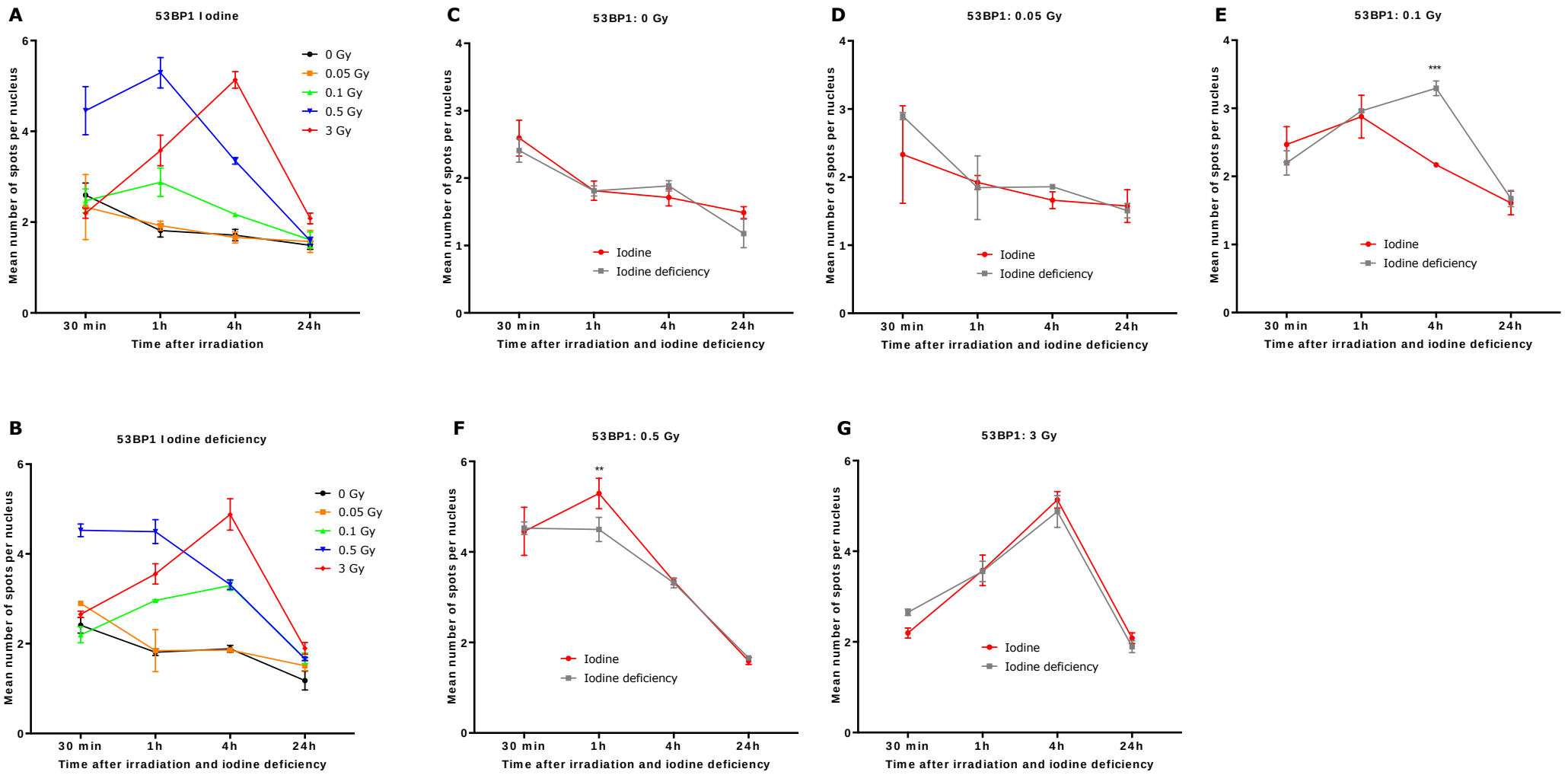

Figure 6: Intermediate and high irradiation doses induce double strand breaks leading to 53BP1 foci in iodine-sufficient and iodine-deficient PCCL3 cells with a maximal number between 30 minutes and 4 hours post-irradiation and ID, and with a minimal number after 24 hours. 53BP1 foci were detected using immunocytochemistry staining of PCCL3 cells that were iodine deprived for 30 min, 1hour, 4 hours and 24 hours and irradiated with low, intermediate and high radiation doses. Results are expressed as mean number of foci per nucleus at each time point in iodine-sufficient conditions **(A)** and iodine-deficient conditions **(B)** ± standard deviation (SD) of three biological replicates (n=3) from 1 representative experiment. Furthermore, the differences between iodine-sufficient and iodine-deficient conditions per radiation dose is visualized for 0 Gy **(C)**, 0.05 Gy **(D)**, 0.1 Gy **(E)**, 0.5 Gy **(F)** and 3 Gy **(G)**. Per biological replicate of each condition, at least 250 nuclei were investigated.

Table 3: Table of significance of the γH2AX (A) and 53BP1 (B) immunostaining in iodine-sufficient and iodine-deficient PCCL3 cells at 30 min, 1 hour, 4 hours or 24 hours after iodine deficiency and ionizing radiation, comparing the different radiation doses to sham-irradiated control cells.

A

Comparison tests	**γH2AX: Iodine**		**γH2AX: Iodine deficiency**	
30 min	Significance	*P-value*	Significance	*P-value*
0 Gy vs. 0.05 Gy	***	<,001	***	<,001
0 Gy vs. 0.1 Gy	***	<,001	***	<,001
0 Gy vs. 0.5 Gy	***	<,001	***	<,001
0 Gy vs. 3 Gy	***	<,001	***	<,001
1h				
0 Gy vs. 0.05 Gy	***	<,001	***	<,001
0 Gy vs. 0.1 Gy	*	0,011	***	<,001
0 Gy vs. 0.5 Gy	***	<,001	***	<,001
0 Gy vs. 3 Gy	***	<,001	***	<,001
4h				
0 Gy vs. 0.05 Gy	***	<,001	***	<,001
0 Gy vs. 0.1 Gy	ns	>,999	***	<,001
0 Gy vs. 0.5 Gy	**	0,006	***	<,001
0 Gy vs. 3 Gy	***	<,001	***	<,001
24h				
0 Gy vs. 0.05 Gy	***	<,001	***	<,001
0 Gy vs. 0.1 Gy	***	<,001	***	<,001
0 Gy vs. 0.5 Gy	***	<,001	***	<,001
0 Gy vs. 3 Gy	*	0,019	ns	0,092

B

Comparison tests	**53BP1: Iodine**		**53BP1: Iodine deficiency**	
30 min	Significance	*P-value*	Significance	*P-value*
0 Gy vs. 0.05 Gy	ns	0,91	*	0,01
0 Gy vs. 0.1 Gy	ns	>,999	ns	0,676
0 Gy vs. 0.5 Gy	***	<,001	***	<,001
0 Gy vs. 3 Gy	ns	0,282	ns	0,457
1h				
0 Gy vs. 0.05 Gy	ns	>,999	ns	>,999
0 Gy vs. 0.1 Gy	***	<,001	***	<,001
0 Gy vs. 0.5 Gy	***	<,001	***	<,001
0 Gy vs. 3 Gy	***	<,001	***	<,001
4h				
0 Gy vs. 0.05 Gy	ns	>,999	ns	>,999
0 Gy vs. 0.1 Gy	ns	0,16	***	<,001
0 Gy vs. 0.5 Gy	***	<,001	***	<,001
0 Gy vs. 3 Gy	***	<,001	***	<,001
24h				
0 Gy vs. 0.05 Gy	ns	>,999	ns	0,14
0 Gy vs. 0.1 Gy	ns	>,999	**	0,009
0 Gy vs. 0.5 Gy	ns	>,999	*	0,011
0 Gy vs. 3 Gy	*	0,035	***	<,001

5. CELL CYCLE ANALYSIS

To investigate the effects of IR and ID on the cell cycle distribution of the thyroid cells, non-cancerous rat PCCL3 cells were cultured in an iodine-sufficient or iodine-deficient state for 6, 24 or 48 hours and exposed to low, intermediate or high radiation doses. To determine the percentages of cells in each phase of the cell cycle, a BrdU/7-AAD staining assay was performed **(Supplemental Figure 13)**.

Six hours after irradiation and ID, the amount of non-irradiated and 0.05 Gy-irradiated, iodine-sufficient cells in the G0/G1 phase was significantly higher compared to the amount of 3 Gy-irradiated, iodine-sufficient cells in the G0/G1 phase (respectively P=0.005 and P=0.024). There were no significant differences observed in the amount of cells in all phases of the cell cycle between the different radiation doses for both iodine-sufficient and iodine-deficient conditions. Furthermore, there were no significant differences detected between iodine-sufficient and iodine-deficient cells **(Figure 7A)**.

24 hours after irradiation and ID, there is a significant increase in the amount of iodine-sufficient cells in the G0/G1 phase after irradiation with a radiation dose of 3 Gy, compared to lower radiation doses. The same counts for iodine-deficient cells **(Table 4, G0/G1 phase)**. However, the percentage of iodine-deficient cells in the G0/G1 phase is significantly lower compared to the percentage of iodine-sufficient cells in the G0/G1 phase for all radiation doses except for the non-irradiated control cells (P<0.001) **(Figure 7B)**. The amount of iodine-sufficient cells in the G2/M phase significantly decreased after irradiation with a radiation dose of 3 Gy, compared to lower radiation doses. In contrast, this change is less pronounced in iodine-deficient conditions, only significant comparing 3 Gy to 0.1 Gy, and 0 Gy to 0.1 Gy **(Table 4, G2/M phase)**. Furthermore, the amount of iodine-deficient cells in the G2/M phase is significantly higher compared to the amount of iodine-sufficient cells in the G2/M phase after irradiation with radiation doses of 0.1 Gy (P=0.003) and 3 Gy (P<0.001) **(Figure 7B)**. Finally, the percentage of iodine-sufficient cells in the S phase started to significantly decrease after irradiation with a radiation dose of 0.5 Gy compared to non-irradiated and 0.1 Gy-irradiated, iodine-sufficient cells. This change was most pronounced after irradiation with 3 Gy, compared to lower irradiation doses. The latter counts for iodine-deficient cells as well **(Table 4, S phase)**. However, the amount of iodine-deficient cells in S phase is higher compared to iodine-sufficient cells for each radiation dose, with a significant difference at 0.05 Gy (P=0.002) and 0.5 Gy (P<0.001) **(Figure 7B)**.

48 hours after irradiation and ID, there are no longer significant differences observed between iodine-sufficient and iodine-deficient cells **(Figure 7C)**. On the other hand, there is still a small significant decrease in the amount of iodine-sufficient cells in the S phase after irradiation with a radiation dose of 3 Gy, compared to lower irradiation doses (0 Gy P=0.01; 0.05 Gy P=0.05; and 0.1 Gy P=0.035). Furthermore, the percentage of iodine-sufficient cells in the G0/G1 phase is still significantly increased after irradiation with 3 Gy compared to sham-irradiated (P=0.019) and 0.1 Gy-irradiated (P=0.047), iodine-sufficient cells. For iodine-deficient cells, there is only a significant decrease in the amount of cells in the S-phase after irradiation with 3 Gy compared to sham-irradiated cells (P=0.041).

Taken together, these results suggest that the cell cycle of PCCL3 cells do not yet change 6 hours after ID and irradiation, even after exposure to high radiation doses. However, the response on these applied stress factors can be detected 24 hours after ID and irradiation. Irradiation with 3 Gy leads to a significant G0/G1 cell cycle arrest in both iodine-sufficient and iodine-deficient cells compared to lower irradiation doses, most likely to repair the DNA damage caused by IR and the generated oxidative stress. Iodine-deficient PCCL3 cells still appear to be less sensitive for this G0/G1 cell cycle arrest even at low irradiation doses and are also more proliferating compared to iodine-sufficient cells. This could represent a stress-response in iodine-deficient cells with subtle changes in their proliferation pathways, which could be triggered by the enhanced ROS production of the co-treatment, with ID as a promoting factor enhancing the effects of IR. This could promote the mutation rate and subsequent pre-cancerous transformation when genetic lesions are not repaired in proliferating iodine-deficient thyroid cells. However, 48 hours after ID and irradiation, the cell cycle profile of iodine-deficient cells no longer significantly differentiates from iodine-sufficient cells. Only following irradiation with 3 Gy, there was still a small significant decrease in the amount of iodine-sufficient and iodine-deficient cells in the S-phase and G0/G1 phase compared to sham-irradiated control cells. This indicates that thyroid cells are able to restore their cell cycle profile to normal conditions 48 hours after ID and irradiation, regardless of their iodine state.

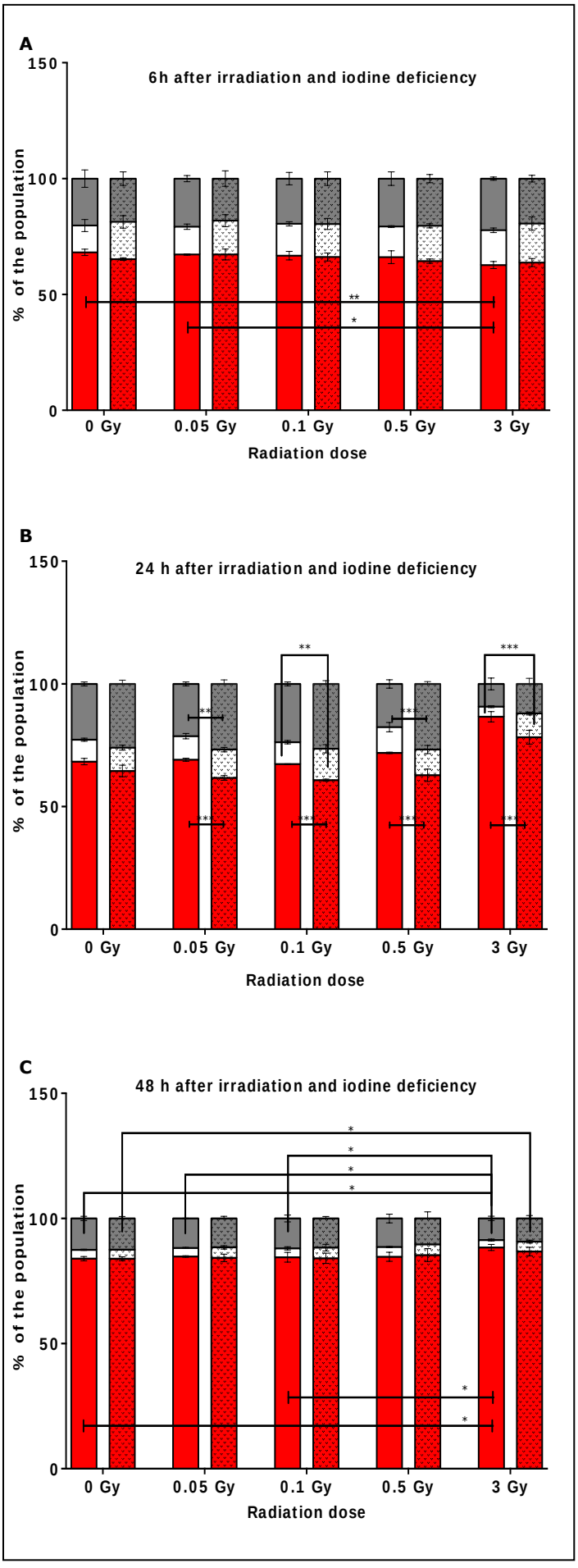

Figure 7: Six hours after irradiation combined with iodine deficiency, the cell cycle of iodine-deficient and iodine-sufficient PCCL3 cells are not altered compared to the control cells. After 24 hours, the cell cycle of iodine-deficient PCCL3 cells altered compared to iodine-sufficient PCCL3 cells, but no longer differentiated after 48 hours. Cell cycle analysis was performed with a BrdU/7-AAD assay on PCCL3 cells that were iodine deprived for 6 hours **(A)**, 24 hours **(B)** or 48 hours **(C)** and irradiated with low, intermediate or high radiation doses. Results are expressed as the mean percentage of cells of the total cell population ± SD of three biological replicates from 1 representative experiment. The cell cycle analysis 6 hours and 24 hours after IR and ID were performed in parallel. The cell cycle analysis 48 hours after IR and ID was performed as a separate experiment, causing technical variation compared to the 6h and 24h experiments.

S iodine
G2/M iodine
G0/G1 iodine
S iodine deficiency
G2/M iodine deficiency
G0/G1 iodine deficiency

Table 4: Table of significance of the cell cycle analysis, 24 hours after iodine deficiency and ionizing radiation, comparing changes between the different radiation doses in iodine-sufficient and iodine-deficient PCCL3 cells in the different cell cycle phases (G0/G1 phase, S phase, G2/M phase).

	G0/G1 phase				S phase				G2/M phase			
Dose (Gy)	I	*P-value*	ID	*P-value*	I	P-value	ID	P-value	I	P-value	ID	P-value
0 - 0.05	Ns	>0.999	Ns	0.475	Ns	>0.999	Ns	>0.999	Ns	>0.999	Ns	0.398
0 - 0.1	Ns	>0.999	Ns	0.117	Ns	>0.999	Ns	>0.999	Ns	>0.999	*	0.024
0 - 0.5	Ns	0.160	Ns	>0.999	**	0.005	Ns	>0.999	Ns	>0.999	Ns	>0.999
0 - 3	***	<0.001	***	<0.001	***	<0.001	***	<0.001	***	<0.001	Ns	>0.999
0.05 - 0.1	Ns	>0.999	Ns	>0.999	Ns	0.635	Ns	>0.999	Ns	>0.999	Ns	>0.999
0.05 - 0.5	Ns	0.513	Ns	>0.999	Ns	0.082	Ns	>0.999	Ns	>0.999	Ns	>0.999
0.05 - 3	***	<0.001	***	<0.001	***	<0.001	***	<0.001	***	<0.001	Ns	0.530
0.1 - 0.5	*	0.028	Ns	>0.999	***	<0.001	Ns	>0.999	Ns	>0.999	Ns	0.214
0.1 - 3	***	<0.001	***	<0.001	***	<0.001	***	<0.001	***	<0.001	*	0.033
0.5 - 3	***	<0.001	***	<0.001	***	<0.001	***	<0.001	***	<0.001	Ns	>0.999

6. MODULATIONS IN SIGNALING PATHWAYS

6.1 THE NOS3/HIF-1A/VEGF-A SIGNALING PATHWAY.

A previous study demonstrated that ID induces NOS3 activation through phosphorylation of Ser1177 (maximal at 4 hours post-ID, but still significant at 6 hours post-ID), thereby increasing NO synthesis and subsequent HIF-1α stabilization leading to VEGF-A release in PCCL3 cells. In an attempt to reproduce these data and to examine a potential enhanced effect of IR and ID on NOS3 activation and HIF-1α stabilization due to increased ROS production, non-cancerous rat thyroid PCCL3 cells were cultured in an iodine-sufficient or iodine-deficient state for 6 hours and exposed to low, intermediate or high radiation doses. Subsequently, protein expressions of NOS3, Ser1177-phosphorylated NOS3 and HIF-1α were analyzed by Western blot **(Figure 8)**.

Bands were detected at approximately ≈140 kDa and ≈70 kDa for (pSer1177) NOS3 protein expression and around ≈120 kDa and ≈80 kDa for HIF-1α protein expression **(Supplemental Figure 10A and B)**. For the (pSer1177) NOS3 protein, the expected band size is ≈140 kDa. For the HIF-1α protein, the expected band size is ≈120 kDa. According to our results, neither ID nor IR or a combined treatment induced a significantly increased activation of NOS3 **(Figure 8A)** and stabilization of HIF-1α **(Figure 8B)** compared to the sham-irradiated, iodine-sufficient thyroid cells. So, despite the same rat cell line used under the same culture conditions, we were not able to reproduce the results from the previous study. Since high standard deviations (SD) occur at n = 3 for each condition, it is difficult to detect a potential small, true effect. Reconsidering optimization of the Western blot protocol and including more biological replicates could reduce the SD values of the observed results and could increase the reproducibility of the experiment.

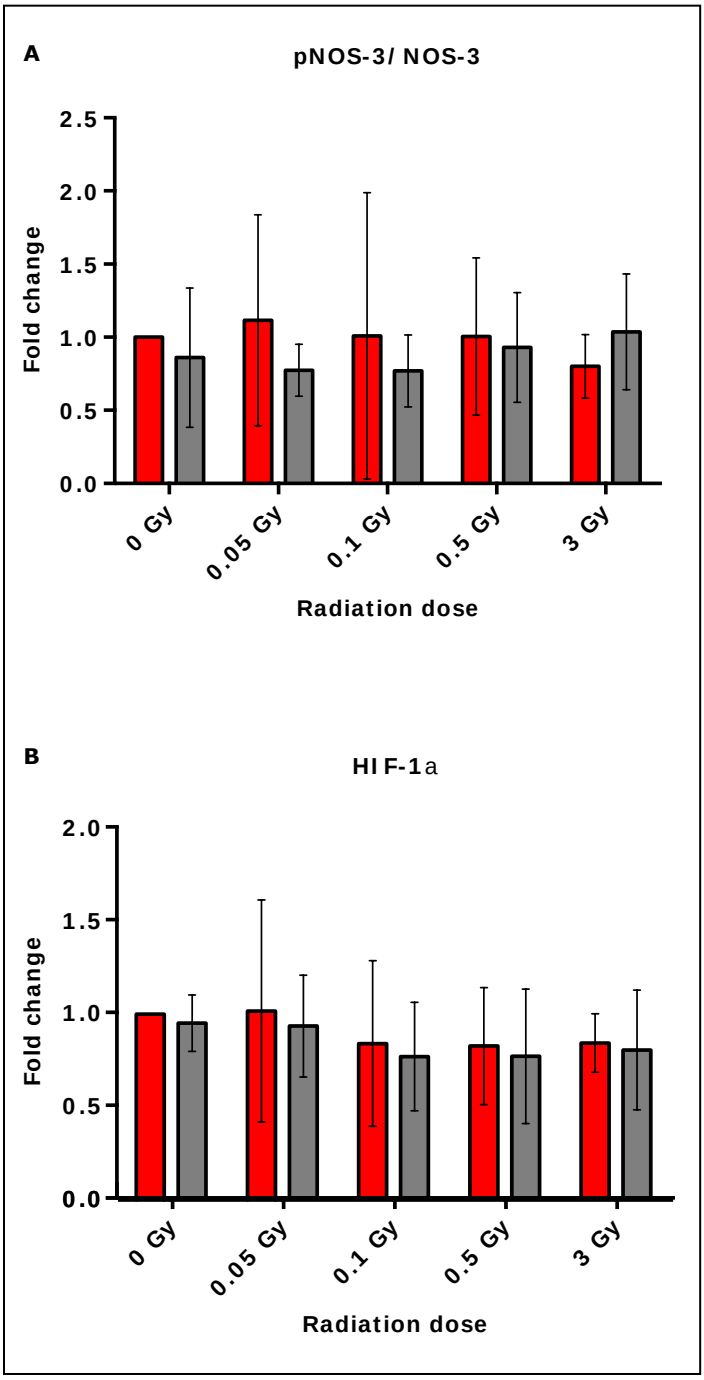

Figure 8: ID, IR or a combined treatment did not significantly changes NOS3 activation and HIF-1α stabilization compared to sham-irradiated, iodine-sufficient PCCL3 cells. NOS3 and pSer1177 NOS3 expression **(A)** and HIF-1α expression **(B)** were analyzed by Western blotting in PCCL3 cells that were iodine deprived for 6 hours and irradiated with low, intermediate or high radiation doses. Densitometric values were normalized against ß-actin. Furthermore, pSer1177 NOS3 protein expression was normalized against total NOS3 protein levels. Results are expressed as the mean fold change relative to non-irradiation, iodine-sufficient thyroid cells ± standard deviation (SD) of 3 biological replicates (n=3) from 1 representative experiment

6.2 CELLULAR PROLIFERATION AND SURVIVAL.

It has been reported that oxidative stress and DNA damage alters signaling pathways involved in cellular proliferation and survival. IR can directly damage DNA but more frequently acts indirectly through the production of ROS, along with ID in thyroid cells. To examine changes in proliferation and survival pathways upon ID and IR, non-cancerous rat thyroid PCCL3 cells were cultured in an iodine-sufficient or iodine-deficient state for 6 hours and exposed to low, intermediate or high radiation doses. Subsequently, protein expression of AKT1, pThr308 AKT1, STAT3, pY705 STAT3 and NFκB p52 were analyzed using Western blot **(Figure 9)**.

Bands were detected at approximately 55 kDa and 62 kDa for AKT1, at 62 kDa for pThr308 AKT1 **(Supplemental Figure 10D)**, at 86 kDa and 91 kDa for STAT3, at 86 kDa and 160 kDa for pY705 STAT3 **(Supplemental Figure 10F)** and at 52 kDa for NFkB p52 protein expression **(Supplemental Figure 10E)**. The predicted band size of (pThr308) AKT1 is 62 kDa. Finally, the predicted band size for NFkB p52 protein expression is 52 kDa which we specifically visualised. There were no significant changes observed in the expression and phosphorylated Thr308 activation of AKT1 upon irradiation or induced ID **(Figure 9A)**. The same counts for NFkB p52 protein expression **(Figure 9B)**. Consequently, there was no enhanced effect observed after combined treatment with ID and IR. These results are consistent with preliminary data on rat FRTL5 cells. However, STAT3 and activated pY705 STAT3 were significantly increased after irradiation with a radiation dose of 3 Gy in FRTL5 cells. Furthermore, there was a significant enhanced effect of combined treatment with IR and ID at 3 Gy. This is in contrast with our results in PCCL3 cells, in which there was no significant change observed in STAT3 and pY705 STAT3 protein expression after irradiation, even with high radiation doses, and induction of ID **(Figure 9C)**. These results indicate that PCCL3 cells and FRTL5 cells are different in their molecular responses on the induction of stress, suggesting that PCCL3 cells are more resistant to changes in their signaling pathways, even at high doses of IR.

There are relatively high standard deviations observed at n=3 for each condition. This could mask small but true significant effects of IR, ID or a potential enhanced effect of IR and ID on the protein expression of (pThr308)AKT1, NFκB p52 and especially (pY705)STAT3. Reconsidering optimization of the Western blot protocol and including more biological replicates could reduce the SD values of the observed results and could increase the reproducibility and in particular the comparability of the experiment with preliminary data on FRTL5 cells.

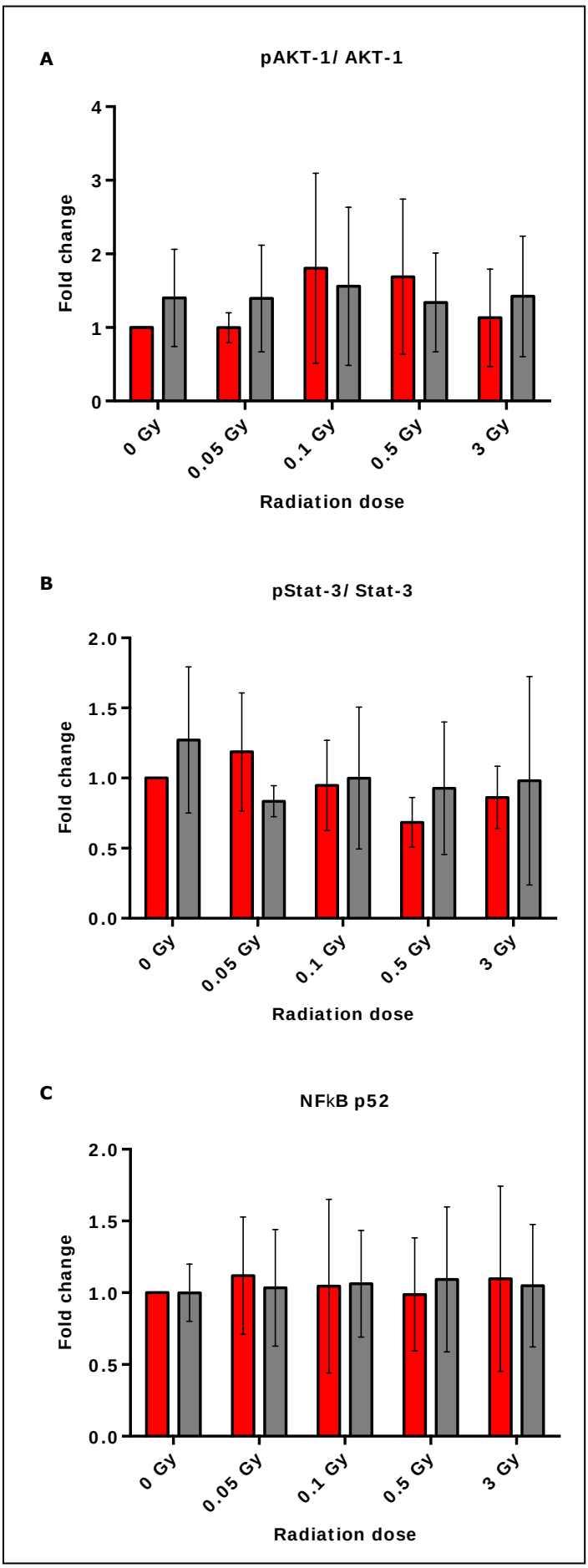

Figure 9: ID, IR or a combined treatment did not alter signaling pathways involved in cellular proliferation and survival. AKT1 and pThr308 AKT1 **(A)** STAT3 and pY705 STAT3 **(B)** and NFB p52 protein expressions **(C)** were analyzed by Western blotting in PCCL3 cells that were iodine deprived for 6 hours and irradiated with low, intermediate or high radiation doses. Densitometric values were normalized against ß-actin. Furthermore, pThr308 AKT1 and pY705 STAT3 protein expressions were normalized against total AKT1 and STAT3 protein levels respectively. Results are expressed as the mean fold change relative to non-irradiation, iodine-sufficient thyroid cells ± standard deviation (SD) of 3 biological replicates (n=3) from 1 representative experiment.

Iodine

Iodine deficiency

DISCUSSION AND OUTLOOK

Nowadays, the general population is increasingly exposed to IR originating from natural and human-made sources. The latter can range from nuclear power generation to medical uses of radiation for diagnosis or treatment, which is the most common human-made source of IR, representing 20% of the total population exposure (111). Post-Chernobyl epidemiological studies appointed IR as high-risk factor for thyroid cancer at doses above 100 mSv. On the other hand, an inadequate supply of iodine, an important element for normal thyroid functioning and thyroid hormone synthesis, affects more than two billion individuals worldwide. It is not only the main cause of some thyroid abnormalities such as goitrogenesis, but it is also a potential risk factor for thyroid cancer development (70). There is still little knowledge about the combined effect of ID and IR exposure on thyroid cells, especially when considering exposure to low-dose IR, which is of major concern for the general public and for the research community. Therefore, our research group at SCK•CEN investigated the molecular effects of a combined treatment with iodine deprivation and X-ray exposure to low, intermediate and high radiation doses on rat thyroid cells. Preliminary research was performed on the FRTL5 thyroid cell line, while in this project the PCCL3 thyroid cell line is used to validate and compare results with preliminary data.

Ionizing radiation is well known for its genotoxic effects on biological systems due to their direct interaction and damage to DNA molecules, but more frequently due to water radiolysis leading to ROS production and subsequent damage to cellular biomolecules, including DNA. In addition, previous studies demonstrated that ID triggers VEGF-A secretion from thyroid cells, which also involves intracellular production of ROS (70). Here, we showed that iodine-deficient PCCL3 cells irradiated with 0.5 Gy up to 3 Gy resulted in an enhanced ROS production 24 hours post-treatment, compared to the irradiated, iodine-sufficient PCCL3 cells. These results suggest that PCCL3 cells irradiated with intermediate and high radiation doses are stressed to a certain extent, which makes them unable to cope with the additional oxidative stress originating from ID, leading to a higher accumulation of ROS compared to irradiated PCCL3 cells cultured in the presence of iodine. In preliminary data, there was also a significantly increased ROS production observed in iodine-deficient FRTL5 cells exposed to a high irradiation dose of 3 Gy compared to the corresponding iodine-sufficient cells. This is an interesting observation since extensive oxidative stress in the thyroid is related to several thyroid abnormalities such as hyperthyroidism, hypothyroidism, thyroiditis and also thyroid cancer.

Although we were unable to observe significant differences in catalase protein expression between iodine-sufficient and iodine-deficient PCCL3 cells, a two-way Anova statistical analysis showed that the iodine state of PCCL3 cells had a significant overall effect on the response we observed. However, post-hoc testing could not indicate a defined significance between groups, probably due to lack of power. A higher number of biological replicates could increase the power of the Western blot analysis, which then could result in a more defined indication of significance between groups. Since catalase has a tetrameric conformation consisting of four 60 kDa monomers, each containing a porphyrin heme group under physiological conditions, the additional

120 kDa protein band that we detected could correspond to a catalase dimer of two subunits. Catalase is an antioxidant enzyme known for its detoxification of H_2O_2. Under adequate iodine supply, iodide is oxidized in thyroid cells by TPO using H_2O_2 as a substrate during the process of thyroid hormone synthesis. However, when thyroid cells are iodine deprived, this detoxification process of H_2O_2 is diminished, leading to H_2O_2 accumulation. Therefore, it could be possible that thyroid cells respond by adjusting their catalase protein expression as a compensatory mechanism. This antioxidant defense topic could be further investigated by examining other antioxidant proteins such as the selenoproteins glutathione peroxidases and thioredoxin reductase. Nadolnik, et al., and Valentyukevich, et al. demonstrated that the thyroid gland was characterized by low activities of catalase and superoxide dismutase, while there was a considerable high concentration of reduced glutathione and a high enzymatic activity of glutathione peroxidase and glutathione reductase (112, 113). Furthermore, there is no thyroid phenotype associated to acatalasemia, while selenium deficiency leads to increased ROS production and even thyroidal damage. As selenium is required for glutathione peroxidase and thioredoxin enzyme activity, it is suggested that these enzymes play a significant role in thyroidal antioxidant defense mechanisms (114). On the other hand, C. Massart, et al. and Ulla Bjijrkman, et al. showed that catalase represents a major H_2O_2-detoxification pathway in respectively PCCL3 and FRTL5 cells exposed to high concentrations of H_2O_2 (115, 116). Taken together, these data suggest that the glutathione peroxidase defense system plays a major role at physiological levels of H_2O_2, while catalase, which has a much higher K_m and V_{max}, is more important to detoxify large and toxic levels of H_2O_2 (114). Another possibility to investigate is peroxiredoxin 5 (PRDX5), which is also expressed in high levels in the thyroid gland and is up-regulated in Graves' disease, a disease associated with the release of large amounts of ROS (117).

The generation of H_2O_2 in stimulated PCCL3 cells is approximately 6 nmol/10 minutes. In activated human leukocytes around 17 nmol/10 minutes. However, activated leukocytes live a few hours, while the life of thyroid cells in adults is 7 years. Thus, thyroid cells may be exposed to high doses of H_2O_2. Hydrogen peroxide exerts the same cytotoxic effect on thyroid cells as on other cell types (114). At concentrations higher than 0.05-0.1 mM, H_2O_2 is able to induce DNA DSBs in PCCL3 cells and in human primary thyroid cells, demonstrated by N Driessens, et al. using Commet assays and Western blot detection of γH2AX (118). Here, we measured the general ROS production in PCCL3 cells and the induction of DNA DSBs at different time points post-treatment by immunocytochemistry against γH2AX and 53BP1. We demonstrated that irradiation of PCCL3 cells with intermediate and high radiation doses (0.5 Gy and 3 Gy) significantly increased the number of γH2AX foci compared to sham-irradiated cells already at 30 minutes post-treatment, after which the number of γH2AX foci decreased due to DNA repair up to 24 hours post-treatment. These are normal γH2AX kinetics seen in literature (119-121). In contrast, after irradiation of PCCL3 cells with 0.05 Gy and 0.1 Gy, we observed a continuous increase in γH2AX foci even up to 24 hours, which is mostly not seen in literature. These data suggest that low-dose irradiated cells failed to repair their DNA damage, which lead to accumulation of γH2AX foci. There are some research groups, which also detect persistence of γH2AX foci after irradiation of cells with low radiation doses. Saskia Grudzenski, et al. used human fibroblasts and showed that the kinetics of γH2AX foci loss are substantially disturbed after an irradiation dose of 10 mGy and even failed to show any

foci loss after irradiation with 2.5 mGy. Furthermore, they performed an *in vivo* study and showed efficient γH2AX and 53BP1 foci removal during 24 hours after irradiation of mice with 1 Gy, but barely observed any γH2AX and 53BP1 foci loss after irradiation with 10 mGy (122). A possible model to explain these findings is that irradiation with low radiation doses induce damage or a stress level which is insufficient to allow an efficient activation of the DDR pathway and subsequent DNA repair. For PCCL3 cells, this could correspond to a radiation dose in the range of 0.05 – 0.1 Gy or lower inducing a mean foci number around 6-8 foci per nucleus at 24 hours post-treatment, while irradiation with intermediate and high irradiation doses lead to a mean foci number of 10 foci per nucleus already at 30 minutes post-treatment. This suggests that an acute induction of 10 foci per nucleus post-irradiation could represent the threshold of DNA damage to activate the DDR pathway. Interestingly, Saskia Grudzenski, et al. also demonstrated that cells irradiated with 10 mGy efficiently started to remove all γH2AX foci when the cells were exposed to an extra stress of 10 μM H_2O_2 (122). At these concentrations, H_2O_2 produces in particularly SSBs and base damages but no DSBs. According to this, it would be the level of radiation damage other than DSBs or cellular lesions, which determine whether or not efficient DNA repair occurs. In addition, they also observed that one gene (Nek1) is up-regulated after high-dose irradiation, but not after low doses. Interestingly, Nek1 appears to be involved in the DNA damage response after irradiation and loss of function is associated with radiosensitivity and impaired DSB repair. The question how the repair of DSBs is associated to the repair of SSB or base damage is interesting to investigate but is out of the scope of this project. A possible explanation could be that the repair of DSBs needs end-processing before ligation which involves factors that are also involved in the repair of SSB and first have to be induced (122). The health risk estimates for low-dose IR is based on a linear extrapolation of high-dose data, assuming a similar DNA repair capacity of IR damage after low dose irradiation as after high dose irradiation. However, if low-dose irradiation leads to persistent DSBs, this could lead to genomic instability promoting malignant transformation. In this case, these data do not support the linear extrapolation assumption and even suggest that it is an underestimation of the carcinogenic risks of low-dose IR. However, this is only of interest when unrepaired DSBs are present in actively proliferating cells. Kai Rothkamn, et al. evaluated the cellular consequences of persistent DSBs by irradiating human primary fibroblasts and then allowed them to proliferate. They observed a similar level of γH2AX foci in the irradiated cells compared to the non-irradiated cells, but detected substantially more micro-nucleated and apoptotic cells, suggesting that the cells exhibiting persistent DSBs are eliminated from the culture. Therefore, they speculated that the observed DSB persistence in low-dose irradiated cells does not increase the carcinogenic risk of low-dose irradiation but rather represents a protective biological mechanism by eliminating these cells. It could be more beneficial for a biological system to remove the damaged cell and replace it by a healthy neighbor cell, instead of repairing the DSBs with the risk of causing genomic instability (10). This model would be of interest when only a small fraction of cells exhibit DSBs, so repair is only necessary at higher levels of damage, for example following high-dose irradiation.

Strikingly, the PCCL3 cells exposed to low-dose irradiation with 0.05 Gy and 0.1 Gy exhibited a significantly lower number of γH2AX foci at early time points of 30 minutes and 1 hour post-treatment compared to sham-irradiated PCCL3 cells. These results indicate hormesis, a hypothesis

suggesting that low-dose irradiation is beneficial. However, approximately around 4 hours post-treatment the number of γH2AX foci in low-dose irradiated cells exceeds the number of γH2AX in sham-irradiated cells, which contradicts the hormesis hypothesis. On the other hand, the number of γH2AX foci in the sham-irradiated cells could be relatively high. Indeed, R. Runge, et al. counted the number of γH2AX foci per nucleus of non-irradiated PCCL3 cells using an automated method (The Aklides algorithms) and measured approximately a mean number of 3 γH2AX foci per cell, while we counted approximately around 6 γH2AX foci per cell (123). The reason for this high mean number is not known. However, it should be mentioned that the presence γH2AX foci is not radiation specific and can also be induced by other stress factors. In contrast to γH2AX foci, the mean number of 53BP1 foci and their kinetics over time is relatively normal. There are no significant differences observed in the mean number of 53BP1 foci and its kinetics between 0.05 Gy-irradiated cells and sham-irradiated cells which could correspond to the basal cellular levels of 53BP1. In contrast, the number of 53BP1 foci reached a peak in cells irradiated with 0.1 Gy or higher up to 3 Gy around 1-4h post-treatment after which the number of 53BP1 foci decreased again to almost basal levels after 24 hours due to DNA repair. It could be possible that irradiation with 0.1 Gy is the threshold level in which PCCL3 cells still accumulate γH2AX foci but are also able to partially recruit 53BP1 to the sites of DNA damage. Another possible model for the increasing γH2AX foci after low-dose irradiation (0.05 Gy and 0.1 Gy) but the decreased 53BP1 foci response after 0.1 Gy could be the failure of dephosphorylation of γH2AX following repair. However, no literature is describing this phenomenon. Finally, although ROS production was enhanced 24h post-treatment in iodine-deficient cells compared to iodine-sufficient cells, there were no major differences observed between iodine-sufficient and iodine-deficient conditions regarding the number of YH2AX and 53BP1 foci at different time points post-treatment.

In conclusion, in order to verify these data, in particularly the continuous increase in γH2AX foci after low-dose irradiation, we could repeat this experiment. Furthermore, it is of interest to investigate the number of γH2AX foci in PCCL3 cells at 48h and 72h after irradiation with low radiation doses (0.05 Gy and 0.1 Gy) to test our speculation of the presence of a DNA damage threshold level (approximately 10 foci per nucleus) required to activate the DDR pathway and induce DNA repair. In addition, in order to test the above described speculations regarding a protective elimination of low-dose irradiated cells with persistent DSBs as a low-dose hyper-radiosensitivity response, it would be of interest to examine apoptosis e.g. by performing TUNEL analysis, and clonogenic assays to investigate the viability and proliferation capacity after irradiation.

Exposure to IR causes perturbations in the cell cycle progression. Ionizing radiation-induced DNA damage activates the DDR pathway which in turn interacts with checkpoint proteins involved in cell cycle arrest at the G0/G1 phase, the S phase or the G2/M phase. These delays provide the required time to repair the damage. An arrest in the G1 phase prevents aberrant replication of damaged DNA, while arrest in the G2 phase avoids cells to segregate defective chromosomes. Cells are most sensitive for the effects of ionizing radiation when they are actively proliferating and thus reside in the M phase or in the G1/S interface (124). In our study, measurements of the cell cycle distribution at 6h, 24h and 48h post-treatment indicated that PCCL3 cells irradiated with low,

intermediate and high radiation doses did not majorly differ in their cell cycle distribution and progression at 6h post-treatment, except for a small significant decrease of iodine-sufficient cells in the G0/G1 phase after irradiation with 3 Gy compared to sham-irradiated control cells. In addition, at this time point, there were no significant differences observed between iodine-deficient and iodine-sufficient cells. However, at 24h post-treatment, the percentage of cells in the G0/G1 phase significantly increased, while the amount of cells in the G2/M phase and S phase significantly decreased after irradiation with 3 Gy compared to sham-irradiated cells for both iodine-sufficient as iodine-deficient cells. These results are in line with Kostic, et al. who also observed a significant G1 block with a decreased amount of cells in the S phase in human thyroid cells at 24 hours after irradiation with short-wavelength ultraviolet light (UVC), the most damaging and energetic type of UV light (125). According to Jiri Bartek, et al., there exist two distinctive waves of checkpoint responses at the G1/S interface **(Supplemental Figure 14)**. The initial transient respond is very rapid and inhibits cyclin-dependent kinase 2 within 20 to 30 minutes and can last for several hours. This prompt cell cycle delay is independent of p53 and protein transcription. It temporarily slows down the cell cycle progression to provide more time for DNA repair. The second response is delayed and considerable more sustained. This response is activated by the classical p53/p21 cascade, which is a multistep process involving induction of effector proteins which requires several hours. This delay is more suitable for repair of highly complex DNA damages or for elimination of cells with severely damaged DNA. The latter is supported by the ability of the p53-pathway to induce apoptosis (126). Although we observed γH2AX and 53BP1 foci, associated with DSBs, around respectively 30 minutes to 4 hours post-treatment, we did not observe a cell cycle arrest 6 hours post-treatment. It could be possible that we missed an early wave of cell cycle arrest at this time point. On the other hand, a significant but not a complete loss of γH2AX and 53BP1 foci, associated with DNA repair, was observed 24 hours post-treatment. At this point, we detected a significant G1 arrest. This could represent the delayed p53-dependent G1 arrest in response to severe and complex DNA damage induced by high irradiation doses. This is supported by William G. Nelson, et al. who demonstrated that DNA strand breaks, especially DSBs, which are typically induced by IR, appeared to be very efficient at triggering p53 protein up-regulation compared to other types of genomic insults (127). However, to ensure the G1 arrest is p53-dependent, we could knockdown p53 in thyroid cells and examine if the G1 arrest will still occur 24 hours after irradiation with 3 Gy. The occurrence of a G1 arrest in irradiated cells is correlated with their radiosensitivity.

Following low-dose and intermediate-dose exposure, there is no significant G1 arrest compared to sham-irradiated cells. This indicates that the PCCL3 cells are relatively radioresistance, since there only occurs a G1 arrest after irradiation with 3 Gy. However, there are differences observed between iodine-sufficient and iodine-deficient cells in which there is a decreased number of cells in the G0/G1 phase and an increased number of cells in the G2/M phase and S phase under iodine-deficient conditions. This trend is observed after irradiation with low, intermediate and high radiation doses, but not in sham-irradiated cells. Therefore, this could indicate that a treatment with low-dose or intermediate-dose irradiation alone, or ID alone does not majorly change the cell cycle progression, while a combined treatment with IR and ID makes PCCL3 cells less sensitive for a G1 arrest and even enhance their proliferation. This could represent a stress-response with

subtle changes in the cellular proliferation pathways, which could be triggered by the enhanced ROS production of the co-treatment as indicated by the ROS assay 24 hours post-treatment, with ID as a promoting factor stimulating the effects of IR. Since there was no complete loss of γH2AX and 53BP1 foci yet at 24h post-treatment, an enhanced proliferation could potentially lead to accumulation of DNA damage increasing the mutation rate and the risk on malignant transformation. Finally, 48h post-treatment, PCCL3 cells irradiated with 3 Gy still exhibited a disturbed cell cycle with a small but significant decreased number of iodine-sufficient and iodine-deficient cells in the S phase compared to the corresponding sham-irradiated cells. Furthermore, there were significantly more iodine-sufficient cells in the G0/G1 phase after irradiation with 3 Gy compared to sham-irradiated cells. However, there were no longer significant differences detected between iodine-deficient and iodine-sufficient cells. This suggests that PCCL3 cells exposed to a combined treatment of low-dose or intermediate-dose irradiation and ID are able to restore their normal cell cycle progression after 48h post-treatment, indicating a transient stress response.

Since the ROS/HIF-1/VEGF-A pathway is activated approximately around 2-6 hours post-ID in PCCL3 cells and since changes in protein expression were observed in FRTL5 cells already at 6 hours post-treatment, we investigated the combined effect of IR and ID on the protein expression in PCCL3 cells at 6 hours post-treatment by performing Western blot analysis. In this study, we first focused on the ROS/HIF-1/VEGF-A pathway. Craps, et al. demonstrated that NO, which is produced by NOS3, is able to stabilize HIF-1α. Indeed, they observed an increased activated phosphorylation of NOS3 and HIF-1α protein expression in human thyroid cells, FRTL5 cells and PCCL3 cells at 4-6 hours post-ID. In this study, we tried to verify these data in PCCL3 cells that were iodine deprived for 6 hours and we tried to find a possible enhanced effect on HIF-1α and NOS3 protein expression when combined with irradiation with low, intermediate or high irradiation doses. The identity of the additional ≈80 kDa protein band that we detected for HIF-1α protein expression is unknown. However, this band is also detected in Western blot results from Life science companies Abcam and Cell Signaling. We used the primary anti-HIF-1α antibody of Cell Signaling. Although this band is not fully characterized, it is suggested to be a degradation or cleavage product of HIF-1α in samples that have experienced multiple freeze-thaw cycles. The identity of the additional ≈70 kDa band that we detected for (pSer1177) NOS3 protein expression is also unknown, but is detected as well in Western blot results from Life science company Abcam. Furthermore, A. Persu, et al. also observed a 70 kDa protein band using primary antibodies from Santa Cruz on endothelial cell lysates submitted to repeated freeze-thaw cycles. They suggested that it might correspond to a proteolytic cleavage product of eNOS containing its C-terminus (128). We used the primary anti-eNOS3 antibody of BD Biosciences which is also directed against the C-terminus of eNOS type III, and thus may also bind to this potential 70 kDa cleavage product. Although we used the same cell line and the same culture method as the research group of J Craps, we were unable to reproduce the described data.

To investigate the effects of IR and ID on the proliferation and survival of PCCL3 cells, we investigated the protein expression of major key factors involved in proliferation and survival pathways at 6 hours post-treatment performing Western blot analysis. We specifically investigated (pY705)STAT3, (pThr308)AKT1 and NFκB p52. The additional 55 kDa protein band that we

detected for AKT1 expression is not identified. This could represent an alternative splice variant or a putative isoform. The 86 kDa and 91 kDa protein bands detected for STAT3 protein expression correspond to respectively the STAT3β and STAT3α isoforms. Furthermore, the additional 160 kDa protein band detected for pY705 STAT3 protein expression could represent a putative dimerisation of activated pSTAT3 in order to enable nuclear translocation, DNA binding and transcriptional activation. We were unable to detect significant differences in protein expressions between the radiation doses and between iodine-sufficient and iodine-deficient cells. Since we did not observe any differences in the cell cycle distribution between sham-, low-, intermediate- and high-dose irradiated PCCL3 cells and between iodine-sufficient and iodine-deficient PCCL3 cells at 6h post-treatment, it is assumable that there are also no differences detected in the expression of proteins which stimulate proliferation at this time point post-treatment. However, a significant increase was detected in the amount of iodine-deficient, irradiated PCCL3 cells in the S phase and G2/M phase at 24 hours post-treatment compared to iodine-sufficient, irradiated PCCL3 cells. Therefore, it would be of interest also to investigate the protein expressions in PCCL3 cells at 24 hours post-treatment.

We cannot ignore the high standard deviations present in the Western blot results. This also contributes to the absence of significance between the different treatment groups and the controls, especially when the effects on protein expression are small. First of all, it would be beneficial to increase the number of the biological replicates per condition to increase the statistical power of the experiments. However, it would also be of interest to investigate if we observe these data because there is no real effect present of IR and ID on protein expression at this time point representing only the variance in the cell cultures or due to variances in the Western blot protocol and/or experimental environment. The following experimental design could investigate this **(Supplemental Figure 15)**. Three to six biological replicates could be treated with ID and/or IR of different radiation doses to create the experimental conditions. Then, in order to determine if the variance is deriving from the Western blot protocol, Western blotting of one specific biological replicate could be performed three times in parallel on one day. If the Western blot protocol is reproducible, then one can expect to obtain the same results from each Western blot experiment. In order to assess if the variance is deriving from environmental factors such as temperature, incubation times, content of the washing buffer and blocking buffer, etc. Western blotting of three to six biological replicates could be performed on three different days. If environmental factors do not affect the results, then one could expect to obtain the same results for each Western blot experiment per biological replicate. If these experiments rule out the origin of the variance from environmental factors or the Western blot protocol, then it can be concluded that there is no real effect of IR and ID on the protein expression in treated PCCL3 cells on that specific time point post-treatment. Optimization of the Western blot protocol is possible by examining the effects on the results by changing the blocking buffer (e.g. BSA or non-fat dry milk), the washing buffer (e.g. PBS-T or TBT-T) and the protein detection method (e.g. with quantum dots or with ECL chemiluminscence) or by changing the incubation times of the blots in the washing buffer and blocking buffer. There are also other techniques to investigate protein expression such as immunocytochemistry and ELISA. The latter is a very sensitive techniques and easy to quantify.

Finally, along with alterations in the cell cycle progression and protein expression, changes in gene expression are also a major component in stress responses. The control of gene expression is tightly regulated and enables the cell to change its transcriptional capacity with much faster response kinetics compared to *de novo* protein synthesis. Therefore, it might be a more initial adaptive response to stress which can be visualized at earlier time points post-treatment compared to changes in protein expression (129). It could be possible that at 6 hours post-treatment, changes in gene expression can be detected by RT-qPCR. However, due to a lack of time, it was not possible to investigate real-time gene expression in PCCL3 cells in response to IR and ID. However, an interesting gene to examine is NQO1, which appears to be up-regulated in primary human thyroid cells from microarray data. NQO1 is known as a multifunctional cytoprotective and antioxidant enzyme. On the other hand, Selmansberger, et al. showed that CLIP2 is up-regulated in post-Chernobyl pediatric PTCs. They suggest the involvement of CLIP2 in fundamental carcinogenic processes including apoptosis, MAPK signaling and genomic instability (130). Other interesting genes to examine are genes, which are involved in DNA repair, antioxidant defense, apoptosis, cellular proliferation and survival.

At the start of this project, we hypothesized that a combined treatment of PCCL3 thyroid cells to ID and IR leads to an enhanced ROS production, which will eventually affect cellular proliferation, survival and resistance to apoptosis. The findings of these studies indicate that iodine-deficient thyroid cells exposed to intermediate and high irradiation doses (0.05 Gy and 3 Gy) showed a significantly increased ROS production 24 hours post-treatment compared to iodine-sufficient cells. This suggests that irradiation with a dose of 0.5 Gy or higher stress the thyroid cells to a certain extent which makes them unable to cope with the additional oxidative stress originating from ID, leading to a significant higher accumulation of ROS compared to irradiated PCCL3 cells cultured in the presence of iodine. When we then examined the extent of DSBs induced by the co-treatment of IR and ID and their repair kinetics, we can conclude that the extent of DNA damage is radiation dose dependent and is not enhanced by iodine deficiency. Furthermore, we can also conclude that the response of PCCL3 cells after low-dose radiation exposure regarding DNA damage repair is different from PCCL3 cells exposed to high-dose radiation, suggesting the presence of a DNA damage threshold level required for an efficient activation of the DDR pathway and subsequent DSB repair. Finally, from the cell cycle data, we can summarize that PCCL3 cells are relatively radioresistance since only after irradiation with 3 Gy, a significant delayed p53-dependent G1 arrest is induced when compared to sham-irradiated cells. Furthermore, a co-treatment of ID and irradiation with low-, intermediate- and high-radiation doses enhances proliferation of the PCCL3 and makes them less sensitive for a G1 arrest. This is an important observation, since this can increase the mutation rate and the risk on carcinogenic transformation when DNA damage is not fully repaired in the actively proliferating PCCL3 cells. Finally, expanding upon the current study with the use of primary human thyroid cells would help to extrapolate the effects of IR exposure and iodine deficiency in humans.

REFERENCES

1. White BA, Porterfield SP. Endocrine and Reproductive Physiology. 4th ed. ed. Philadelphia: Elsevier Mosby; 2013.
2. Nikiforov YE, Nikiforova MN. Molecular genetics and diagnosis of thyroid cancer. Nature reviews Endocrinology. 2011;7(10):569-80.
3. Nikiforova MN, Nikiforov YE. Molecular diagnostics and predictors in thyroid cancer. Thyroid : official journal of the American Thyroid Association. 2009;19(12):1351-61.
4. Xing M. Molecular pathogenesis and mechanisms of thyroid cancer. Nature reviews Cancer. 2013;13(3):184-99.
5. LiVolsi VA. Papillary thyroid carcinoma: an update. Modern pathology : an official journal of the United States and Canadian Academy of Pathology, Inc. 2011;24 Suppl 2:S1-9.
6. Registry BC. Cancer Incidence in Belgium, 2008. Brussels2011.
7. Yu GP, Li JC, Branovan D, McCormick S, Schantz SP. Thyroid cancer incidence and survival in the national cancer institute surveillance, epidemiology, and end results race/ethnicity groups. Thyroid : official journal of the American Thyroid Association. 2010;20(5):465-73.
8. Zimmermann MB, Galetti V. Iodine intake as a risk factor for thyroid cancer: a comprehensive review of animal and human studies. Thyroid research. 2015;8:8.
9. Navarro Silvera SA, Miller AB, Rohan TE. Risk factors for thyroid cancer: a prospective cohort study. International journal of cancer Journal international du cancer. 2005;116(3):433-8.
10. Rothkamm K, Lobrich M. Evidence for a lack of DNA double-strand break repair in human cells exposed to very low x-ray doses. Proceedings of the National Academy of Sciences of the United States of America. 2003;100(9):5057-62.
11. Statkiewicz Sherer MA, Visconti PJ, Ritenour ER, Haynes K. Radiation Protection in Medical Radiography. 7th ed. Elsevier Mosby; 2015.
12. Wei H, K N Y. Ionizing Radiation, DNA Double Strand Break and Mutation In: Urbano KV, editor. Advances in Genetics Research 4: Nova Science Publishers 2010.
13. Chen CC, Motegi A, Hasegawa Y, Myung K, Kolodner R, D'Andrea A. Genetic analysis of ionizing radiation-induced mutagenesis in Saccharomyces cerevisiae reveals TransLesion Synthesis (TLS) independent of PCNA K164 SUMOylation and ubiquitination. DNA repair. 2006;5(12):1475-88.
14. Mullenders L, Atkinson M, Paretzke H, Sabatier L, Bouffler S. Assessing cancer risks of low-dose radiation. Nature reviews Cancer. 2009;9(8):596-604.
15. Miron SD, Astarastoae V. Long-term biological effects induced by ionizing radiation--implications for dose mediated risk. Revista medico-chirurgicala a Societatii de Medici si Naturalisti din Iasi. 2014;118(3):717-23.
16. Lin EC. Radiation risk from medical imaging. Mayo Clinic proceedings. 2010;85(12):1142-6; quiz 6.
17. Little MP, Wakeford R, Tawn EJ, Bouffler SD, Berrington de Gonzalez A. Risks associated with low doses and low dose rates of ionizing radiation: why linearity may be (almost) the best we can do. Radiology. 2009;251(1):6-12.
18. Imaizumi M, Usa T, Tominaga T, Neriishi K, Akahoshi M, Nakashima E, et al. Radiation dose-response relationships for thyroid nodules and autoimmune thyroid diseases in Hiroshima and Nagasaki atomic bomb survivors 55-58 years after radiation exposure. Jama. 2006;295(9):1011-22.
19. Ron E, Lubin JH, Shore RE, Mabuchi K, Modan B, Pottern LM, et al. Thyroid cancer after exposure to external radiation: a pooled analysis of seven studies. Radiation research. 1995;141(3):259-77.
20. Committee to Assess Health Risks from Exposure to Low Levels of Ionizing Radiation BoRER, Division on Earth and Life Studies, National Research Council. Health Risks from Exposure to Low Levels of Ionizing Radiation:: BEIR VII Phase 2: National Academies Press; 2006. 424 p.
21. Su YP, Niu HW, Chen JB, Fu YH, Xiao GB, Sun QF. Radiation dose in the thyroid and the thyroid cancer risk attributable to CT scans for pediatric patients in one general hospital of China. International journal of environmental research and public health. 2014;11(3):2793-803.
22. Tsuda T, Tokinobu A, Yamamoto E, Suzuki E. Thyroid Cancer Detection by Ultrasound Among Residents Ages 18 Years and Younger in Fukushima, Japan: 2011 to 2014. Epidemiology (Cambridge, Mass). 2016;27(3):316-22.
23. Furukawa K, Preston D, Funamoto S, Yonehara S, Ito M, Tokuoka S, et al. Long-term trend of thyroid cancer risk among Japanese atomic-bomb survivors: 60 years after exposure. International journal of cancer Journal international du cancer. 2013;132(5):1222-6.

24. Zablotska LB, Ron E, Rozhko AV, Hatch M, Polyanskaya ON, Brenner AV, et al. Thyroid cancer risk in Belarus among children and adolescents exposed to radioiodine after the Chornobyl accident. British journal of cancer. 2011;104(1):181-7.
25. Yamashita S, Suzuki S. Risk of thyroid cancer after the Fukushima nuclear power plant accident. Respiratory investigation. 2013;51(3):128-33.
26. Dreger S, Pfinder M, Christianson L, Lhachimi SK, Zeeb H. The effects of iodine blocking following nuclear accidents on thyroid cancer, hypothyroidism, and benign thyroid nodules: design of a systematic review. Systematic reviews. 2015;4:126.
27. Cardis E, Hatch M. The Chernobyl accident--an epidemiological perspective. Clinical oncology (Royal College of Radiologists (Great Britain)). 2011;23(4):251-60.
28. Reiners C. Clinical experiences with radiation induced thyroid cancer after chernobyl. Genes. 2011;2(2):374-83.
29. White SC, Mallya SM. Update on the biological effects of ionizing radiation, relative dose factors and radiation hygiene. Australian dental journal. 2012;57 Suppl 1:2-8.
30. UNSCEAR. Sources of Ionizing Radiation: Medical radiation exposures. New York: 2008 Contract No.: Annex A.
31. Lee NY, Le QT. New developments in radiation therapy for head and neck cancer: intensity-modulated radiation therapy and hypoxia targeting. Seminars in oncology. 2008;35(3):236-50.
32. Inskip PD. Thyroid cancer after radiotherapy for childhood cancer. Medical and pediatric oncology. 2001;36(5):568-73.
33. Green DM, Hyland A, Barcos MP, Reynolds JA, Lee RJ, Hall BC, et al. Second malignant neoplasms after treatment for Hodgkin's disease in childhood or adolescence. Journal of clinical oncology : official journal of the American Society of Clinical Oncology. 2000;18(7):1492-9.
34. Bhatia S, Yasui Y, Robison LL, Birch JM, Bogue MK, Diller L, et al. High risk of subsequent neoplasms continues with extended follow-up of childhood Hodgkin's disease: report from the Late Effects Study Group. Journal of clinical oncology : official journal of the American Society of Clinical Oncology. 2003;21(23):4386-94.
35. Somerville HM, Steinbeck KS, Stevens G, Delbridge LW, Lam AH, Stevens MM. Thyroid neoplasia following irradiation in adolescent and young adult survivors of childhood cancer. The Medical journal of Australia. 2002;176(12):584-7.
36. Sigurdson AJ, Ronckers CM, Mertens AC, Stovall M, Smith SA, Liu Y, et al. Primary thyroid cancer after a first tumour in childhood (the Childhood Cancer Survivor Study): a nested case-control study. Lancet (London, England). 2005;365(9476):2014-23.
37. Lawrence L, Kwan-Hoong N. Radiological Safety and Quality: Paradigms in Leadership and Innovation. Springer Science & Business Media; 2013. p. 471.
38. Vanmarcke H, Bosmans H, Eggermont G, editors. Ionizing radiation exposure of the Belgian population in 2006. Proceedings of Third European IRPA Congress; 2010; Helsinki, Finland.
39. Mettler FA, Jr., Wiest PW, Locken JA, Kelsey CA. CT scanning: patterns of use and dose. Journal of radiological protection : official journal of the Society for Radiological Protection. 2000;20(4):353-9.
40. Mazonakis M, Tzedakis A, Damilakis J, Gourtsoyiannis N. Thyroid dose from common head and neck CT examinations in children: is there an excess risk for thyroid cancer induction? European radiology. 2007;17(5):1352-7.
41. Brenner DJ, Doll R, Goodhead DT, Hall EJ, Land CE, Little JB, et al. Cancer risks attributable to low doses of ionizing radiation: assessing what we really know. Proceedings of the National Academy of Sciences of the United States of America. 2003;100(24):13761-6.
42. Ory C, Ugolin N, Schlumberger M, Hofman P, Chevillard S. Discriminating gene expression signature of radiation-induced thyroid tumors after either external exposure or internal contamination. Genes. 2011;3(1):19-34.
43. Luckey TD. Radiation hormesis: the good, the bad, and the ugly. Dose-response : a publication of International Hormesis Society. 2006;4(3):169-90.
44. Ina Y, Sakai K. Prolongation of life span associated with immunological modification by chronic low-dose-rate irradiation in MRL-lpr/lpr mice. Radiation research. 2004;161(2):168-73.
45. Feinendegen LE. Evidence for beneficial low level radiation effects and radiation hormesis. The British journal of radiology. 2005;78(925):3-7.
46. Kaiser J. Hormesis. A healthful dab of radiation? Science (New York, NY). 302. United States2003. p. 378.
47. Redpath JL. Radiation-induced neoplastic transformation in vitro: evidence for a protective effect at low doses of low LET radiation. Cancer metastasis reviews. 2004;23(3-4):333-9.
48. Portulano C, Paroder-Belenitsky M, Carrasco N. The Na+/I- symporter (NIS): mechanism and medical impact. Endocrine reviews. 2014;35(1):106-49.
49. Gerard AC, Humblet K, Wilvers C, Poncin S, Derradji H, de Ville de Goyet C, et al. Iodine-deficiency-induced long lasting angiogenic reaction in thyroid cancers occurs via a vascular endothelial growth factor-hypoxia inducible factor-1-dependent, but not a reactive oxygen species-

dependent, pathway. Thyroid : official journal of the American Thyroid Association. 2012;22(7):699-708.
50. Pearce EN, Andersson M, Zimmermann MB. Global iodine nutrition: Where do we stand in 2013? Thyroid : official journal of the American Thyroid Association. 2013;23(5):523-8.
51. Dal Maso L, Bosetti C, La Vecchia C, Franceschi S. Risk factors for thyroid cancer: an epidemiological review focused on nutritional factors. Cancer causes & control : CCC. 2009;20(1):75-86.
52. Knudsen N, Bulow I, Jorgensen T, Laurberg P, Ovesen L, Perrild H. Goitre prevalence and thyroid abnormalities at ultrasonography: a comparative epidemiological study in two regions with slightly different iodine status. Clinical endocrinology. 2000;53(4):479-85.
53. Knudsen N, Laurberg P, Perrild H, Bulow I, Ovesen L, Jorgensen T. Risk factors for goiter and thyroid nodules. Thyroid : official journal of the American Thyroid Association. 2002;12(10):879-88.
54. Carle A, Krejbjerg A, Laurberg P. Epidemiology of nodular goitre. Influence of iodine intake. Best practice & research Clinical endocrinology & metabolism. 2014;28(4):465-79.
55. Campbell MJ, Seib CD, Candell L, Gosnell JE, Duh QY, Clark OH, et al. The underestimated risk of cancer in patients with multinodular goiters after a benign fine needle aspiration. World journal of surgery. 2015;39(3):695-700.
56. La Vecchia C, Malvezzi M, Bosetti C, Garavello W, Bertuccio P, Levi F, et al. Thyroid cancer mortality and incidence: a global overview. International journal of cancer Journal international du cancer. 2015;136(9):2187-95.
57. Feldt-Rasmussen U. Iodine and cancer. Thyroid : official journal of the American Thyroid Association. 2001;11(5):483-6.
58. Bacher-Stier C, Riccabona G, Totsch M, Kemmler G, Oberaigner W, Moncayo R. Incidence and clinical characteristics of thyroid carcinoma after iodine prophylaxis in an endemic goiter country. Thyroid : official journal of the American Thyroid Association. 1997;7(5):733-41.
59. Besic N, Hocevar M, Zgajnar J. Lower incidence of anaplastic carcinoma after higher iodination of salt in Slovenia. Thyroid : official journal of the American Thyroid Association. 2010;20(6):623-6.
60. Farahati J, Geling M, Mader U, Mortl M, Luster M, Muller JG, et al. Changing trends of incidence and prognosis of thyroid carcinoma in lower Franconia, Germany, from 1981-1995. Thyroid : official journal of the American Thyroid Association. 2004;14(2):141-7.
61. Pettersson B, Coleman MP, Ron E, Adami HO. Iodine supplementation in Sweden and regional trends in thyroid cancer incidence by histopathologic type. International journal of cancer Journal international du cancer. 1996;65(1):13-9.
62. Axelrad AA, Leblond CP. Induction of thyroid tumors in rats by a low iodine diet. Cancer. 1955;8(2):339-67.
63. Isler H, Leblond CP, Axelrad AA. Influence of age and of iodine intake on the production of thyroid tumors in the rat. Journal of the National Cancer Institute. 1958;21(6):1065-81.
64. Isler H. Effect of iodine on thyroid tumors induced in the rat by a low-iodine diet. Journal of the National Cancer Institute. 1959;23:675-93.
65. Schaller RT, Jr., Stevenson JK. Development of carcinoma of the thyroid in iodine-deficient mice. Cancer. 1966;19(8):1063-80.
66. Fortner JG, George PA, Sternberg SS. The development of thyroid cancer and other abnormalities in Syrian hamsters maintained on an iodine deficient diet. Surgical forum. 1958;9:646-50.
67. al-Saadi AA, Beierwaltes WH. Chromosomal changes in rat thyroid cells during iodine depletion and repletion. Cancer research. 1966;26(4):676-88.
68. Gerard AC, Poncin S, Caetano B, Sonveaux P, Audinot JN, Feron O, et al. Iodine deficiency induces a thyroid stimulating hormone-independent early phase of microvascular reshaping in the thyroid. The American journal of pathology. 2008;172(3):748-60.
69. Gerard AC, Poncin S, Audinot JN, Denef JF, Colin IM. Iodide deficiency-induced angiogenic stimulus in the thyroid occurs via HIF- and ROS-dependent VEGF-A secretion from thyrocytes. American journal of physiology Endocrinology and metabolism. 2009;296(6):E1414-22.
70. Craps J, Wilvers C, Joris V, De Jongh B, Vanderstraeten J, Lobysheva I, et al. Involvement of nitric oxide in iodine deficiency-induced microvascular remodeling in the thyroid gland: role of nitric oxide synthase 3 and ryanodine receptors. Endocrinology. 2015;156(2):707-20.
71. Golkowski F, Szybinski Z, Rachtan J, Sokolowski A, Buziak-Bereza M, Trofimiuk M, et al. Iodine prophylaxis--the protective factor against stomach cancer in iodine deficient areas. European journal of nutrition. 2007;46(5):251-6.
72. Aceves C, Anguiano B, Delgado G. Is iodine a gatekeeper of the integrity of the mammary gland? Journal of mammary gland biology and neoplasia. 2005;10(2):189-96.

73. Venturi S, Donati FM, Venturi A, Venturi M, Grossi L, Guidi A. Role of iodine in evolution and carcinogenesis of thyroid, breast and stomach. Advances in clinical pathology : the official journal of Adriatic Society of Pathology. 2000;4(1):11-7.
74. Tabaeizadeh M, Haghpanah V, Keshtkar A, Semnani S, Roshandel G, Adabi K, et al. Goiter frequency is more strongly associated with gastric adenocarcinoma than urine iodine level. Journal of gastric cancer. 2013;13(2):106-10.
75. Aceves C, Anguiano B, Delgado G. The extrathyronine actions of iodine as antioxidant, apoptotic, and differentiation factor in various tissues. Thyroid : official journal of the American Thyroid Association. 2013;23(8):938-46.
76. Leung AM, Braverman LE. Consequences of excess iodine. Nature reviews Endocrinology. 2014;10(3):136-42.
77. Shakhtarin VV, Tsyb AF, Stepanenko VF, Orlov MY, Kopecky KJ, Davis S. Iodine deficiency, radiation dose, and the risk of thyroid cancer among children and adolescents in the Bryansk region of Russia following the Chernobyl power station accident. International journal of epidemiology. 2003;32(4):584-91.
78. Cardis E, Kesminiene A, Ivanov V, Malakhova I, Shibata Y, Khrouch V, et al. Risk of thyroid cancer after exposure to 131I in childhood. Journal of the National Cancer Institute. 2005;97(10):724-32.
79. Boice JD, Jr. Radiation-induced thyroid cancer--what's new? Journal of the National Cancer Institute. 97. United States2005. p. 703-5.
80. Boltze C, Brabant G, Dralle H, Gerlach R, Roessner A, Hoang-Vu C. Radiation-induced thyroid carcinogenesis as a function of time and dietary iodine supply: an in vivo model of tumorigenesis in the rat. Endocrinology. 2002;143(7):2584-92.
81. Ward JM, Ohshima M. The role of iodine in carcinogenesis. Advances in experimental medicine and biology. 1986;206:529-42.
82. Poncin S, Gerard AC, Boucquey M, Senou M, Calderon PB, Knoops B, et al. Oxidative stress in the thyroid gland: from harmlessness to hazard depending on the iodine content. Endocrinology. 2008;149(1):424-33.
83. Xing M. Oxidative stress: a new risk factor for thyroid cancer. Endocrine-related cancer. 2012;19(1):C7-11.
84. Aslan M, Cosar N, Celik H, Aksoy N, Dulger AC, Begenik H, et al. Evaluation of oxidative status in patients with hyperthyroidism. Endocrine. 2011;40(2):285-9.
85. Torun AN, Kulaksizoglu S, Kulaksizoglu M, Pamuk BO, Isbilen E, Tutuncu NB. Serum total antioxidant status and lipid peroxidation marker malondialdehyde levels in overt and subclinical hypothyroidism. Clinical endocrinology. 2009;70(3):469-74.
86. Erdamar H, Demirci H, Yaman H, Erbil MK, Yakar T, Sancak B, et al. The effect of hypothyroidism, hyperthyroidism, and their treatment on parameters of oxidative stress and antioxidant status. Clinical chemistry and laboratory medicine. 2008;46(7):1004-10.
87. Erdamar H, Cimen B, Gulcemal H, Saraymen R, Yerer B, Demirci H. Increased lipid peroxidation and impaired enzymatic antioxidant defense mechanism in thyroid tissue with multinodular goiter and papillary carcinoma. Clinical biochemistry. 2010;43(7-8):650-4.
88. Wang D, Feng JF, Zeng P, Yang YH, Luo J, Yang YW. Total oxidant/antioxidant status in sera of patients with thyroid cancers. Endocrine-related cancer. 2011;18(6):773-82.
89. Lobrich M, Rief N, Kuhne M, Heckmann M, Fleckenstein J, Rube C, et al. In vivo formation and repair of DNA double-strand breaks after computed tomography examinations. Proceedings of the National Academy of Sciences of the United States of America. 2005;102(25):8984-9.
90. Rube CE, Grudzenski S, Kuhne M, Dong X, Rief N, Lobrich M, et al. DNA double-strand break repair of blood lymphocytes and normal tissues analysed in a preclinical mouse model: implications for radiosensitivity testing. Clinical cancer research : an official journal of the American Association for Cancer Research. 2008;14(20):6546-55.
91. Kuo LJ, Yang LX. Gamma-H2AX - a novel biomarker for DNA double-strand breaks. In vivo (Athens, Greece). 2008;22(3):305-9.
92. Iliakis G, Wang Y, Guan J, Wang H. DNA damage checkpoint control in cells exposed to ionizing radiation. Oncogene. 2003;22(37):5834-47.
93. Norbury CJ, Zhivotovsky B. DNA damage-induced apoptosis. Oncogene. 2004;23(16):2797-808.
94. Lomax ME, Folkes LK, O'Neill P. Biological consequences of radiation-induced DNA damage: relevance to radiotherapy. Clinical oncology (Royal College of Radiologists (Great Britain)). 2013;25(10):578-85.
95. Narang H, Krishna M. Mitogen-activated protein kinases: specificity of response to dose of ionizing radiation in liver. Journal of radiation research. 2004;45(2):213-20.
96. Evan GI, Vousden KH. Proliferation, cell cycle and apoptosis in cancer. Nature. 2001;411(6835):342-8.

97. Reuter S, Gupta SC, Chaturvedi MM, Aggarwal BB. Oxidative stress, inflammation, and cancer: how are they linked? Free radical biology & medicine. 2010;49(11):1603-16.
98. Sofia Vala I, Martins LR, Imaizumi N, Nunes RJ, Rino J, Kuonen F, et al. Low doses of ionizing radiation promote tumor growth and metastasis by enhancing angiogenesis. PloS one. 2010;5(6):e11222.
99. Osaki M, Oshimura M, Ito H. PI3K-Akt pathway: its functions and alterations in human cancer. Apoptosis : an international journal on programmed cell death. 2004;9(6):667-76.
100. Zhan M, Han ZC. Phosphatidylinositide 3-kinase/AKT in radiation responses. Histology and histopathology. 2004;19(3):915-23.
101. Ahmed KM, Li JJ. NF-kappa B-mediated adaptive resistance to ionizing radiation. Free radical biology & medicine. 2008;44(1):1-13.
102. Karin M. How NF-kappaB is activated: the role of the IkappaB kinase (IKK) complex. Oncogene. 1999;18(49):6867-74.
103. Basseres DS, Baldwin AS. Nuclear factor-kappaB and inhibitor of kappaB kinase pathways in oncogenic initiation and progression. Oncogene. 2006;25(51):6817-30.
104. Criswell T, Leskov K, Miyamoto S, Luo G, Boothman DA. Transcription factors activated in mammalian cells after clinically relevant doses of ionizing radiation. Oncogene. 2003;22(37):5813-27.
105. Brach MA, Hass R, Sherman ML, Gunji H, Weichselbaum R, Kufe D. Ionizing radiation induces expression and binding activity of the nuclear factor kappa B. The Journal of clinical investigation. 1991;88(2):691-5.
106. Jin S, Borkhuu O, Bao W, Yang YT. Signaling Pathways in Thyroid Cancer and Their Therapeutic Implications. Journal of clinical medicine research. 2016;8(4):284-96.
107. Trovato M, Grosso M, Vitarelli E, Ruggeri RM, Alesci S, Trimarchi F, et al. Distinctive expression of STAT3 in papillary thyroid carcinomas and a subset of follicular adenomas. Histology and histopathology. 2003;18(2):393-9.
108. Sosonkina N, Starenki D, Park JI. The Role of STAT3 in Thyroid Cancer. Cancers. 2014;6(1):526-44.
109. Zhang J, Gill A, Atmore B, Johns A, Delbridge L, Lai R, et al. Upregulation of the signal transducers and activators of transcription 3 (STAT3) pathway in lymphatic metastases of papillary thyroid cancer. International journal of clinical and experimental pathology. 2011;4(4):356-62.
110. Lau J, Ilkhanizadeh S, Wang S, Miroshnikova YA, Salvatierra NA, Wong RA, et al. STAT3 Blockade Inhibits Radiation-Induced Malignant Progression in Glioma. Cancer research. 2015;75(20):4302-11.
111. (WH0) WHO. Ionizing radiation, health effects and protective measures. 2016.
112. Nadolnik LI, Valentyukevich OI. Peculiarities of the antioxidant status of the thyroid gland. Bulletin of experimental biology and medicine. 2007;144(4):529-31.
113. Poncin S, Colin IM, Gerard AC. Minimal oxidative load: a prerequisite for thyroid cell function. The Journal of endocrinology. 2009;201(1):161-7.
114. Song Y, Driessens N, Costa M, De Deken X, Detours V, Corvilain B, et al. Roles of hydrogen peroxide in thyroid physiology and disease. The Journal of clinical endocrinology and metabolism. 2007;92(10):3764-73.
115. Massart C, Hoste C, Virion A, Ruf J, Dumont JE, Van Sande J. Cell biology of H2O2 generation in the thyroid: investigation of the control of dual oxidases (DUOX) activity in intact ex vivo thyroid tissue and cell lines. Molecular and cellular endocrinology. 2011;343(1-2):32-44.
116. Bjorkman U, Ekholm R. Hydrogen peroxide degradation and glutathione peroxidase activity in cultures of thyroid cells. Molecular and cellular endocrinology. 1995;111(1):99-107.
117. Gerard AC, Many MC, Daumerie C, Knoops B, Colin IM. Peroxiredoxin 5 expression in the human thyroid gland. Thyroid : official journal of the American Thyroid Association. 2005;15(3):205-9.
118. Driessens N, Versteyhe S, Ghaddhab C, Burniat A, De Deken X, Van Sande J, et al. Hydrogen peroxide induces DNA single- and double-strand breaks in thyroid cells and is therefore a potential mutagen for this organ. Endocrine-related cancer. 2009;16(3):845-56.
119. Mariotti LG, Pirovano G, Savage KI, Ghita M, Ottolenghi A, Prise KM, et al. Use of the gamma-H2AX assay to investigate DNA repair dynamics following multiple radiation exposures. PloS one. 2013;8(11):e79541.
120. Anderson L, Henderson C, Adachi Y. Phosphorylation and rapid relocalization of 53BP1 to nuclear foci upon DNA damage. Molecular and cellular biology. 2001;21(5):1719-29.
121. Zhang X, Ye C, Sun F, Wei W, Hu B, Wang J. Both Complexity and Location of DNA Damage Contribute to Cellular Senescence Induced by Ionizing Radiation. PloS one. 2016;11(5):e0155725.
122. Grudzenski S, Raths A, Conrad S, Rube CE, Lobrich M. Inducible response required for repair of low-dose radiation damage in human fibroblasts. Proceedings of the National Academy of Sciences of the United States of America. 2010;107(32):14205-10.

123. Runge R, Wendisch M, Wunderlich G, Roggenbuck D, Hiemann R, Kasten-Pisula A, et al. Visual and automatic interpretation of yH2AX immunofluorescence microscopy images after irradiation with open radionuclides. Germany: Technical University Dresden, 2010.
124. Chaudhry MA. Base excision repair of ionizing radiation-induced DNA damage in G1 and G2 cell cycle phases. Cancer cell international. 2007;7:15.
125. Kostic I, Toffoletto B, Toller M, Beltrami CA, Ambesi-Impiombato FS, Curcio F. UVC radiation-induced effect on human primary thyroid cell proliferation and HLA-DR expression. Hormone and metabolic research = Hormon- und Stoffwechselforschung = Hormones et metabolisme. 2010;42(12):846-53.
126. Bartek J, Lukas J. Pathways governing G1/S transition and their response to DNA damage. FEBS letters. 2001;490(3):117-22.
127. Nelson WG, Kastan MB. DNA strand breaks: the DNA template alterations that trigger p53-dependent DNA damage response pathways. Molecular and cellular biology. 1994;14(3):1815-23.
128. Persu A, Stoenoiu MS, Messiaen T, Davila S, Robino C, El-Khattabi O, et al. Modifier effect of ENOS in autosomal dominant polycystic kidney disease. Human molecular genetics. 2002;11(3):229-41.
129. de Nadal E, Ammerer G, Posas F. Controlling gene expression in response to stress. Nature reviews Genetics. 2011;12(12):833-45.
130. Selmansberger M, Feuchtinger A, Zurnadzhy L, Michna A, Kaiser JC, Abend M, et al. CLIP2 as radiation biomarker in papillary thyroid carcinoma. Oncogene. 2015;34(30):3917-25.

Supplemental Table 1: thyroid cancer types and their mutational profiles (2)**.**

Characteristics	**Papillary carcinoma**	**Follicular carcinoma**	**Anaplastic carcinoma**	**Medullary carcinoma**
Cell type	Follicular cells	Follicular cells	Follicular cells	C-cells
Prevalence	80-85%	10-15%	1-2%	3-5%
Typical route of spread	Local lymph node metastasis.	Hematogenous metastasis, typically to bones and lungs.	Invasive local growth, lymph node and hematogeneous metastases.	Lymph node and hematogeneous metastases.
10-years survival	95-98%	90-95%	<10%	60-80%
Common mutations and their prevalence	BRAF 40–45% RAS 10–20% RET/PTC 10–20% TRK <5%	RAS 40–50% PAX8/PPARγ 30–35% PIK3CA <10% PTEN <10%	TP53 50–80% CTNNB1 5–60% RAS 20–40% BRAF 20–40% PIK3CA 10–20% PTEN 5–15% AKT1 5-10%	<u>Familial forms:</u> RET >95% <u>Sporadic:</u> RET 40–50% RAS 25%

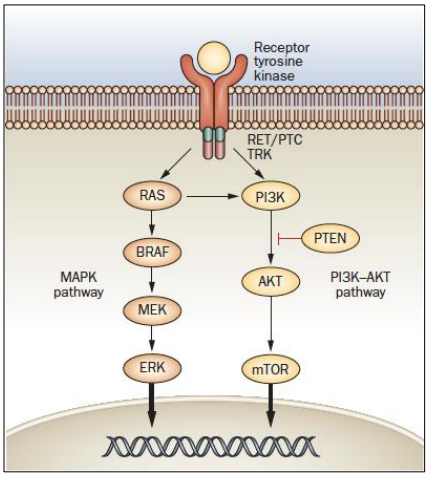

Supplemental Figure 1: The main signaling pathways involved in thyroid carcinogenesis are the MAPK and PI3K–AKT pathways. These pathways regulate multiple cellular processes including proliferation, differentiation and survival. Constitutive activation of the MAPK pathway by mutated BRAF and RAS genes or by the chimeric fusion proteins RET/PTC and tyrosine receptor kinase (TRK) are a common tumor-initiating event in well-differentiated papillary carcinoma and in some follicular carcinomas. Mutations involving the effectors of the PI3K–AKT pathway such as the PI3K subunit PIK3CA, AKT1 and PTEN are found more frequently in follicular carcinomas and in undifferentiated types of thyroid cancer (2).

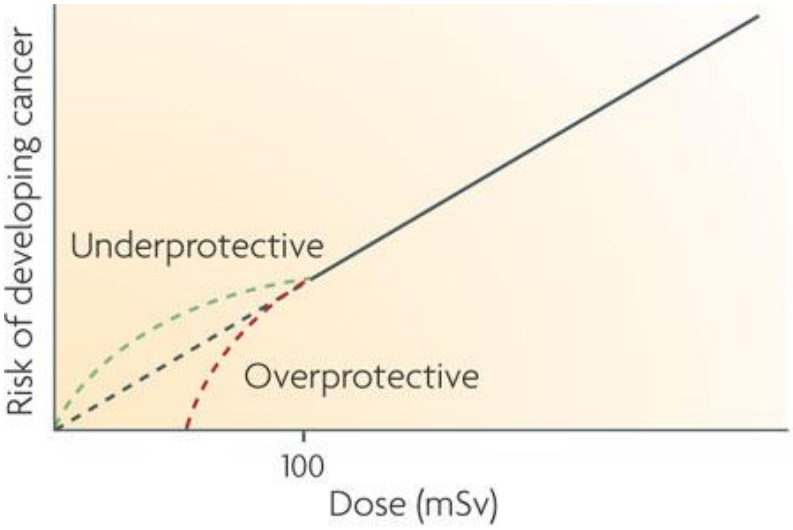

Supplemental Figure 2: Possible relationships between low-dose radiation of cancer risk. Epidemiological data provide direct measurements down to ~ 100 mSv (solid black line). However, there are still uncertainties about the health effects of radiation doses below 100 mSv. Below this level a linear non-threshold extrapolation is used to estimate the risks to develop cancer at low radiation doses (dashed black line) (14).

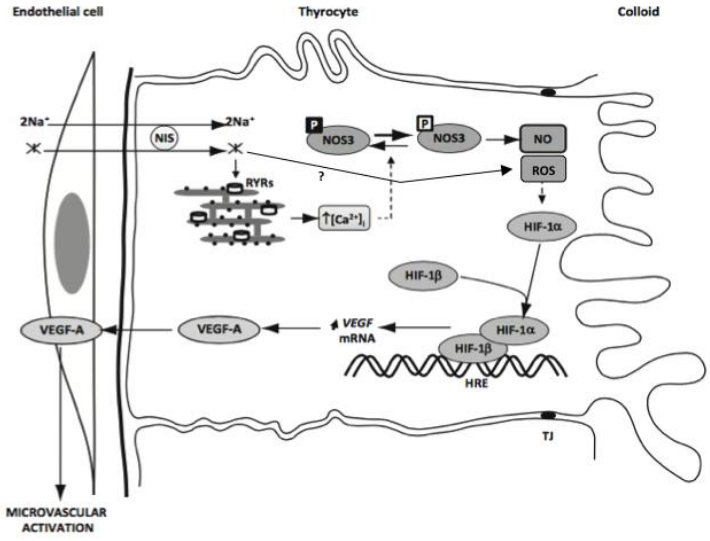

Supplemental Figure 3: Proposed mechanism of iodide deprivation-induced angiogenesis in thyroid angiofollicular units. As soon as intracellular iodide levels drop due to an acute decrease in iodine supply, an increase in intracellular ROS levels is observed. Furthermore, ID induces RYR-dependent Ca^{2+} release from the endoplasmic reticulum, leading to phosphorylation and subsequent activation of NOS3 and NO production. The produced ROS and NO stabilize HIF-1α which associates with HIF-1ß to form the transcription factor HIF- 1. HIF-1 binds to the hypoxia-response element (HRE) site localized in the promoter region of the VEGF-A gene, thereby initiating VEGF-A transcription and VEGF-A protein synthesis. VEGF-A then acts as a paracrine factor to stimulate the proliferation of adjacent endothelial cells and promote microvascular thyroid reshaping. Adapted from (69) and (70).

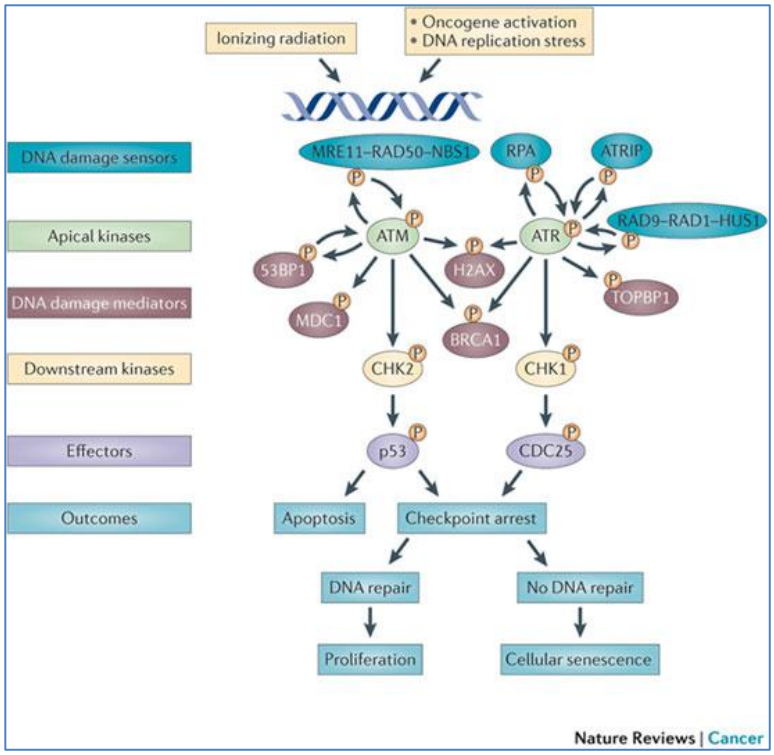

Supplemental figure 4: DNA damage response pathway

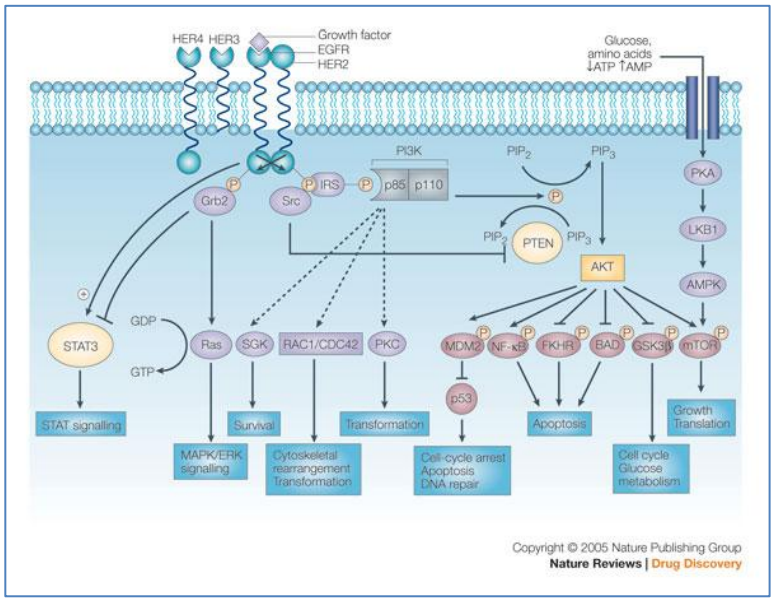

Supplemental figure 5: PI3K/AKT pathway

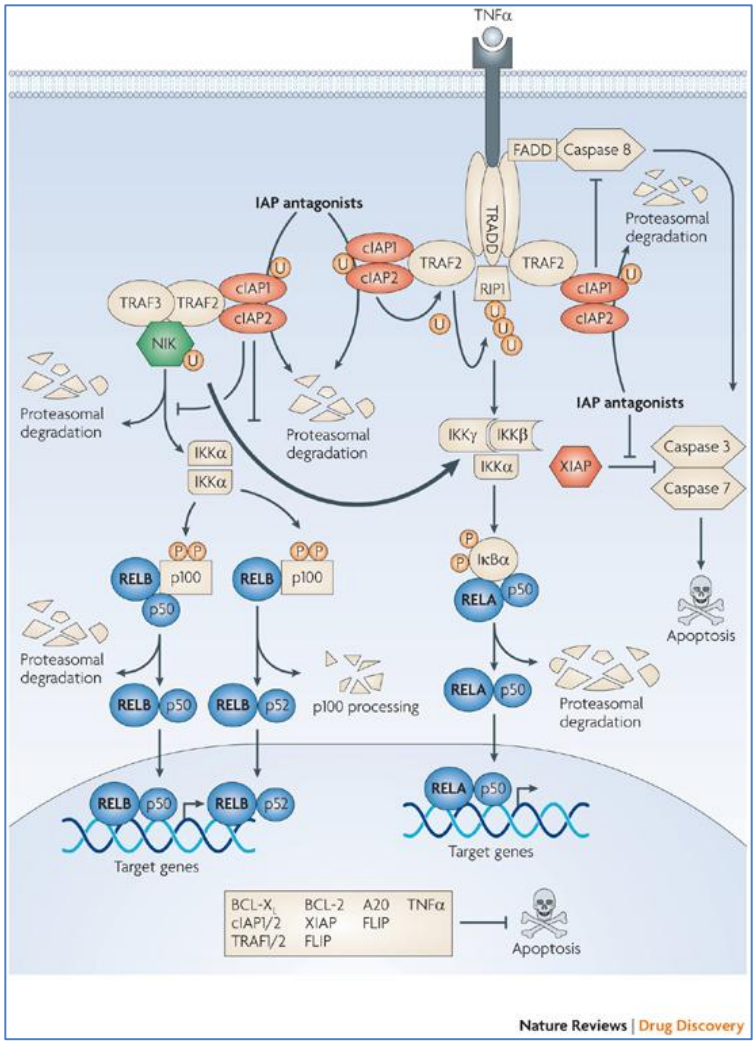

Supplemental figure 6: NFκB pathway

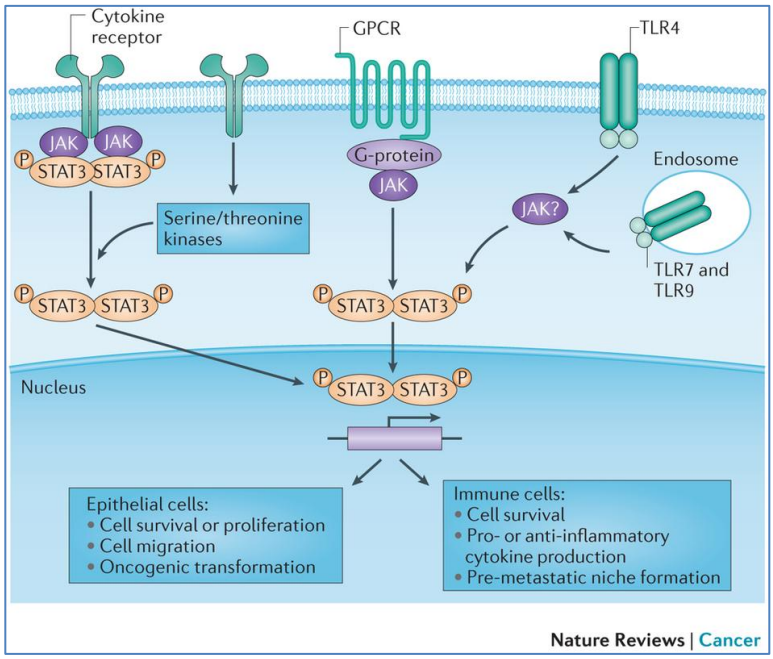

Supplemental figure 7: JAK/STAT pathway

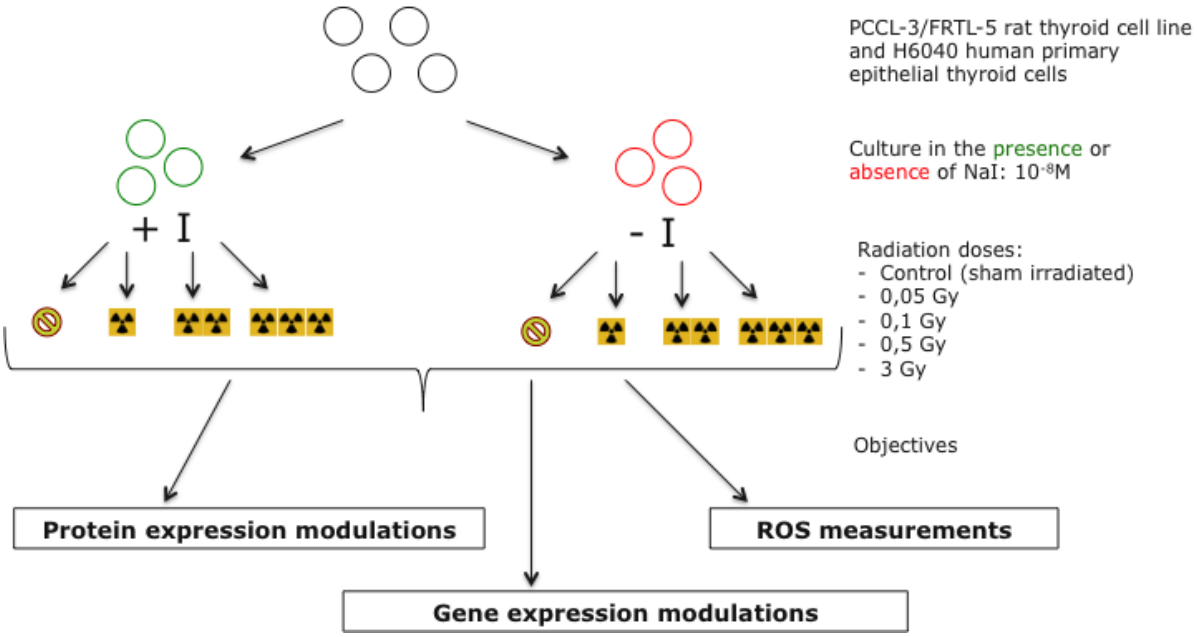

Supplemental figure 8: Experimental set-up with the different condition (iodine, iodine deficiency, and the different radiation doses).

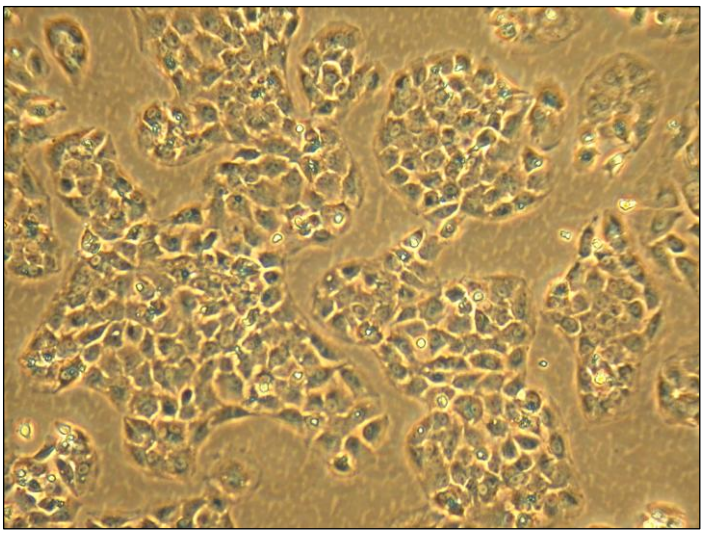

Supplemental figure 9: Cultured rat PCCL3 thyroid cells.

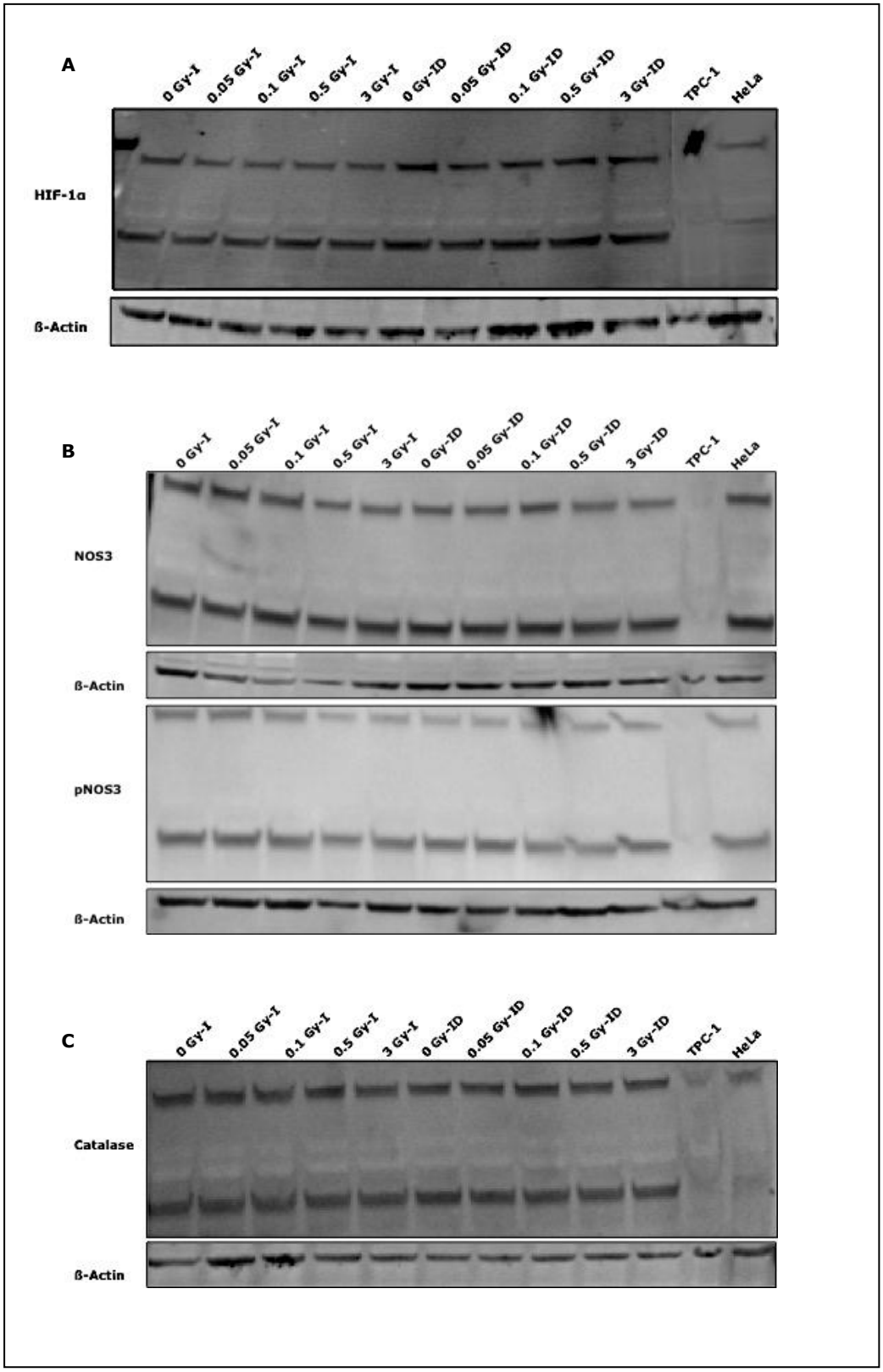
A
0 Gy-I
0.05 Gy-I
0.1 Gy-I
0.5 Gy-I
3 Gy-I
0 Gy-ID
0.05 Gy-ID
0.1 Gy-ID
0.5 Gy-ID
3 Gy-ID
TPC-1
HeLa
HIF-1α
ß-Actin
B
NOS3
ß-Actin
pNOS3
ß-Actin
C
Catalase
ß-Actin

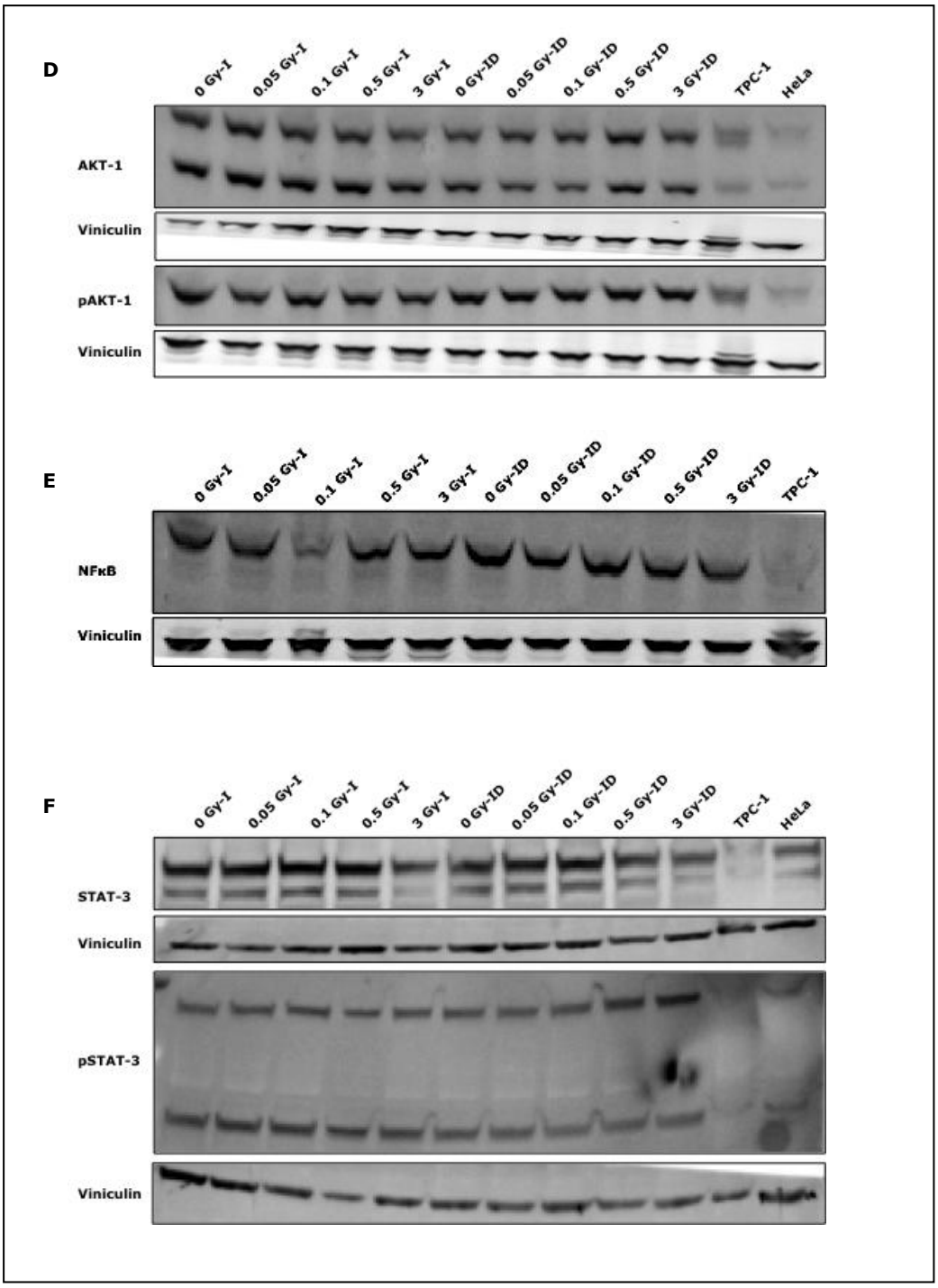

Supplemental figure 10: Western blot results of HIF-1α and β-Actin **(A)**; NOS, pNOS3 and β-Actin **(B)**; Catalase and β-Actin **(C)**; AKT-1, pAKT-1 and viniculin **(D)**; NFκB p52 and viniculin **(E)**; STAT-3, pSTAT-3 and viniculin **(F)**. Viniculin and β-Actin are housekeeping proteins to normalize for equal loading.

A

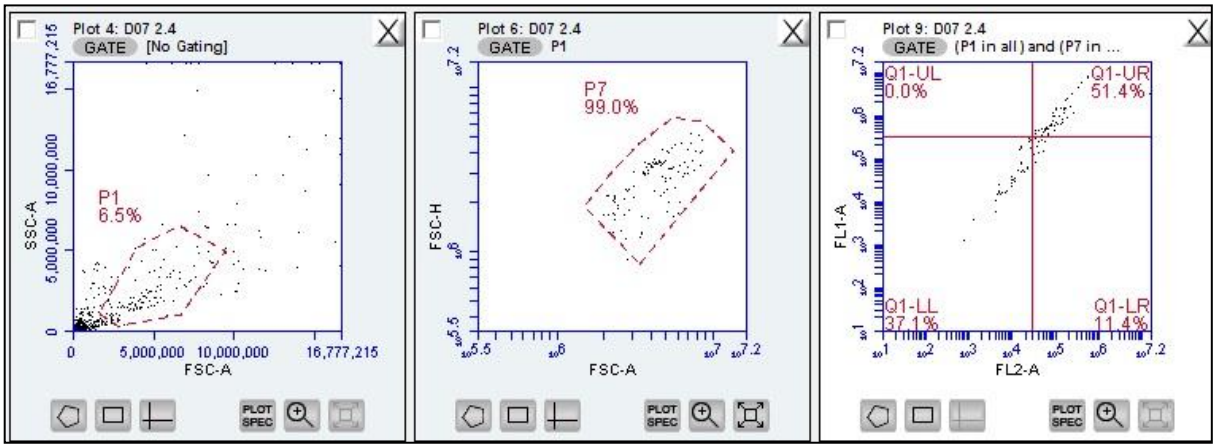

B

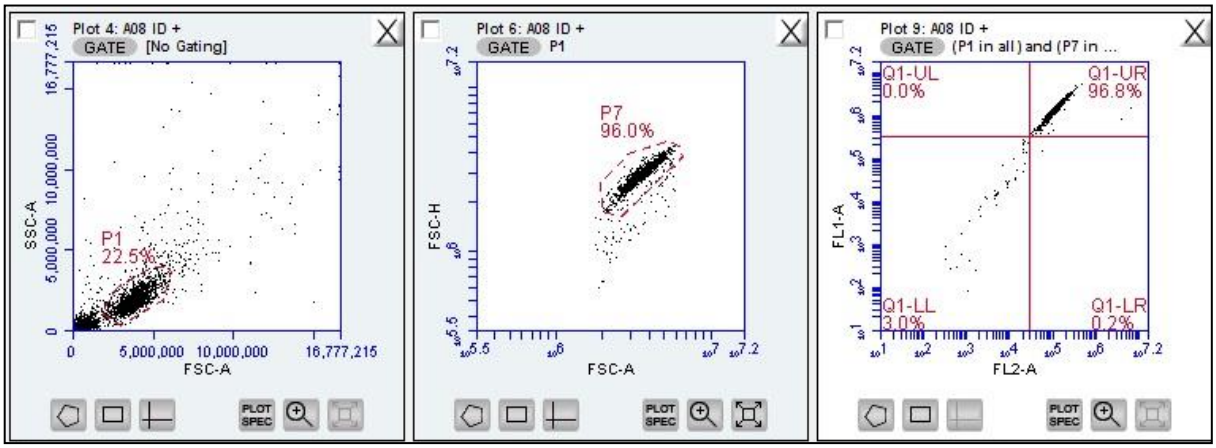

C

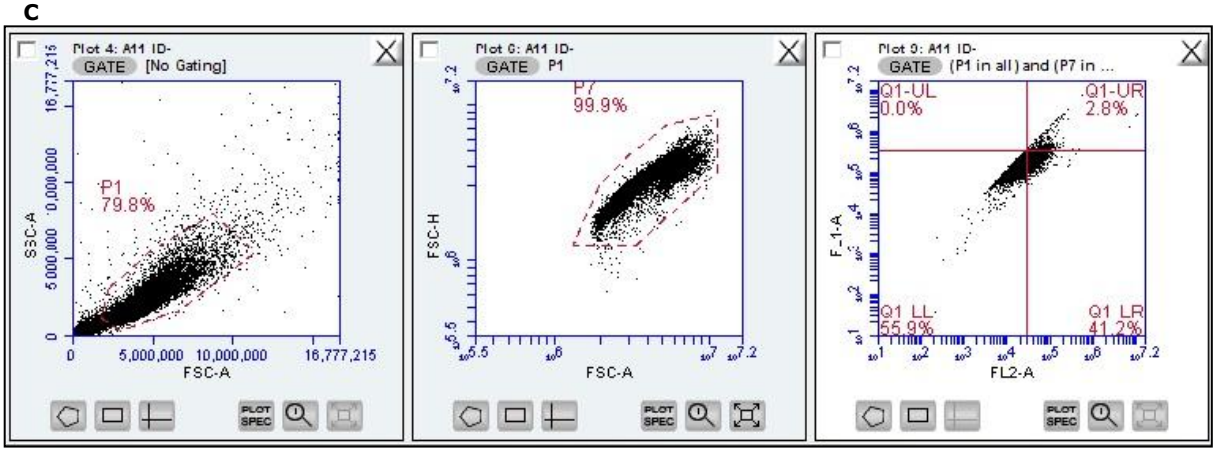

Supplemental figure 11: TUNEL staining and subsequent flow cytometry analysis of PCCL3 cells. PCCL3 cells were iodine deprived for 48 hours and were irradiated with 0.05 Gy **(A)**, Sham-irradiated and treated with DNase 1 **(B)**, and sham-irradiated without DNase 1 treatment **(C)**. Left plots represent the forward and sideward scatter, distinguishing debris from cells. Middle plots discriminate doublets from singlet cells. Finally, the right plots visualize the presence of BrdUTP, measured in the FL1-A channel and cleaved caspase 3, measured in the FL2-A channel. In these plots, the lower left quadrant represent living cells, the lower right quadrant early apoptotic cells and the right upper quadrant late apoptotic cells. Many cell samples had low cell counts such as represented in example **(A)**. The positive control sample treated with DNase 1 showed a major cell population in the late apoptotic quadrant **(B)**. However, there were no clearly separated cell populations of living and apoptotic cells detected in **(C)**, which was not treated with DNase 1.

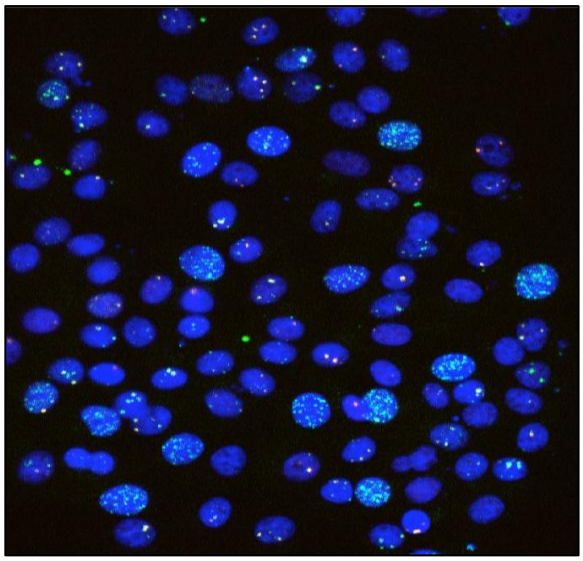

Supplemental figure 12: γH2AX and 53BP1 foci in 3 Gy-irradiated iodine-deficient PCCL3 cells at 1 hour post-treatment. (Magnification: 40X).

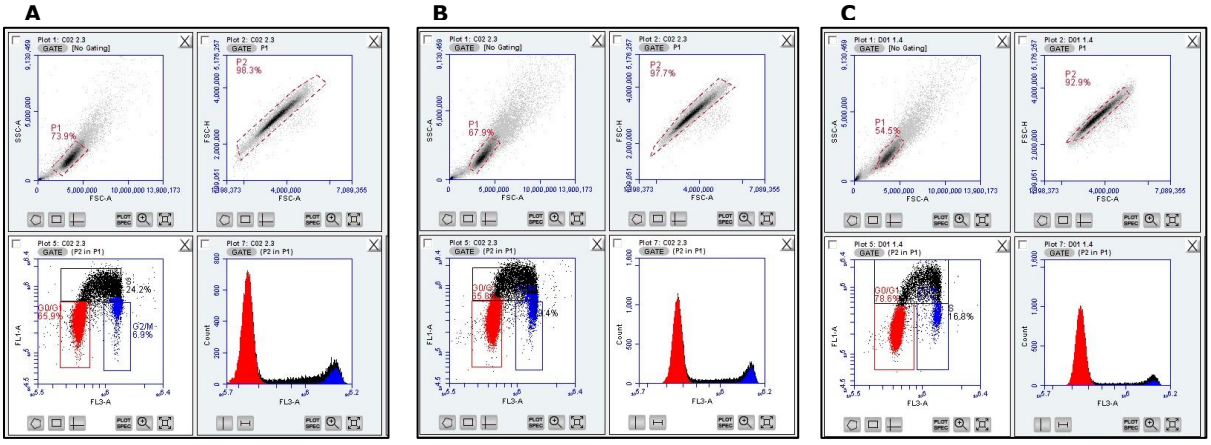

Supplemental figure 13: Cell cycle analysis by 7-AAD/BrdU staining measured by flow cytometry. PCCL3 cells were iodine deprived for 6 hours **(A)**, 24 hours **(B)** and 48 hours **(C)** and were irradiated with 0.05 Gy in (A) and (B) and were sham-irradiated in (C). Upper left plots represent the forward and sideward scatter, distinguishing debris from cells. Upper right plots discriminate doublets from singlet cells. Lower left plots visualize the presence of BrdU in the FL1-A channel and 7-AAD in the FL3-A channel. Lower right plots represent a DNA histogram with the fluorescence intensity on the X-axis and the number of cells in the G0/G1 phase, S phase and G2/M phase in the Y-axis.

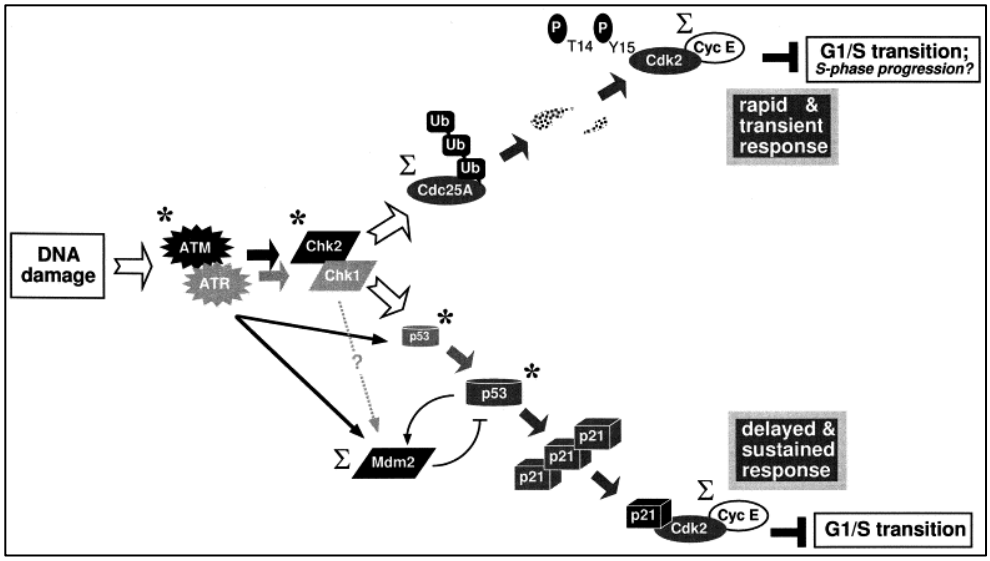

Supplemental figure 14: p53-independent rapid and transient G1 arrest and the p53 dependent delayed and sustained G1 arrest.

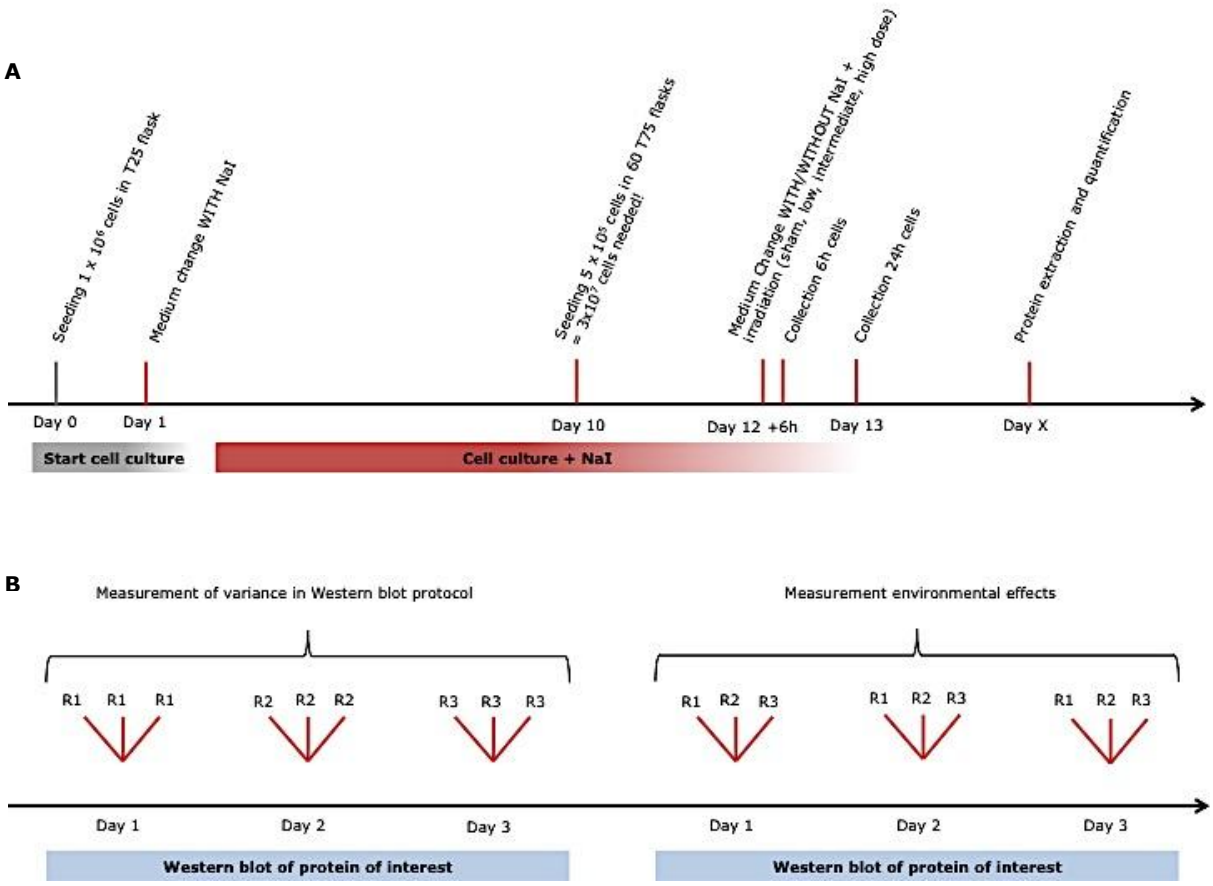

Supplemental figure 15: Experimental scheme for the cell culture process (A) and the possibilities to measure potential variances deriving from the Western blot protocol or the environment (B).

Auteursrechtelijke overeenkomst

Ik/wij verlenen het wereldwijde auteursrecht voor de ingediende eindverhandeling:
Cellular and molecular effects of iodine deficiency and ionizing radiation on non-cancerous thyroid cells

Richting: **master in de biomedische wetenschappen-klinische moleculaire wetenschappen**
Jaar: **2016**

in alle mogelijke mediaformaten, - bestaande en in de toekomst te ontwikkelen - , aan de Universiteit Hasselt.

Niet tegenstaand deze toekenning van het auteursrecht aan de Universiteit Hasselt behoud ik als auteur het recht om de eindverhandeling, - in zijn geheel of gedeeltelijk -, vrij te reproduceren, (her)publiceren of distribueren zonder de toelating te moeten verkrijgen van de Universiteit Hasselt.

Ik bevestig dat de eindverhandeling mijn origineel werk is, en dat ik het recht heb om de rechten te verlenen die in deze overeenkomst worden beschreven. Ik verklaar tevens dat de eindverhandeling, naar mijn weten, het auteursrecht van anderen niet overtreedt.

Ik verklaar tevens dat ik voor het materiaal in de eindverhandeling dat beschermd wordt door het auteursrecht, de nodige toelatingen heb verkregen zodat ik deze ook aan de Universiteit Hasselt kan overdragen en dat dit duidelijk in de tekst en inhoud van de eindverhandeling werd genotificeerd.

Universiteit Hasselt zal mij als auteur(s) van de eindverhandeling identificeren en zal geen wijzigingen aanbrengen aan de eindverhandeling, uitgezonderd deze toegelaten door deze overeenkomst.

Voor akkoord,

Daems, Noami

Datum: **8/06/2016**